R92-917981-2

(2)

CARBON FIBER REINFORCED GLASS MATRIX COMPOSITES FOR SATELLITE APPLICATIONS

Prepared by

W. K. Tredway
P. H. McCluskey
K. M. Prewo

ANNUAL REPORT

Contract N00014-89-C-0046

for

Department of the Navy
Office of Naval Research
Arlington, VA 22217

June 30, 1992

UNITED TECHNOLOGIES RESEARCH CENTER

REPORT DOCUMENTATION PAGE

Form Approved
OMB No 0704-0188

1. AGENCY USE ONLY (Leave blank)	2. REPORT DATE	3. REPORT TYPE AND DATES COVERED
	30 June 1992	Annual January 1989 - June 1992

4. TITLE AND SUBTITLE

CARBON FIBER REINFORCED GLASS MATRIX COMPOSITES FOR SATELLITE APPLICATIONS

5. FUNDING NUMBERS

N00014-89-C-0046

6. AUTHOR(S)

W. K. Tredway, P. H. McCluskey and K. M. Prewo

7. PERFORMING ORGANIZATION NAME(S) AND ADDRESS(ES)

United Technologies Research Center
East Hartford, CT 06108

8. PERFORMING ORGANIZATION REPORT NUMBER

R92-917981-2

9. SPONSORING / MONITORING AGENCY NAME(S) AND ADDRESS(ES)

Department of the Navy
Office of Naval Research
Arlington, VA 22217

10. SPONSORING / MONITORING AGENCY REPORT NUMBER

11. SUPPLEMENTARY NOTES

12a. DISTRIBUTION / AVAILABILITY STATEMENT

Unclassified/Unlimited

12b. DISTRIBUTION CODE

13. ABSTRACT *(Maximum 200 words)*

The development of carbon fiber reinforced glass and glass-ceramic matrix composites for satellite applications is described. A variety of carbon fibers (HMU, P-100, FT700, K1100X) have been used to reinforce borosilicate glass and BMAS glass-ceramics to create high performance composite materials useful for structural applications in space. Fundamental material properties that are described in this report include tensile and compressive stress-strain behavior, tensile and compressive fatigue behavior, effect of fiber orientation on tensile strength and elastic modulus, notch sensitivity, high temperature strength characteristics, thermal expansion behavior, thermal conductivity characteristics, and space environmental durability. Also included is a section describing methods that have been developed for improving the tensile proportional limit in these materials as well as a section describing the application of hot isostatic pressing for the fabrication of structural components such as thin-walled tubes and angle brackets. The final section describes two satellite applications that have been identified for carbon fiber reinforced glass composites, specifically tubes for satellite truss structures and radiator fins for space power applications.

14. SUBJECT TERMS

glass matrix composites
carbon fiber reinforced composites
ceramic matrix composites

15. NUMBER OF PAGES
88

16. PRICE CODE

17. SECURITY CLASSIFICATION OF REPORT	18. SECURITY CLASSIFICATION OF THIS PAGE	19. SECURITY CLASSIFICATION OF ABSTRACT	20. LIMITATION OF ABSTRACT
Unclassified	Unclassified	Unclassified	SAR

R92-917981-2

Carbon Fiber Reinforced Glass Matrix Composites for Satellite Applications

ANNUAL REPORT

Contract N00014-89-C-0046

REPORTED BY William K. Tredway
William K. Tredway
Philip H. McCluskey
Philip H. McCluskey
Karl M. Prewo
Karl M. Prewo

APPROVED BY Earl R. Thompson
Earl R. Thompson
Asst. Director of Research
for Materials Technology

DATE June 30, 1992

TABLE OF CONTENTS

SECTION PAGE

I. PREFACE

This report contains the results of work performed during the period from January, 1989 to June, 1992 on ONR Contract N00014-89-C-0046 to develop carbon fiber reinforced glass matrix (C/Glass) composites for structural satellite applications. Section II contains the bulk of the information and has been consolidated in a form that makes it possible to gain important information regarding behavior of C/Glass composites relevant to space-based applications. This section was intended to serve as a primer which could provide an introduction to C/Glass composites and present all of the information that is important in understanding how this material would perform in the space environment. Subsequent sections contain additional detailed information on work that was performed during the program as well as a section describing satellite applications for C/Glass composites.

This program is supported by the Strategic Defense Initiative Organization / Innovative Science and Technology through Office of Naval Research contract N00014-89-C-0046.

II. FIBER REINFORCED GLASS MATRIX COMPOSITES FOR SPACE STRUCTURES

II.1. INTRODUCTION

Advanced materials being developed for structural applications in space will have extraordinary requirements placed on them due to the challenging demands of space structures. Depending on the particular application, issues such as dimensional stability, density, specific strength and stiffness, near-zero thermal expansion, and space environmental durability can be critically important factors. One of the materials being developed for utilization in space structures is carbon fiber reinforced glass (C/Glass). This exceptional class of materials has been the subject of investigation for many years due to the unique combination of high strength, stiffness, and toughness, low thermal expansion, low density, excellent tribological characteristics, and ease of fabrication. C/Glass composites offer performance equivalent or better than polymer and metal matrix systems in many areas. In addition, the superior temperature capability and extreme resistance to the space environment make C/Glass composites an attractive material for many space based applications. This section describes the behavior of C/Glass composites pertinent to use as a structural material in space.

II.2. MATERIALS

II.2.1 Fibers

One of the most attractive features of using carbon fibers as a reinforcement is the wide variety of carbon fibers that are available in terms of strength, elastic modulus, thermal expansion, and thermal conductivity. This makes possible the idea of tailoring, or engineering, composites for specific applications. Table II-1 summarizes some of the carbon fibers that are currently available along with the pertinent property data. It is clear from the data that density,

thermal expansion, and thermal conductivity are all closely related to fiber elastic modulus. In fact, all of these characteristics (including modulus) are established by the internal structure of the fiber, with crystallite size and the degree of crystallite orientation being the most dominant factors [1-2]. Fiber strength is somewhat dependent on these factors but is influenced to a greater extent by the presence and size of internal and surface defects. The internal and surface structure and surface chemistry can vary greatly for different types of fiber, with corresponding differences in fiber properties. For example, a polyacrylonitrile (PAN) based fiber such as HMU has a "skin-core" type microstructure, with an inner core consisting of curled and bent graphite crystallites surrounded by an outer skin of crystallites that are highly aligned with their basal planes parallel to the fiber surface (Figure II-1a). This results in a smooth fiber surface with a low surface energy characteristic of graphite basal planes. On the other hand, a high elastic modulus fiber derived from a mesophase pitch precursor, such as P-100, has a radial microstructure, with highly oriented graphite crystallites exhibiting radial alignment about the fiber axis (Figure II-1b). A significant fraction of these high energy edge planes intersect the fiber surface, resulting in an increase in fiber surface energy. Understanding the fiber surface morphology and chemistry is important since these characteristics are known to affect the nature of the fiber-matrix interface, which probably exerts the strongest influence on overall composite performance [3].

Table II-1 - Carbon Fiber Room Temperature Property Data

Fiber	Manufacturer	Density (g/cm^3)	Tensile Strength (MPa)	Tensile Modulus (GPa)	Axial Thermal Expansion (10^{-6} cm/cm K)	Axial Thermal Conductivity (W/m K)
T-300	APP*.	1.76	3100	234	-0.5	8.5
HMU	Hercules	1.84	2760	380	-0.7	80
FT500	Tonen	2.14	3000	500	-1.0	150
FT700	Tonen	2.16	3300	700	-1.5	360
P-100	APP*	2.16	2240	724	-1.6	520
P-120	APP*	2.18	2070	827	-1.6	520
K1100X	APP*	2.23	2350	920	-1.6	1030

* Amoco Performance Products

II.2.2 Matrices

A large number of glass and glass-ceramic compositions can be successfully utilized as matrix materials for C/Glass composites. Table II-2 lists some of the systems from which matrix compositions are commonly derived along with typical values of density, thermal expansion, and maximum temperature capability. Glass-ceramics are materials that exhibit the viscous characteristics of glass at temperatures above their melting point, thus enabling them to be formed into a variety of complex shapes. They also have the unique trait of being able to be converted from an amorphous material to a dense polycrystalline material through an appropriate heat treatment, thus imparting superior mechanical and temperature characteristics to the matrix. Again, it is important to realize that matrix chemistry can play a large role in determining overall composite performance. Reactions between the matrix and the fiber, or the lack thereof, can affect the strength of the fiber-matrix interface, which in turn controls many important aspects of composite behavior [3]. Also, it has been recently shown that the wetting behavior of the matrix on the carbon fiber is an important factor in determining fiber-matrix interfacial bond strength and subsequent composite performance [4].

Table II-2 - Matrix Materials Used for Carbon Fiber Reinforced Glass Composites

Matrix Type	Matrix System	Density (g/cm^3)	Thermal Expansion (10^{-6} m/m K)	Temperature Capability (°C)
Glass	Borosilicate	2.2	3.2	500-560
Glass-Ceramic	LAS*	2.45	1.0	1000
"	BMAS**	2.7	3.0	1200
"	MAS†	2.6	1.0	1250

* LAS = Lithium aluminosilicate

** BMAS = Barium magnesium aluminosilicate

† MAS = Magnesium aluminosilicate

II.3. FABRICATION METHODS

The most common method of fabricating C/Glass composites is by hot-pressing multi-ply laminates consisting of carbon fiber and glass powder at a temperature well above the softening point of the glass [5-6]. In the case of glass-ceramic matrix compositions, the hot-pressing

temperature is also dependent on the crystallization behavior of the glass. Unitape prepregs are made by a slurry impregnation process whereby fiber tows are unwound from the supply spool, pulled through a slurry consisting of water, glass powder, and an acrylic binder, and then wound onto a hexagonal mandrel and allowed to dry. Prepregged fabric can also be produced by dipping the fabric in slurry and allowing it to dry. A composite preform is then made by cutting the prepreg into plies, stacking in the desired orientation, and thermally decomposing the binder. Final consolidation is achieved by loading the preform into a graphite die and hot-pressing using the appropriate conditions of temperature and pressure. C/Glass composites fabricated via this method are typically fully densified with less than 1% porosity.

The size of composite articles that can be fabricated via hot-pressing is limited only by the size of the furnace chamber. As part of this program, flat panels of [0/90] reinforced C/Glass up to 51 cm x 20 cm in size and 0.25 cm thick have been fabricated in a large hot-press at United Technologies Research Center (UTRC). Composite thickness can also vary considerably, ranging from a practical maximum of 1.25 cm all the way down to as thin as 0.25 mm. While the complexity of parts that can be fabricated via hot-pressing is somewhat limited, the geometries that can be produced are not restricted to flat panels. Curved "hat-section" beams, airfoil shapes, and other complex structures have also been successfully fabricated using hot-pressing techniques.

Other techniques have also been utilized to produce C/Glass composite articles in situations where external and/or internal structural geometries are too complex for hot-pressing. Examples of such techniques are: (1) injection molding, where chopped carbon fiber and glass powder are injected into a die cavity at high temperature; (2) matrix transfer molding, where molten glass is transferred from a reservoir into a rigidized fiber preform at high temperature, and; (3) hot isostatic pressing (HIP), where isostatic pressure is used to consolidate the composite preform inside a vacuum-evacuated can. The technique that has been investigated most recently at UTRC for its potential to fabricate C/Glass composites for space structures is HIP. Specifically, HIP has been used to fabricate continuously reinforced circular cross-section (2.5 to 4.4 cm diameter) and square cross-section (2.5 cm square) thin-walled tubular elements as well as L-beams in lengths up to 30 cm (Figure II-2). Details of the steps involved in HIP processing were summarized in a previous report [7]. A comparison of properties of composites fabricated by hot-pressing and by HIP'ing is described in a subsequent section (Section IV) of this report. One of the major advantages of using HIP for fabrication of tubes and beams is that it allows for the scale-up of parts to lengths of 3 meters. Such structural elements are commonly envisioned as the main components of satellite truss structures. The fabrication and compression testing of HIP'ed C/Glass tubes was described in a previous report [7].

II.4. MECHANICAL PROPERTIES

II.4.1 Monotonic Tensile Stress-Strain Behavior

C/Glass composites typically exhibit non-linear tensile stress-strain behavior that is quite unique in its characteristics. In general, the high tensile strength of the carbon fibers used as reinforcement translates to reasonably high composite strength, with values for unidirectionally reinforced composites ranging from 500 MPa to 900 MPa, depending on the type of fiber and the fiber volume fraction. C/Glass composites also generally exhibit significant fiber pullout and crack bridging during fracture, indicating a reasonable degree of toughness. However, the aforementioned ditferences in fiber surface morphology, fiber surface chemistry, matrix chemistry, and matrix wetting behavior can lead to substantial differences in composite stress-strain behavior depending on the exact nature of the fiber-matrix interface. In this section the tensile stress-strain behavior of two borosilicate glass matrix composites, one containing PAN-based HMU fiber and the other reinforced with pitch-based fiber (P-100 or FT700), will be described and compared with respect to various features of the stress-strain curve and how they relate to interfacial strength.

Figure II-3 shows a typical stress-strain curve for a unidirectional HMU reinforced borosilicate glass (HMU/BSG) composite containing approximately 45 vol% fiber. Upon initial loading the composite displays linear elastic behavior up to a stress and strain of about 400 MPa and 0.25%, respectively. In this initial linear region, the composite elastic modulus is predictable based on a combination of stiffness from the carbon fibers and the glass matrix. At the upper level of this initial linear region, the stress-strain curve deviates significantly from linearity, passing through a transition region of increasing strain with very little increase in stress. The point where the curve deviates from linearity is commonly referred to as the proportional limit (PL). In the HMU/BSG composite system, it has been suggested that the PL and the subsequent "plateau" region correspond to wide-scale microcracking of the matrix and fiber-matrix debonding [8]. However, recent evidence in the literature obtained using acoustic emission indicates that the initiation of microcracking in this composite system actually begins much earlier at about 125 MPa [9]. It is likely that the microcrack density continues to increase on extended loading from 125 MPa until it reaches a saturation level, followed by fiber-matrix debonding at the PL and plateau region. Similar behavior has been observed in other fiber reinforced ceramic composites. The occurrence of wide-scale microcracking in the HMU/BSG composite is verified by the fact that on unloading and reloading after passing through the plateau region, the composite elastic modulus is decreased from the original by an amount attributable to a loss of matrix stiffness.

Following the transition region, the curve again exhibits linear behavior representative of the fibers carrying the load alone after matrix microcracking. The mechanism of fiber-matrix debonding prior to this stage is critical to the fibers being able to carry the load until they reach their inherent failure strain of 0.7%. If significant debonding did not occur, matrix cracks would experience little if any deflection and would instead propagate directly through the fibers, resulting in lower composite strength and near-brittle failure. A considerable amount of fiber pullout typifies fracture surfaces in HMU/BSG composites, indicative of low fiber-matrix interfacial strength.

While the performance of HMU/BSG composites is exceptional in terms of strength and toughness, stiffness-critical applications in space structures will most likely require the utilization of higher elastic modulus pitch-based carbon fibers, such as P-100 or FT700. The tensile stress-strain behavior of P-100/BSG and FT700/BSG composites differs in several respects from that of HMU/BSG composites. The curve in Figure II-3 illustrates the tensile behavior of a unidirectionally reinforced P-100/BSG composite containing approximately 40 vol% fiber (this curve is also typical of the behavior of FT700/BSG composites). The initial portion of the curve is again representative of linear elastic behavior which is predictable based on a rule-of-mixtures approach, with the elastic modulus being at an acceptably high level for many stiffness-critical space applications. The curve experiences a PL at a stress and strain of about 125 MPa and 0.03%, respectively, followed by a secondary region of steadily decreasing slope. The fibers continue to carry the load until they reach their failure strain of approximately 0.2%.

The stress-strain curves of the HMU and P-100 reinforced materials differ in two main respects: 1) the P-100/BSG composite does not exhibit the sudden increase in strain following the PL, and; 2) the secondary region representative of fibers carrying the load alone in the P-100/BSG composite is not linear, but instead exhibits a negative curvature with increasing strain. The two materials also differ in the sense that, in contrast to the HMU reinforced system, strain cycling of the P-100/BSG composite past the PL does not result in any change in the initial elastic modulus. The mechanism for this is described below. The fracture behavior of the P-100/BSG composite also differs from that of the HMU/BSG composite, with fiber pullout not being as extensive in the P-100/BSG material. These dissimilarities between the two composite systems are due in large part to differences in the nature of the fiber-matrix interface caused by the unlike surface structure and surface chemistry of HMU and P-100 carbon fiber. Stronger interfacial bonding in the P-100/BSG composite resulting from a rougher surface and a higher surface energy along with the lower *in-situ* strength of the P-100 fibers are thought to lead to shorter pullout lengths and reduced composite toughness.

The PL in the P-100/BSG composite, as in the HMU/BSG system, seems to correspond to a loss in the matrix contribution to the composite elastic modulus. However, the mechanism by

which the matrix stiffness is decoupled from the composite in the P-100/BSG composite is not yet certain. Calculations of residual matrix tensile stress in the P-100/BSG system using the composite cylinder assemblage model show that the magnitude of matrix tensile stress generated during cooling parallel to the fiber direction is approximately 125 MPa at room temperature [10]. This level of stress is great enough to generate a considerable number of *pre-existing* matrix microcracks in the P-100/BSG composite due to thermal residual stresses alone, as shown in Figure II-4. This figure shows an optical micrograph of a replica of the surface of a 0° reinforced P-100/BSG composite after fabrication and before any testing. It is evident from the micrograph that a large number of evenly spaced microcracks exist running normal to the fiber direction, with an average crack spacing of about 160 μm. Other experimental evidence regarding pre-existing matrix microcracks has been gathered using acoustic emission monitoring of FT700/BSG composite specimens during tensile testing. Signals normally associated with matrix cracking were not detected throughout the entire loading cycle, suggesting that the matrix may have already been fully microcracked from thermal residual stresses. Also, cyclic tensile testing [11] and tensile fatigue testing of P-100/BSG and FT700/BSG composites at UTRC have shown that loading of tensile specimens to a point well beyond the PL does not result in any loss of initial composite stiffness during reloading in subsequent cycles.

This behavior is in sharp contrast to the HMU/BSG system, where loading above the PL results in a permanent decrease in initial modulus on reloading by an amount corresponding to the matrix contribution to composite stiffness [8], indicating that the matrix has fully cracked and debonded from the fibers. The "recoverable" loss in modulus observed in the P-100/BSG and FT700/BSG systems suggests that another mechanism is responsible for the non-linear stress-strain behavior in these composites. One possible mechanism proposed here is that Poisson contraction of the fibers away from the matrix during loading coupled with the high interfacial tensile stress (from thermal expansion mismatch) in the P-100/BSG and FT700/BSG systems results in gradual decoupling of the fibers from the matrix during loading, causing a progressive reduction in load transfer from the matrix to the fibers. This would account for the steadily decreasing slope of the stress-strain curve in the secondary region after the PL (Figure II-3) as well as the recovery of the original composite stiffness on unloading. Continued work is underway at UTRC to confirm the mechanism(s) responsible for the non-linear stress-strain behavior in the P-100/BSG, FT700/BSG, and other high modulus pitch fiber reinforced systems.

II.4.2 Effect of Fiber Orientation on Composite Behavior

The effect of fiber orientation on the tensile stress-strain behavior of HMU/BSG composites has been studied previously [8]. In that study, it was found that the dependence of

the UTS and elastic modulus on ply angle θ (for unidirectional composites) or $\pm\theta$ (for angle-ply composites) could be well-described using classical laminate theory (Figures II-5 and II-6). The UTS was accurately predicted in these composites by the Tsai-Hill (maximum work) failure criterion. More recently, work has been performed at UTRC to determine the effect of fiber orientation on the performance of FT700/BSG composites. As in the previous study, both unidirectional (θ) and angle-ply ($\pm\theta$) composites were investigated. The particular aspects of performance that were assessed as a function of fiber angle were UTS and elastic modulus.

Classical laminate theory [12] was used to predict the elastic modulus of the FT700/BSG composites as a function of ply angle θ. The results for both unidirectional and angle-ply composites are shown in Figure II-7. The values used for composite longitudinal modulus (329 GPa) Poisson's ratio (0.18) are the experimentally measured values for the 0° reinforced composite. The value used for transverse elastic modulus was estimated based on transverse tensile tests of P-100/BSG composites. The composite shear modulus G was used as an adjustable parameter to fit the data. In order to obtain the best fit, the value of G for the angle-ply composites was only half that of the unidirectional composites. This is similar to behavior exhibited in the HMU/BSG system [8] and may be due to higher interply stresses in the angle-ply composites caused due to ply anisotropy in thermal expansion. In general, good agreement was seen between the predicted and measured elastic moduli in both the unidirectional and angle-ply composites.

Two different strength theories, the maximum stress failure criterion and the maximum work failure criterion, were used to predict the ultimate tensile strength of the unidirectionally reinforced composites as a function of θ. In the maximum stress failure criterion, composite failure is assumed to occur by either tensile fiber failure, shear failure of the fiber-matrix interface or the matrix, or tensile failure of the fiber-matrix interface or matrix [12]. The maximum stress theory predicts that composite failure will occur by the mechanism exhibiting the lowest value of strength at a particular value of θ. The maximum work failure criterion is based on the von Mises failure criterion describing a failure "envelope" or surface in three-dimensional space [12]. This approach takes account of interactions that occur between tensile and shear stresses in the material and considers the complex nature of fracture that typically occurs in composites.

Both the maximum stress failure criterion and the maximum work failure criterion provided very good descriptions of the tensile strength exhibited by the unidirectionally reinforced composites as a function of θ (Figure 8a). In these calculations, the value of τ (shear strength) was used as an adjustable parameter to fit the data. A value of 28 MPa was found to provide the best fit and agrees well with the previously reported work on the HMU/BSG system [8]. The variation of strength as a function of θ for each of the three mechanisms of the maximum stress

theory is shown along with the prediction of the maximum work theory. It appears from the figure that the good agreement with the maximum strength theory was fortuitous; a composite with a 20° off-axis orientation may not have fit the theory as well. The fit of the angle-ply composite data to the maximum work theory was not as good as that seen in the unidirectionally reinforced composites. Figure II-8b shows the predicted (maximum work) and experimental strengths for both unidirectional and angle-ply reinforced FT700/BSG composites. The ±10° and ±45° angle-ply orientations do not show particularly good agreement with the maximum work prediction. The reason for this lack of agreement in the angle-ply composites is not understood. It may relate to complex interactions and failure mechanisms in these angle-ply FT700/BSG composites that are not accounted for in the maximum work theory.

II.4.3 Tensile Fatigue Behavior

The tensile fatigue behavior of unidirectional and [0/90] reinforced HMU/BSG composites has been evaluated previously [13]. Testing was performed at North Carolina A&T State University on material that was fabricated at UTRC. Samples were tested in a tensile-tensile mode at a frequency of 10 Hz and an R-ratio (maximum stress/minimum stress) of 0.10. All tests where failure did not occur during fatigue were stopped after 10^6 cycles and then uploaded to failure to determine the residual strength after fatigue. Samples were tested at several peak stress levels below and above the PL stress. The results for both unidirectional and [0/90] reinforced HMU/BSG composites are shown in Figures II-9 and II-10. For both composites, runout to 10^6 cycles was observed up to peak stress levels representing about 75-80% of the ultimate tensile strength (as determined via monotonic tensile testing on samples obtained from each composite panel). Above this peak stress level, fatigue failures were observed, with the number of cycles to failure decreasing with increasing peak stress. The residual strength of the samples that experienced runout was equal to or greater than the monotonic tensile strength in every case. This aspect of the fatigue behavior of these materials is not fully understood; however, similar behavior has been observed in other carbon fiber reinforced ceramic matrix composite systems [14].

More recently, evaluation of the tensile-tensile fatigue behavior of pitch carbon fiber reinforced BSG composites has been conducted at UTRC. Specific composite systems under investigation to date have been 0° FT700/BSG and [0/90] P-100/BSG. While not as extensive as the fatigue testing just described for the HMU/BSG system, the initial trends that have been demonstrated are similar to those exhibited by the HMU/BSG composites. Figures II-11 and II-12 illustrate the tensile-tensile fatigue results obtained so far for the two different composites. The same parameters that were described for the HMU/BSG testing were also used for evaluation of the [0/90] P-100/BSG composites. For the 0° FT700/BSG composites, the

frequency was reduced to 0.33 Hz and testing was stopped after reaching 10^5 cycles. (Cycle time was reduced for the FT700/BSG composites to allow for better data acquisition during each cycle.) It is clear from Figure II-11 that the behavior of the 0° FT700/BSG system is similar to that of the HMU/BSG system. Again, runout was observed up to a peak stress level of about 75-80% of the monotonic tensile strength, with higher peak loads resulting in fatigue failures. Residual tensile strength after fatigue was again equal to or greater than the monotonic tensile strength, indicating that fatigue at these peak stress levels was not inducing fiber damage. The behavior of the [0/90] P-100/BSG composite shown in Figure II-12 indicates that similar trends will also be exhibited; additional testing at higher peak stresses will be required to indicate where fatigue failures begin to occur.

The tensile-tensile fatigue behavior of all the C/Glass systems just described indicates that fatigue failures will not be a concern for peak stress levels up to at least 60% of the ultimate tensile strength (for lifetimes of up to 10^6 cycles). The fatigue failures that were observed at higher peak stresses (> 75% of the ultimate tensile strength) are thought to be at least partially related to the statistical nature of fiber tensile strength. As the ultimate composite strength is approached at the higher peak stress levels, weaker fibers in the composite begin to fail, leaving fewer fibers to carry the load. These remaining fibers are then subjected to a higher level of stress, resulting in composite failure at loads below the ultimate (monotonic) tensile strength.

II.4.4 Notch Sensitivity of C/Glass Composites

Another aspect of the performance of C/Glass composites that has been evaluated is the sensitivity of the materials to the presence of a notch, which acts as a stress concentrator during mechanical loading. For elliptical shaped holes oriented with the major axis of the ellipse normal to the direction of the applied stress, the stress concentration factor (K) depends on the degree of elongation of the ellipse [12]. Long flat elliptical holes or cracks that are oriented with the long direction normal to the direction of the applied stress result in very large stress concentration factors at the tip of the notch. When taking into account the smaller load-bearing cross-section resulting from the presence of the notch, materials that are notch insensitive will maintain a constant level of strength irrespective of the value of K. Notch sensitive materials, on the other hand, will show a steady decrease in strength with increasing K (i.e., sharper notches). For the special geometrical case of a circular notch, the stress concentration factor K is 3 at the edge of the hole and is independent of hole diameter. Notch sensitive materials containing circular holes would exhibit a decrease in strength compared to unnotched material. However, unlike the case for elliptical holes, the strength drop would be constant for any size hole since the stress concentration factor is always the same.

To evaluate the degree of notch sensitivity in C/Glass composites, circular holes ranging in diameter from 1.6 mm to 6.5 mm were drilled ultrasonically in the center of [0/90] reinforced tensile samples in the HMU/BSG, FT700/BSG, and P-100/BSG systems. The effect of the notches on the tensile strength of the [0/90] HMU/BSG composites has been reported previously [15]. Figure II-13(a) shows the tensile strength as a function of the ratio of hole diameter to specimen width (d/b) for the HMU/BSG system. The dashed lines on the figure indicate a "scatter band" of strengths that were observed in this material (*i.e.*, all of the observed strengths fall within the scatter band). It is clear that the level of strength in the HMU/BSG system is fairly constant for both unnotched and notched samples, indicating that the composites in this system are notch insensitive. The notch sensitivity of the FT700/BSG and P-100/BSG systems has been investigated more recently. Figure II-14(a) shows the results for the FT700/BSG system. As described for the HMU/BSG system, the strength of the FT700/BSG composites is essentially constant within the scatter band for all the samples, indicating that this system is also notch insensitive. The results for the P-100/BSG system are shown in Figure II-15(a). Unlike the other two systems described previously, the P-100/BSG composites containing circular holes exhibited a decrease in strength (~15-25%) compared to the unnotched material. As expected with circular notches, the degree of strength loss was fairly constant for all of the notched samples. This behavior indicates that the P-100/BSG system is sensitive to the presence of a notch, although the degree of notch sensitivity is not that large (*viz.*, the material still retains at least 75% of its original strength).

The reason for the notch insensitivity observed in the HMU/BSG and FT700/BSG composites is thought to be related to the relatively weak fiber-matrix interfacial bond that exists in these systems. The degree of notch sensitivity in a material is related to the way that the material responds to the concentrated stress field at the notch tip [12]. Mechanisms such as matrix microcracking and fiber-matrix debonding can serve to quickly dissipate the concentrated stress and make the material notch insensitive. Examination of fracture surfaces in the vicinity of the notch in the HMU/BSG and FT700/BSG systems indicated a significant degree of fiber pullout [Figures II-13(b) and II-14(b)], suggesting that the primary means of concentrated stress relief in these composites was via fiber-matrix debonding. The reason for the slight notch sensitivity observed in the P-100/BSG system is unclear, since every other aspect of its mechanical behavior is similar to that of the FT700/BSG system. Adding to the inconsistency is the appearance of the notched P-100/BSG composite fracture surfaces [Figure II-15(b)], which exhibited an amount of fiber pullout very similar to that observed in the FT700/BSG composites.

II.4.5 Compression Behavior

Many types of space structures, such as tubes for satellite trusses, will be loaded primarily in compression. The compression behavior of unidirectional and [0/90] reinforced HMU/BSG,

FT700/BSG, and P-100/BSG composites as determined using the Celanese specimen geometry and test fixture is summarized in Table II-3. (The HMU/BSG composites were tested at Martin Marietta as part of an Air Force/SDIO program to generate mechanical and thermal property data on potential spacecraft structural materials. Complete information can be found in the handbook prepared at the end of the Martin Marietta program [16]). The elastic moduli for all three composite systems agree well with those predicted using a rule-of-mixtures approach. The ultimate compressive strength (UCS) for the HMU/BSG composite is essentially equivalent to the tensile strength exhibited by this system. The high values of the ratio of UCS to UTS as compared to polymer matrix or metal matrix composites is due to the excellent compressive strength of the ceramic matrix, which provides full support for the carbon fibers until they fail either by kinking, bending, or shearing. The lower values of UCS demonstrated by the FT700/BSG and P-100/BSG composites are due to the poor compressive strength of high modulus pitch based carbon fibers that results from the highly oriented radial internal structure of the fiber. Inherent to this structure is a relatively low shear strength between graphite basal planes, which inevitably leads to failure by shear when loaded in compression [17-18]. However, the values of UCS for this system are comparable to P-100 reinforced polymer matrix and metal matrix composites.

Table II-3 - Compression Behavior of HMU/BSG and P-100/BSG Composites

Composite System	Fiber Volume %	Orientation	Number of Samples	Ultimate Compressive Strength (MPa)	Elastic Modulus (GPa)
HMU/BSG	44	0°	4	870 ± 18	147 ± 3
	40	[0/90]	3	600 ± 32	86 ± 8
FT700/BSG	52	0°	3	419 ± 42	391 ± 14
	46	[0/90]	3	215 ± 19	169 ± 16
P-100/BSG	43	0°	3	385 ± 5	356 ± 42
	44	[0/90]	2	230 ± 2	162 ± 7

II.4.6 Cyclic Compression and Compression Fatigue Behavior

Cyclic compression and compression fatigue testing at room temperature was performed on P-100/BSG-2 composites having fiber orientations of either 0° or $(0/+20/0/0/-20/0)_S$.

Unidirectional samples were chosen as the baseline material, while the 0/±θ/0 orientation was selected to compare with the results obtained for thin-walled tubes.that had been compression tested in work reported previously [7]. Samples for both types of testing had a 1.27 cm gage length and were machined from flat panels fabricated using conventional hot-pressing methods.

Cyclic Compression Testing

Cyclic compression testing was performed by loading the composites to successively higher stress levels over a four or five period cycle, with the composite being loaded to failure on the final cycle . A cross-head displacement rate of 0.13 cm/min was used. Each specimen was completely unloaded in-between loading cycles. Figure II-16 contains the compressive stress-strain curves for the first, second and fourth cycles for a unidirectional P-100/BSG-2 composite, while data for all cycles are given in Table II-4. The stress-strain curves indicate that as the load was increased during successive cycles, the area of the hysteresis loop increases, indicating an increase in the amount of energy dissipated in the specimen. Examples of processes that could be responsible for energy dissipation during loading-unloading could be fiber-matrix interfacial sliding or slipping between individual graphite planes within the carbon fiber. A small amount of permanent deformation was introduced into the sample during cycling, indicated by the failure of the loop to close during unloading. As can be seen from the data in Table II-4, no significant change in the elastic modulus of the material was observed during successive loading cycles.

Shown in Figure II-17 is the cyclic stress-strain response for the first, second and fourth cycles on a $(0/+20/0/0/-20/0)_s$ P-100/BSG-2 composite, with the data for all cycles being shown in Table II-4. As in the unidirectional material, the amount of energy dissipated in the multiaxial composite (as measured by the area of the hysteresis loop) increased with increasing load level, a small amount of permanent strain was introduced during cycling, and no change in the elastic modulus was seen during the four successive loading cycles.

Both the unidirectional and the multiaxial reinforced materials were loaded to failure in compression following cyclic compressive testing. Determination of the ultimate compressive properties after cyclic loading showed only a slight deviation in the compressive strength and modulus compared to the monotonic properties. It is interesting that although the cyclic stress-strain curves of Figures II-16 and II-17 represent energy having been dissipated in the composites, this energy did not result in severe degradation of the ultimate compressive properties of either composite. It is believed that the work performed on the composites during cyclical loading induced some damage in the high modulus P-100 fibers by creating shear bands, as described previously. The fact that a slight degradation in the UCS was observed following cyclic testing supports this belief. During successively higher loads, the damage is most likely

increased, but this damage is not manifested in a severe UCS degradation because the matrix still supports the fibers. As discussed later in this report, tensile testing of P-100/BSG-2 samples that were loaded initially in compression showed a significant decrease in the ultimate tensile properties. In this case, the damage to the fibers was not supported by the glass matrix, because the matrix has little strength in tension, and a dramatic drop in composite UTS was observed.

Table II-4 - Cyclic Compression Properties of P-100/BSG-2 Composites

Fiber Orientation	Cycle No.	Maximum Stress (MPa)	E (GPa)
0°	*Monotonic Data*	*366*	*242*
	1	123	249
	2	190	259
	3	248	254
	4	316	261
	UCS	326	257
(0/+20/0/0/-20/0)	*Monotonic Data*	*351*	*308*
	1	82	269
	2	186	260
	3	224	262
	4	261	265
	5	300	260
	UCS	301	259

Compressive Fatigue Testing

Compressive fatigue testing was carried out at a compressive peak stress of 250 MPa (70% of the UCS) an R ratio of 0.1, and a loading frequency of 0.33 Hz. This frequency corresponds to a crosshead displacement of approximately 0.07cm/min for these specimens.

Figure II-18 shows the change in the compressive elastic modulus (measured during loading) with increasing number of cycles for both fiber orientations. The unidirectional

composite shows no decrease in modulus, even after 200,000 cycles. At approximately 208,000 cycles, the sample was uploaded to failure and exhibited a compressive strength of 362 MPa. This compares favorably with the monotonic UCS of 366 MPa for this composite (Table II-4), indicating that compressive fatigue loading did not affect the residual compressive strength of the unidirectionally reinforced material. The multiaxial composite exhibited markedly different behavior. At some point during the first cycle, damage was imparted into the specimen, as evidenced by the sharp decrease in the elastic modulus measured during the second cycle loading. From the second cycle to the 26,000th cycle, the elastic modulus continued to decrease until the composite failed during uploading at 246 MPa.

Insight into the difference in behavior for the two specimens can be found by examining the fracture surfaces seen in Figure II-19. The unidirectional composite (Fig. II-19A) showed no degradation of material compressive properties after 208,000 cycles, and the fracture surface is very similar to monotonic compressive fracture surfaces. The unidirectional fibers show a classic shear failure surface at 45°, typical of P-100/BSG composites. In the case of the $(0/+20/0/0/-20/0)_S$ composite, severe degradation of the compressive strength and modulus resulted from fatigue loading. From Figure II-19B, it is evident that the degradation of the properties was associated with a delamination along the fiber axis in the ±20 direction. The fracture surface indicates fiber-matrix debonding in the off axis plies, while in the 0° fibers, classic shear failure is seen in the high modulus carbon fibers. Further evidence for this damage mode is shown by calculating the properties of a $(0/+20/0/0/-20/0)_S$ composite assuming the ±20° plies do not contribute. In the $(0/+20/0/0/-20/0)_S$ composite, 33% of the reinforcing fiber is in the off-axis direction. A calculated 33% reduction in the monotonic UCS and elastic modulus (Table II-4) gives values of 244 MPa for strength and 191 GPa for modulus. The dashed line in Figure II-19 corresponds to an elastic modulus of 191 GPa. As is seen in the figure, the $(0/+20/0/0/-20/0)_S$ composite modulus decreases during fatigue testing to this value, indicating that contribution to the modulus by the ±20° plies decreases with increasing fatigue. The composite failed at a strength of 246 MPa, which is in good agreement with the calculated value.

Although evident in fatigue testing, fiber-matrix debonding and the associated decrease in composite modulus was not seen in the $(0/+20/0/0/-20/0)_S$ composite panels studied in cyclic compression testing (described previously). This discrepancy is not completely understood at this time.

II.4.7 Reversed Mode Loading Behavior of C/Glass Composites

The effects of reversed mode loading on carbon fiber reinforced borosilicate glass composites was investigated for both unidirectionally reinforced HMU/BSG and P-100/BSG

composites. Reversed mode loading consists of loading a sample in compression to a fixed level (below failure), and subsequently loading the same sample in tension until failure, or, conversely, loading a sample to a fixed level in tension, and subsequently determining the ultimate residual compressive strength. This type of testing is important, as any component in service would most likely be subjected to differing loading conditions.

The HMU/BSG composite samples showed no degradation in mechanical properties as a result of reversed mode loading. Initially, specimens were pre-loaded in tension at levels of 11, 46, and 68% of the UTS of the material (Table II-5). The first two loading levels were below the proportional limit of the composite, with the third level (68%) being slightly above the proportional limit. Subsequent compression testing to failure of these specimens showed no decrease in the UCS (compared to the baseline) regardless of the level of tensile pre-stressing (Table II-5). Pre-loading of samples in compression at levels of 24, 48, and 73% of the UCS followed by subsequent tensile testing to failure revealed no degradation in the UTS or elastic modulus of the composite. In fact, the UTS of the prestressed materials showed an increase of approximately 20% after prestressing in compression (Table II-5).

Table II-5 - Reversed Mode Mechanical Test Results for 0° HMU/BSG-2 Composites

Initial Load (MPa)	Ultimate Load (MPa)	E (GPa)
None (Monotonic test)	589 (UCS)	*
None (Monotonic test)	568 (UTS)	170
63 (tension/11% UTS)	752 (UCS)	190
264 (tension/46% UTS)	641 (UCS)	190
389 (tension/68% UTS)	704 (UCS)	175
142 (compression/24% UCS)	711 (UTS)	168
284 (compression/48% UCS)	697 (UTS)	168
428 (compression/73% UCS)	665 (UTS)	169

Evaluation of P-100/BSG composite specimens indicated a dependance of compressive pre-loading on the residual tensile properties of the material, but not vice versa. Tensile pre-loading was performed at levels of 24 and 46% of the UTS, followed by compressive loading to failure (Table II-6). Both of these loading levels occurred in the linear region of the stress-strain curve. No change in the residual compressive strength of the specimens was observed after tensile pre-loading, although the compressive elastic modulus increased. When specimens were pre-loaded in compression at levels of 28, 43, and 69% of the UCS, a significant decrease in the residual tensile strength was observed. As shown in Table II-6, the UTS of the P-100/BSG-2 materials decreased dramatically after compressive pre-loading compared to the monotonic UTS. However, no change in the residual tensile elastic modulus was observed after compressive pre-loading.

Table II-6 - Reversed Mode Mechanical Test Results for 0° P-100/BSG-2 Composites

Initial Load (MPa)	Ultimate Load (MPa)	E (GPa)
None (Monotonic test)	351 (UCS)	308
None (Monotonic test)	631 (UTS)	319
150 (tension/24% UTS)	334 (UCS)	344
293 (tension/46% UTS)	383 (UCS)	383
97 (compression/28% UTS)	351 (UTS)	333
150 (compression/43% UTS)	293 (UTS)	333
243 (compression/69% UTS)	277 (UTS)	331

When samples were pre-loaded in compression, stress-strain curves showed inelastic behavior. Figure II-20 shows a typical compression stress-strain curve obtained in the longitudinal direction during pre-loading. As can be seen, the curve exhibits hysteresis during the loading-unloading cycle. The hysteresis is thought to be an indication of an energy dissipation process occurring within the material during compressive pre-loading. Examples of

such processes could be fiber-matrix interfacial sliding or slipping between individual graphite planes within the carbon fiber. In both fiber systems, pre-loading to any level of compression prior to tensile testing resulted in this type of stress-strain behaviour, with the area of the curve being dependant on the level of pre-stressing.

The amount of energy dissipation within the composites during compressive pre-loading was calculated based on the area of the compression-stress-strain hysteresis loop and the tested volume of each specimen. The calculated values of energy dissipation occurring within each specimen during compressive loading and unloading is shown in Table II-7. The HMU/BSG system withstood over seventy times (70x) the amount of energy dissipation in the P-100/BSG system without any degradation of the resultant tensile properties. For levels of energy dissipation as low as 2.1 mJ/cm^3, the P-100 fiber composites showed a dramatic decrease in the residual tensile strength, while the HMU fiber system showed no degradation in tensile properties after having over 153 mJ/cm^3 of compressive energy dissipated during pre-loading.

Table II-7 - Energy Dissipated During Compressive Pre-stressing of Composites Studied in Reversed Mode Loading

Composite System	Initial Compressive Load (MPa)	Cross-Sectional Area (10^{-3} cm^2)	Energy Dissipated per Unit Volume (mJ/cm^3)
HMU/BSG-2	142 (24% UCS)	67.7	4.0
	284 (48% UCS)	67.2	34.0
	428 (73% UCS)	67.3	153.8
P-100/BSG-2	97 (28% UCS)	71.1	2.1
	150 (43% UCS)	68.0	19.2
	243 (69% UCS)	69.2	46.9

The explanation of the dramatic differences in the levels of energy that can be dissipated in compressive pre-loading, both with and without degradation to the resultant tensile properties for the two materials can be found in the fibers themselves. As described earlier, HMU fiber has a disordered carbon structure, while P-100 fibers have a highly structured, radial sheet-like

structure. Because of these structural differences, HMU fibers have higher compressive strengths than P-100 fibers. During compressive testing, HMU fibers typically fail in a fiber buckling and kinking mode, requiring great amounts of strain. Pitch-based fibers such as P-100 fail in a classical shear fashion, leaving a 45° angle at the fracture surface. These shear failures require very little strain. PAN based fibers have been reported to have up to ten times the strain to compressive failure of P-100 fibers [18]. For HMU/BSG composites, the fibers respond to the induced strain during compressive loading by buckling or kinking. The glass matrix supports the fibers and prevents failure. In P-100 fiber reinforced materials, the fibers respond to the strain induced during compressive loading by shearing, even at very low loads. Shear bands are introduced into the fiber without completely failing it. Evidence that the fibers have not completely failed is seen in the unchanged tensile modulus measured during the subsequent tensile loading to failure. The shear bands act as defects when loaded in tension, however, leading to a decrease in the residual tensile strength of the specimen after compressive pre-loading. Evidence of shear damage in the fibers is seen in scanning electron micrographs of the tensile fracture surfaces of the pre-stressed specimens. Figure II-21 compares tensile fracture surfaces of monotonic specimens and specimens after compression pre-stressing. In the pre-stressed material, a great many more shear failures are seen in the fibers, evidence of damage induced during the compressive pre-stressing as described above.

The results of cyclic testing and fatigue testing (described previously), together with the results of reversed mode testing combine to demonstrate the various critical functions that the carbon fiber or the glass matrix perform during composite loading. In tensile loading, the fiber controls the ultimate properties of the composite, not the matrix. Composite specimens that have been stressed such that the fibers are damaged (compression loaded), show a dramatic decrease in the tensile properties. During compressive loading, no effect is seen for either pre-tensile or pre-compressive loaded materials. In a compression test, the matrix contributes significantly to the UCS by supporting the fiber such that even specimens with damaged fibers still maintain the UCS of unstressed materials.

II.4.8 High Temperature Behavior

The ability of C/Glass composites to maintain mechanical performance at elevated temperatures in a non-oxidizing atmosphere such as space is dependent on the inherent temperature capability of the glass or glass-ceramic matrix. In order to fully evaluate high temperature composite properties, it is usually necessary to employ both flexural and tensile testing. Flexural testing provides a better indication of matrix integrity at temperature because it provides a means of highly stressing the matrix in shear. Tensile testing furnishes information on fiber strength, elastic modulus, and environmental stability at elevated temperature.

Composites in the HMU/BSG system have been shown to retain their flexural and tensile strength and stiffness in argon and air (for short times) up to a temperature of 560°C, corresponding to softening and relaxation of the BSG matrix [19]. BMAS glass-ceramic matrix composites unidirectionally reinforced with FT700 carbon fiber have demonstrated full retention of flexural strength in argon up to a temperature of 1200°C (Figure II-22). Post-test examination of samples tested at 1200°C indicated that the samples had failed in tension, with no indication of any plastic deformation induced during testing. Higher temperatures result in plastic deformation due to viscous flow of the residual glassy phase that still exists after crystallization of the matrix.

A limited amount of short-time flexural creep testing was performed on samples from the FT700/BMAS system at temperatures ranging from 1000°C to 1200°C in argon to determine the time dependent deformation behavior of this material. Samples were held at constant stress levels of 240 MPa and 480 MPa for one hour at temperature and then examined for signs of plastic deformation. Mid-span deflection was monitored throughout the duration of the test. Table II-8 shows the results of the very limited amount of testing that was performed. Up to a temperature of 1100°C, a stress level of 240 MPa resulted in no permanent deformation after one hour. The higher stress level of 480 MPa resulted in slight deformation after one hour at 1100° and 1200°C, with approximately 0.10 mm and 0.13 mm of permanent mid-span deflection, respectively. These preliminary results suggest that BMAS matrix composites are quite resistant to short-time creep up to 1150°C at moderate stress levels (at least up to 240 MPa). More rigorous evaluation of the creep behavior of these composites is planned for the next phase of the program.

Table II-8 - Flexural Creep Behavior in Argon of 0° FT700/BMAS Composites

Temperature (°C)	Stress Level (MPa)	Mid-Span Deflection* (mm)	Comments
1000	240	0	No deformation
1100	240	0	No deformation
1100	480	0.10	Slightly deformed
1150	240	0	No deformation
1200	480	0.12	Slightly deformed

* After one hour at temperature

As stated previously, it is clear that under inert atmosphere conditions composite failure is solely a function of the temperature capability of the matrix. Under oxidizing conditions, however, oxidation of the carbon fiber becomes an issue. In a previous study, strength loss in unstressed unidirectionally reinforced HMU/BSG composites became noticeable after approximately 100 hours at temperatures above 450°C [20]. Under applied stress, strength degradation was found to take place more rapidly. Factors affecting the rate of strength loss are numerous, but consist mainly of the level of applied stress, specimen geometry, and fiber architecture within the composite. The primary mechanism for strength loss was found to be oxidation of carbon fiber in a direction normal to the fiber direction, *i.e.* oxidation from the sides and faces of the composite. The effective load-bearing cross-section of the composite became gradually smaller as oxidation progressed. More recent work at UTRC has shown that fiber coatings can significantly reduce the transverse oxidation rate in HMU/BSG composites at a temperature of 450°C, which translates to slower rate of strength loss.

Higher temperature oxidation behavior under stress (stress rupture) has recently been evaluated for 0° reinforced FT700/BMAS composites. Prior to the stress rupture evaluation, the inherent flexural strength of the material in argon at 800°C was determined to be 1170 MPa. Samples were then loaded in a 3-point flexural configuration and held at constant stress levels of 172, 345, 517, and 690 MPa in air at a temperature of 800°C until failure. Each sample that was evaluated had a thickness of approximately 1.8 mm and had been machined only along the longer edge faces. The time to failure at each stress level is shown graphically in Figure II-24. It is clear that the time to failure decreases with an increasing level of applied stress. This was the expected trend based on the strength degradation mechanism previously described for the HMU/BSG system. A similar oxidation mode was observed in the FT700/BMAS samples, *i.e.* transverse oxidation was the primary mechanism of strength degradation. The fact that the composites could last for more than one hour at 800°C at stress levels up to 345 MPa was thought to be fairly remarkable. This suggests that these materials may be candidates for limited life applications such as missile components. Samples with a larger cross-section or containing coated fiber could be expected to exhibit even longer life under similar loading conditions.

II.5. THERMOPHYSICAL PROPERTIES

II.5.1 Thermal Expansion

A requirement of nearly all space structures is that they exhibit low values of thermal expansion and a high level of dimensional stability so that any change in dimension due to temperature fluctuations during orbit is minimized. Because of the low coefficient of thermal

expansion (CTE) values of carbon fiber and the glass matrices, C/Glass composites offer the potential of obtaining extreme dimensional stability and a near-zero CTE over a wide temperature range.. Since carbon fiber has a negative axial CTE (up to a temperature of 400 to 500°C), a resultant in-plane composite CTE of very close to zero is achievable by combining the fibers with a matrix which has a positive CTE, such as glass. Through control of fiber orientation and fiber content, it is possible to tailor thermal expansion behavior to achieve composites whose in-plane CTE is nearly zero over a wide temperature range. Figure II-25 shows the in-plane thermal strain as a function of temperature for a quasi-isotropic [0/±60°] reinforced HMU/BSG composite over the temperature range of interest for most space applications (-150°C to +100°C). The curve is essentially flat over the entire temperature range, indicating a near-zero CTE, with less than 15×10^{-6} cm/cm hysteresis over the entire thermal cycle. This exceptional combination of near-zero CTE and extreme dimensional stability makes HMU/BSG composites potential candidates to replace monolithic glasses and polymer matrix composites for large space based mirrors and optical structures [21].

The thermal expansion behavior of C/Glass composites containing high modulus pitch-based carbon fibers has also been characterized since these materials will be necessary for stiffness-critical applications in space. The thermal strain behavior of unidirectionally reinforced P-100/BSG and FT700/BSG composites is characterized by closed hysteresis loops and shows similar levels of hysteresis as that of the HMU/BSG composite described above, with values of less than 25×10^{-6} cm/cm over the entire thermal cycle (Figure II-26). The more negative axial CTE for the high modulus pitch based fibers results in composite CTE's being more negative than those of HMU-reinforced composites, varying from approximately -1.1 to -0.75×10^{-6} cm/cm K over the temperature range of -150°C to +100°C. This compares with a CTE range of -0.5 to -0.25×10^{-6} cm/cm K for unidirectionally reinforced HMU/BSG composites of similar fiber content (Figure II-27). Even though these ranges of composite CTE for the P-100/BSG and FT700/BSG composites are somewhat negative, they still fall within an acceptable CTE window for many space-related structures. As an example, many satellite truss structures require high stiffness materials with CTE's that can vary from -1.4 to $+1.4 \times 10^{-6}$ cm/cm K over the temperature range of -150 to +100°C [10]. Unidirectionally reinforced P-100/BSG and FT700/BSG composites definitely satisfy both of these criteria.

The in-plane CTE of P-100/BSG and FT700/BSG composites can be brought closer to zero by going to an angle-ply configuration in a similar manner as the HMU/BSG composite described previously. However, going to the off-axis orientation required for zero CTE drastically reduces the in-plane elastic modulus, thereby defeating the original purpose for using the high modulus fiber. Preserving high composite stiffness is imperative for many space-based structures. One means of achieving this combination of high stiffness and near-zero CTE that

has been developed at UTRC is to incorporate a second high modulus fiber with a positive CTE into the composite microstructure [22]. Boron and silicon carbide monofilaments have both been successfully combined with P-100 fiber to create a dual fiber reinforced glass matrix composite possessing a combination of high elastic modulus and near-zero CTE. Figure II-27 shows the CTE as a function of temperature for one of these dual fiber reinforced glass matrix composites along with the CTE curves for a P-100/BSG and a HMU/BSG composite. This is a good example of the remarkable tailorability afforded by the wide variety of fibers that can be used for fiber reinforced glass matrix composites.

II.5.2 Thermal Conductivity

One of the unique characteristics of carbon fiber is the extremely high thermal conductivity that exists along the direction of the fiber. The fiber data summarized earlier in Table II-1 includes information on axial thermal conductivity. Thermal conductivity is another property that is strongly dependent on the internal microstructure of the fiber, with the two most important factors being crystallite size and the degree of crystallite orientation [1]. It can be seen in the table that the ultra-high modulus pitch based carbon fibers approach or exceed the thermal conductivity of copper (400 W/m K). In fact, a carbon fiber under development at Amoco Performance Products (K1100X) for the Navy exhibits an axial thermal conductivity nearly three times that of copper (1030-1100 W/m K).

Power generation systems in space will require the expulsion of waste heat, typically envisioned as being accomplished through a system of high thermal conductivity radiator fins [23-24]. C/Glass composites have been identified as a candidate material for radiator fins because of their high strength and stiffness, inherent space environmental durability, thin-gage fabrication capability, and the potential for high in-plane thermal conductivity (the trade study will be described in a subsequent section of this report). To demonstrate the potential of glass matrix composites containing the very highest thermal conductivity carbon fiber, unidirectionally reinforced K1100X/BSG composites were fabricated and tested. Samples of K1100X fiber were supplied to UTRC by Amoco Performance Products at the request of the Naval Surface Warfare Center. The unusual structure of the K1100X fiber can be seen in Figure II-28, which shows a picture of the composite microstructure. The split "Pac-Man" structure is prevalent in the majority of the fibers and arises during fiber manufacture due to thermal stresses generated in the fiber during cooling. Despite the split fiber structure, the tensile stress-strain behavior of the K1100X/BSG composite was very similar to that of P-100/BSG composites described in a previous section. The non-linear shape of the stress-strain curve (Figure II-29) was nearly identical to that shown in Figure II-3 for P-100/BSG, with values of tensile strength ranging from 470 to 515 MPa and the elastic modulus being in the range of 360 GPa for a composite containing 41 volume % fiber. The degree of fiber pullout observed on the fracture surface of

the K1100X/BSG composite is considerably greater than that typically observed in a P-100/BSG composite, presumably indicating comparable or even higher toughness. The difference is thought to be related to the more highly aligned fiber structure which results in significant shearing of the fiber during composite tensile fracture.

The thermal conductivity characteristics of several C/Glass composites was assessed in the in-plane fiber direction and the through-thickness direction using a laser flash technique. Composites evaluated were [0/90] reinforced HMU/BSG, 0° reinforced P-100/BSG, and 0° reinforced K1100X/BSG. Figure II-30 shows the results of the measured in-plane thermal conductivities as a function of temperature as well as the calculated room temperature conductivities for the three composites. The calculated values were obtained using a standard rule-of-mixtures approach. For the HMU/BSG composite, the agreement between the measured and calculated values is excellent. However, the measured values for the P-100/BSG and K1100X/BSG composites are only about 75-80% of the theoretical values, suggesting that some damage may have occurred to these high modulus fibers during fabrication. With respect to the measured thermal conductivities, of note is that the specific in-plane thermal conductivity (thermal conductivity/density) of the P-100/BSG composite is approximately twice the specific thermal conductivity of copper. Also measured was the through-thickness thermal conductivity, which was predictably quite low (2 W/m K) due to the insulating qualities of the glass matrix.

II.6. SPACE ENVIRONMENTAL DURABILITY

One of the most crucial requirements of materials to be utilized in space-based applications is that they be resistant to the rigors of the space environment. Atomic oxygen, micrometeoroids and orbital debris, solar radiation, and thermal cycling are but a few of the environmental factors that can seriously damage materials in space. The effects of atomic oxygen (AO) on carbon-containing materials in space can be especially severe. Erosion due to AO is a line-of-sight process, meaning that only material that is directly impinged by AO is affected. AO species are highly energetic and rapidly react with oxidizable materials, especially those that are carbon-based, in the temperature regime of the space environment. Analysis of carbon fiber reinforced polymer materials that have been exposed in low earth orbit has revealed that AO attack leads to significant erosion of both the epoxy matrix and the carbon fibers [25], with the formation of a cone-like surface morphology resulting from the release of volatile oxidation products. Most metal and ceramic materials have shown extreme stability when exposed to similar conditions, with erosion yields of less than 0.02×10^{-24} cm^3/atom compared with erosion yields greater than 1×10^{-24} cm^3/atom for carbon and polymer-based materials [25].

C/Glass composites were exposed to the space environment for a period of nearly 6 years aboard the Long Duration Exposure Facility (LDEF) satellite. The LDEF satellite was placed in low earth orbit by the shuttle orbiter Challenger in April of 1984 and was retrieved by the shuttle orbiter Columbia in January of 1990. The LDEF satellite was situated in a stable orbit with the cylindrical axis Earth pointing and the same edge always facing in the direction of the velocity vector. The purpose of the experiment was to expose potential spacecraft and satellite materials to the space environment in a controlled fashion, such that materials placed in a "leading edge" or "trailing edge" orientation would remain that way for the duration of the experiment. C/Glass composite materials were located in both leading edge (Row 8) and trailing edge (Row 4) positions, with end-of-mission AO fluences for those positions being 6.93×10^{21} atoms/cm^2 and 9.32×10^4 atoms/cm^2, respectively.

Analysis of the C/Glass composites, performed at UTRC under corporate funding, indicated that they experienced negligible weight loss resulting from fiber erosion, with no change in flexural strength or thermal expansion behavior [26]. Figure II-31 shows optical micrographs of a polished cross-section of a C/Glass composite that was exposed on the leading edge (Row 8) of LDEF. A coating of nickel was deposited on the surface of the composite prior to sectioning and polishing to fill in and decorate any voids present due to carbon fiber that had been eroded away by AO. The micrographs clearly show that only fiber that was exposed at the surface of the samples (due to polishing) was eroded away, with the glass matrix providing excellent protection for interior fibers. In fact, even fibers near the surface that were covered by only a thin layer (< 5 μm) of glass were fully intact following exposure. This inherent resistance to the effects of AO suggests that C/Glass composites will not require additional protective measures, such as coatings, making them very attractive for space applications requiring long-term durability.

II.7. SUMMARY

Carbon fiber reinforced glass matrix composites have been developed which exhibit an outstanding combination of mechanical performance, high temperature capability, low density, near-zero thermal expansion, dimensional stability, and space environmental durability. The ability to choose from different fibers, a variety of matrices, and different ply orientations affords a remarkable degree of tailorability to these C/Glass composite materials. These attributes combine to make C/Glass composites an excellent candidate for many space-based structural applications.

REFERENCES

1. W. Johnson, "The Structure of PAN Based Carbon Fibres and Relationship to Physical Properties"; pp. 389-473 in *Handbook of Composites, Volume 1 - Strong Fibres.* Edited by W. Watt and B. V. Perov. Elsevier Science Publishers B. V., Amsterdam, 1985.

2. B. Rand, "Carbon Fibres from Mesophase Pitch"; pp. 495-575 in *ibid.*.

3. W. K. Tredway, K. M. Prewo and C. G. Pantano, "Fiber-Matrix Interfacial Effects in Carbon Fiber Reinforced Glass Matrix Composites," *Carbon*, **27** (1989) 717-727.

4. W. K. Tredway, C. G. Pantano and G. Chen, "Influence of Matrix Wetting on The Fiber-Matrix Interfacial Strength and Subsequent Performance of Carbon Fiber Reinforced Glass Composites," presented at the 93rd Annual Meeting of the American Ceramic Society, Cincinnati, OH, April 28-May 2, 1991.

5. K. M. Prewo, J. J. Brennan and G. K. Layden, "Fiber Reinforced Glasses and Glass-Ceramics for High Performance Applications," *Am. Ceram. Soc. Bull.*, **65** (1986) 305-313.

6. J. J. Brennan, "Glass and Glass-Ceramic Matrix Composites"; pp. 222-259 in *Fiber Reinforced Ceramic Composites: Materials, Processing and Technology.* Edited by K. S. Mazdiyasni. Noyes Publications, Park Ridge, New Jersey, 1990.

7. W. K. Tredway and P. H. McCluskey, "Compression Testing of Continuous P-100 Fiber Reinforced Glass Matrix Composite Tubes," UTRC Contract Report R91-917981-1, Office of Naval Research Contract N00014-89-C-0046, October 1, 1991.

8. V. C. Nardone and K. M. Prewo, "Tensile Performance of Carbon-Fibre-Reinforced Glass," *J. Mater. Sci.*, **23** (1988) 168-180.

9. R. Y. Kim and N. J. Pagano, "Crack Initiation in Unidirectional Brittle-Matrix Composites," *J. Am. Ceram. Soc.*, **74** (1991) 1082-1090.

10. D. Volk, C. F. Yen and K. Buesking, "Structural Development of Fiber Reinforced Glass Matrix Composites," Materials Sciences Corporation Contract Report MSC TFR 2112/8601, Office of Naval Research Contract N00014-89-C-0211, June, 1990.

11. W. K. Tredway and K. M. Prewo, "Carbon Fiber Reinforced Glass Matrix Composites for Structural Space Based Applications," UTRC Contract Report R89-917704-1, Office of Naval Research Contract N00014-85-C-0332, July 31, 1989.

12. D. Hull, *An Introduction to Composite Materials*, Cambridge University Press, Cambridge, Great Britain, 1981.

13. V. S. Avva, North Carolina A&T State University, 1987, personal communication.

14. J. W. Holmes, University of Michigan, 1991, personal communication.

15. W. K. Tredway and K. M. Prewo, "Carbon Fiber Reinforced Glass Matrix Composites for Space Based Applications," UTRC Contract Report R87-917470-1, Office of Naval Research Contract N00014-85-C-0332, August 30, 1987.

16. *SDS Spacecraft Structural Composite Materials Selection Guide*, prepared by Ketema, Inc., Composite Materials Division, for WPD L502, AFWAL, Materials Laboratory, WPAFB, May, 1989.

17. J. M. Prandy and H. T. Hahn, "Compressive Strength of Carbon Fibers," *SAMPE Quart.*, **22** (1991) 47-52.

18. M. G. Dobb, D. J. Johnson and C. R. Park, "Compressional Behaviour of Carbon Fibers," *J. Mater. Sci.*, **25** (1990) 829-834.

19. K. M. Prewo, "Carbon Fibre Reinforced Glass Matrix Composite Tension and Flexure Properties," *J. Mater. Sci.*, **23** (1988) 2745-2752.

20. K. M. Prewo and J. A. Batt, "The Oxidative Stability of Carbon Fibre Reinforced Glass-Matrix Composites," *J. Mater. Sci.*, **23** (1988) 523-527.

21. K. M. Prewo and E. Minford, "Thermally Stable Composite (TSC™) - Graphite Fiber Reinforced Glass for Dimensionally Stable Applications," Proc. of SPIE, Vol. 505, *Advances in Optical Materials*, San Diego, California, August, 1984, pp. 188-191.

22. W. K. Tredway and K. M. Prewo, "Development of Dual Fiber Reinforced Glass Matrix Composites for Structural Space Based Applications," UTRC Contract Report R90-917886-1, Office of Naval Research Contract N00014-88-C-0251, May 31, 1990.

23. T. Mahefkey, "Thermal Management Issues and Technology Needs for SDI," *AIAA 22nd Thermophysics Conference*, Honolulu, Hawaii, 1987, Paper AIAA-87-1478.

24. A. Choudhury and G. Peterson, "A Review of Advanced Radiator Technologies for Spacecraft Thermal Control," *AIAA/ASME 5th Joint Thermophysics and Heat Transfer Conference*, Seattle, WA, 1990, Paper AIAA 90-1706.

25. B. A. Banks, et al., "Atomic Oxygen Effects on Materials," *NASA/SDIO Space Environmental Effects on Materials Workshop*, Hampton, VA, 1988, NASA CP-3035, pp. 197-239.

26. W. K. Tredway and K. M. Prewo, "Analysis of the Effect of Space Environmental Exposure on Carbon Fiber Reinforced Glass," UTRC Internal Report R91-112542-4, May 31, 1991.

Figure II-1 (a). Structure of Hercules HMU Carbon Fiber

Figure II-1 (b). Structure of Amoco P-100 Carbon Fiber

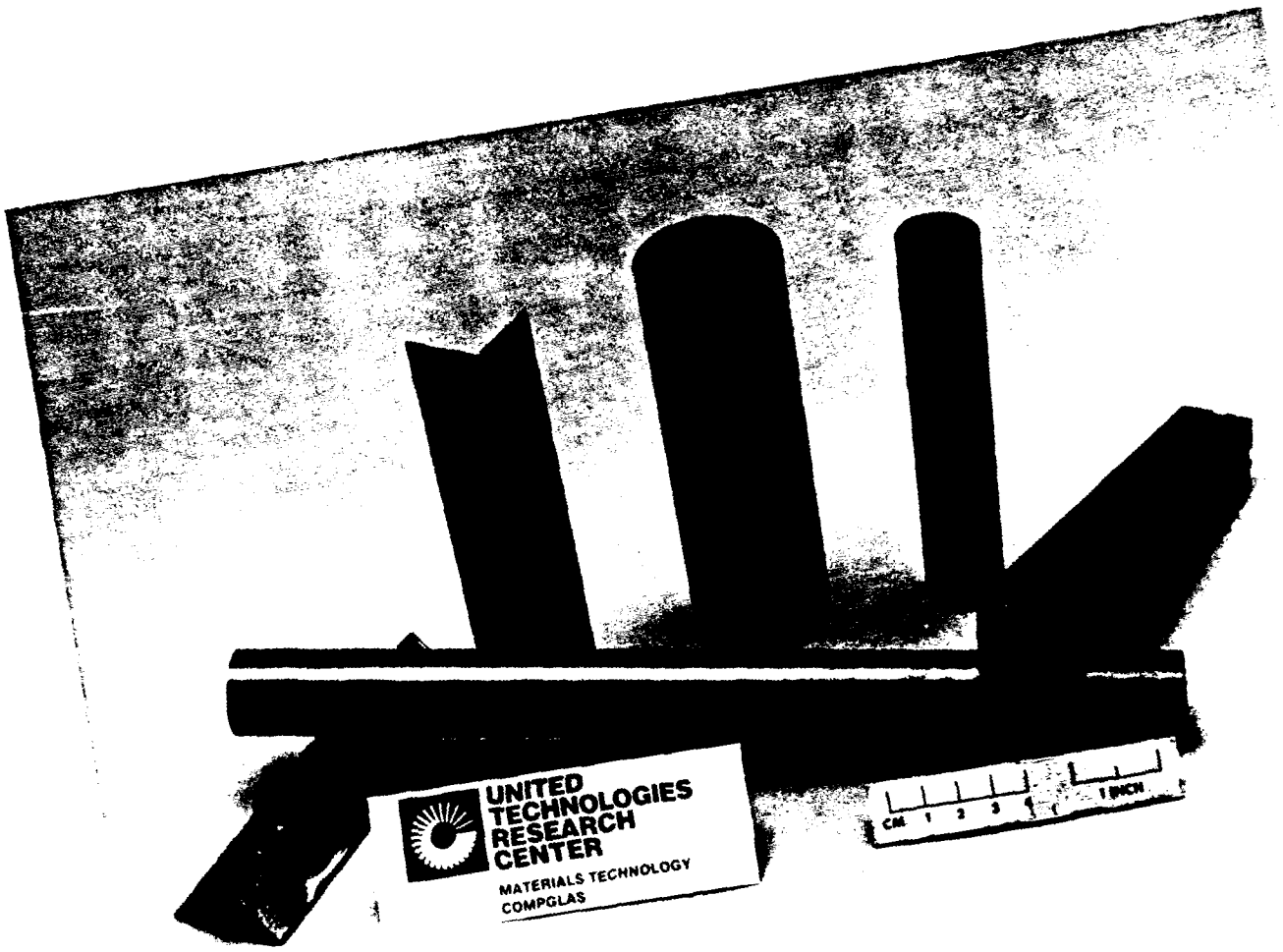

Figure II-2. Carbon Fiber Reinforced Glass Components Fabricated Using Hot Isostatic Pressing (HIP)

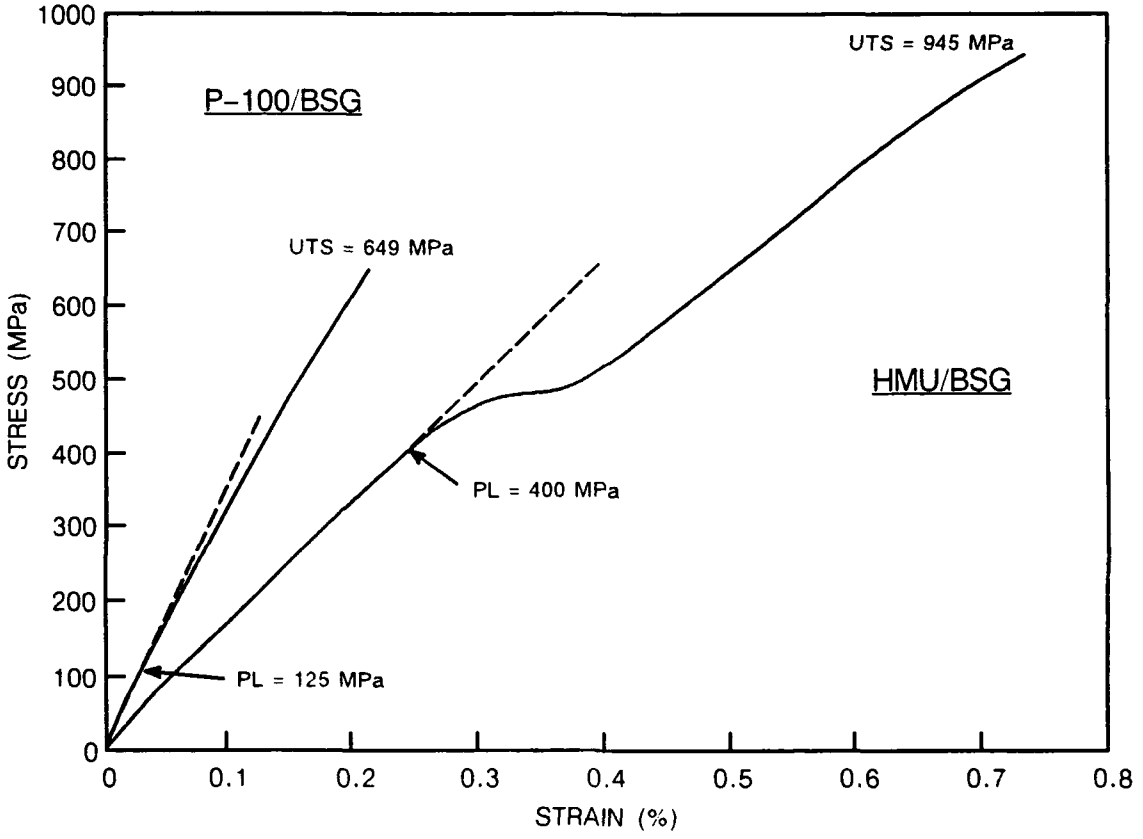

Figure II-3. Tensile Stress-Strain Behavior of 0° Reinforced P-100/BSG and HMU/BSG Composites

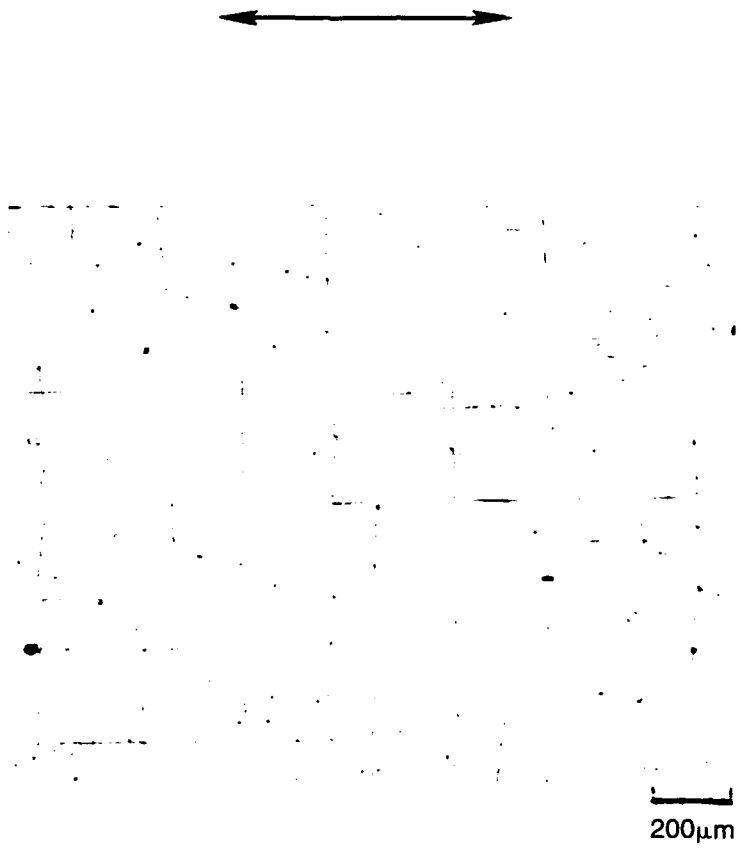

Figure II-4. Replica of the Surface of a 0°-Reinforced P-100/BSG Composite Showing Matrix Microcracks Formed Due to Thermal Residual Stress. The Arrow Indicates the Fiber Direction.

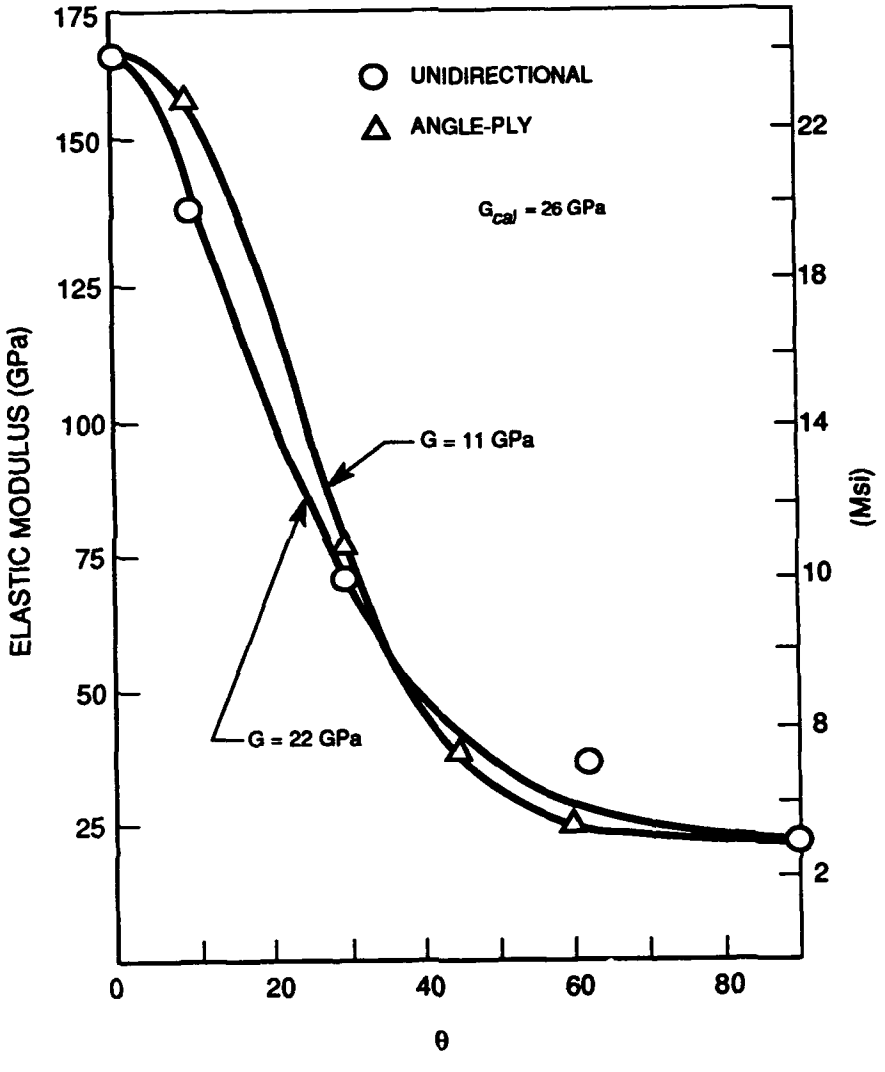

Figure II-5. Comparison of Measured and Calculated Elastic Modulus Values for Unidirectional and Angle-Ply 43 v/o HMU/BSG Composites

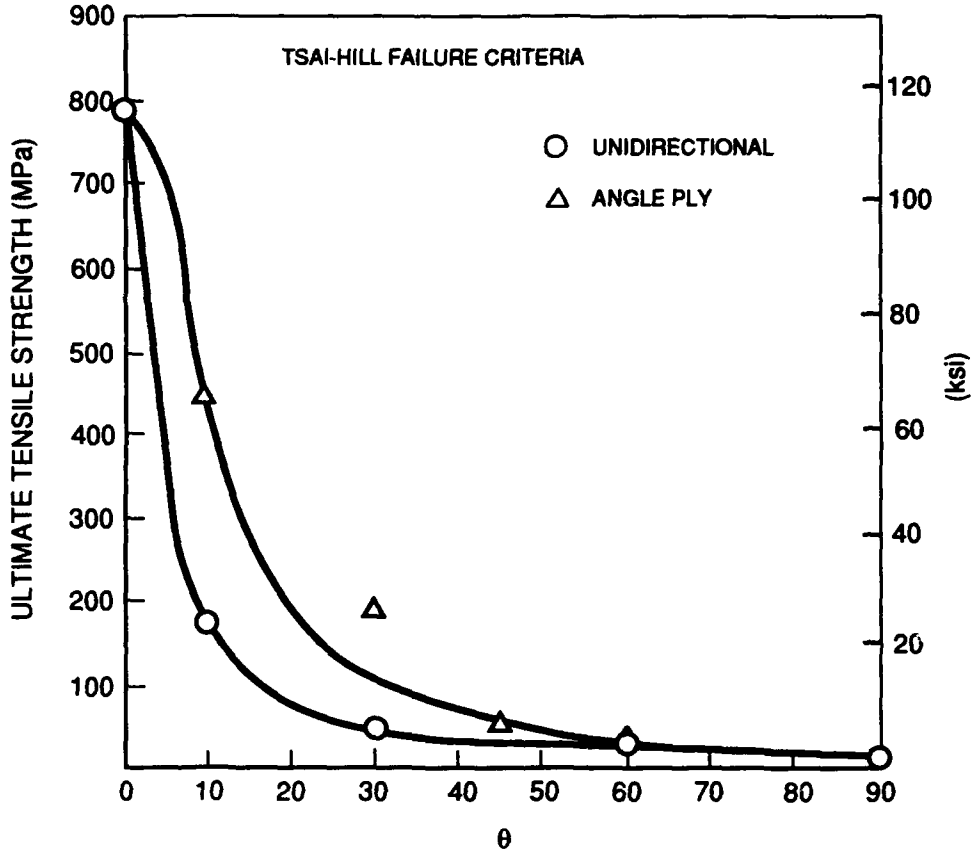

Figure II-6. Comparison of Measured and Predicted Strength of Unidirectional and Angle-Ply 43 v/o HMU/BSG Composites

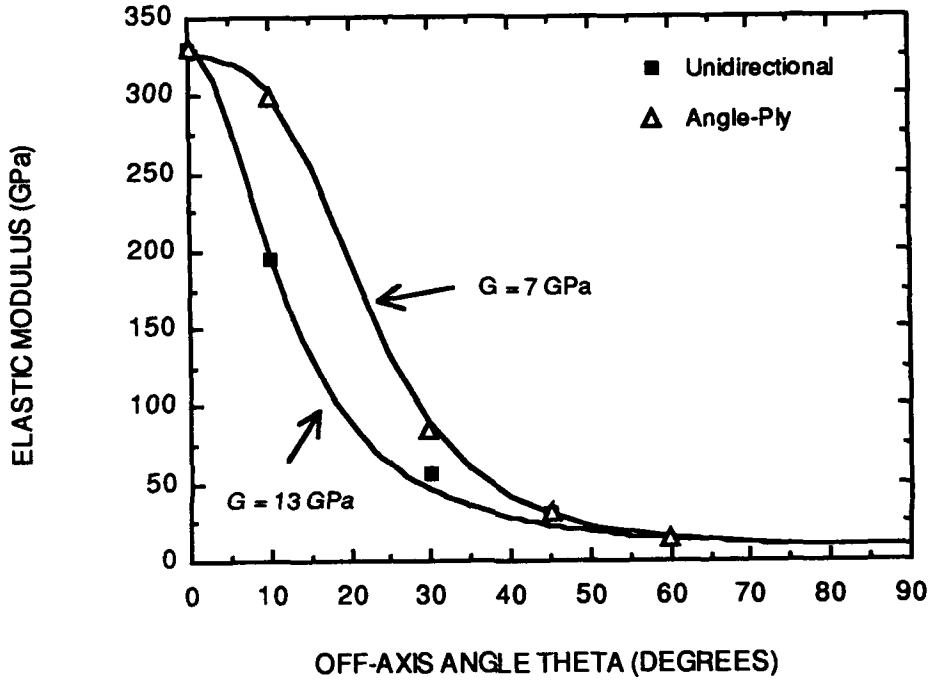

Figure II-7. Comparison of Measured and Predicted Elastic Modulus of Unidirectional and Angle-Ply FT700/BSG Composites

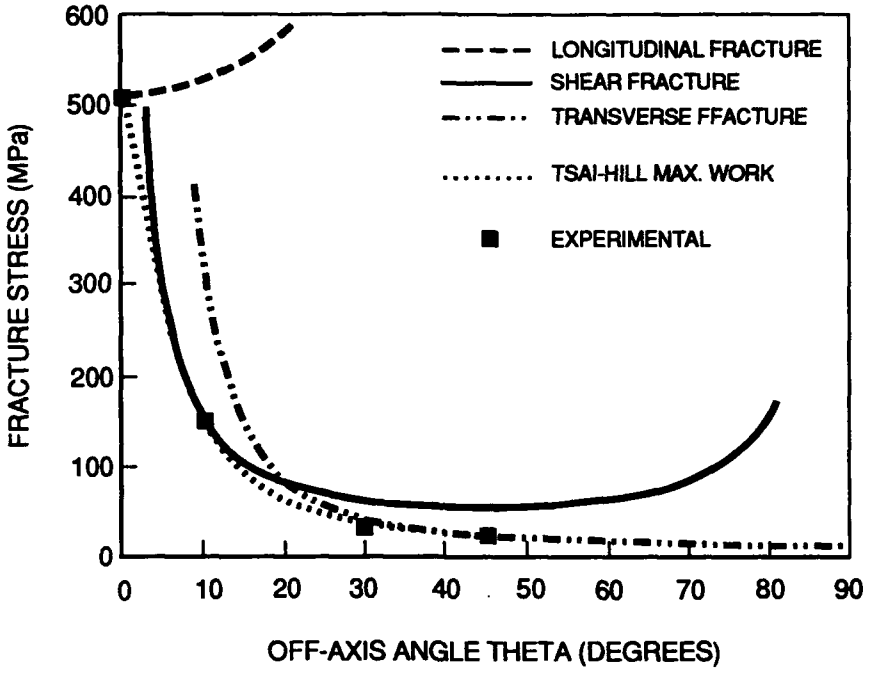

Figure II-8a. Comparison of Measured and Predicted Strength of Unidirectional FT700/BSG Composite

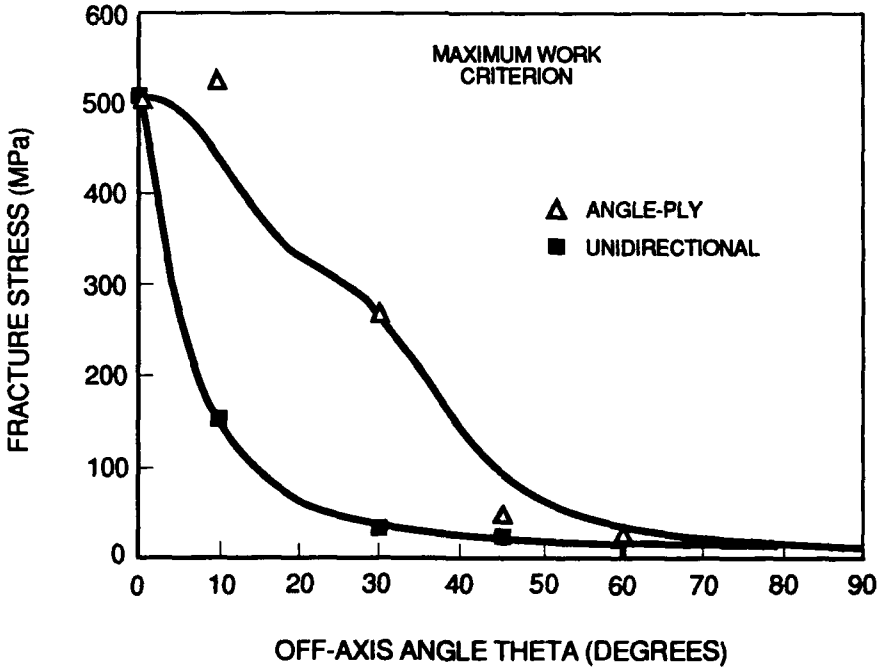

Figure II-8b. Comparison of Measured and Predicted Strength of Unidirectional and Angle-Ply FT700/BSG Composites Using Maximum Work Criterion

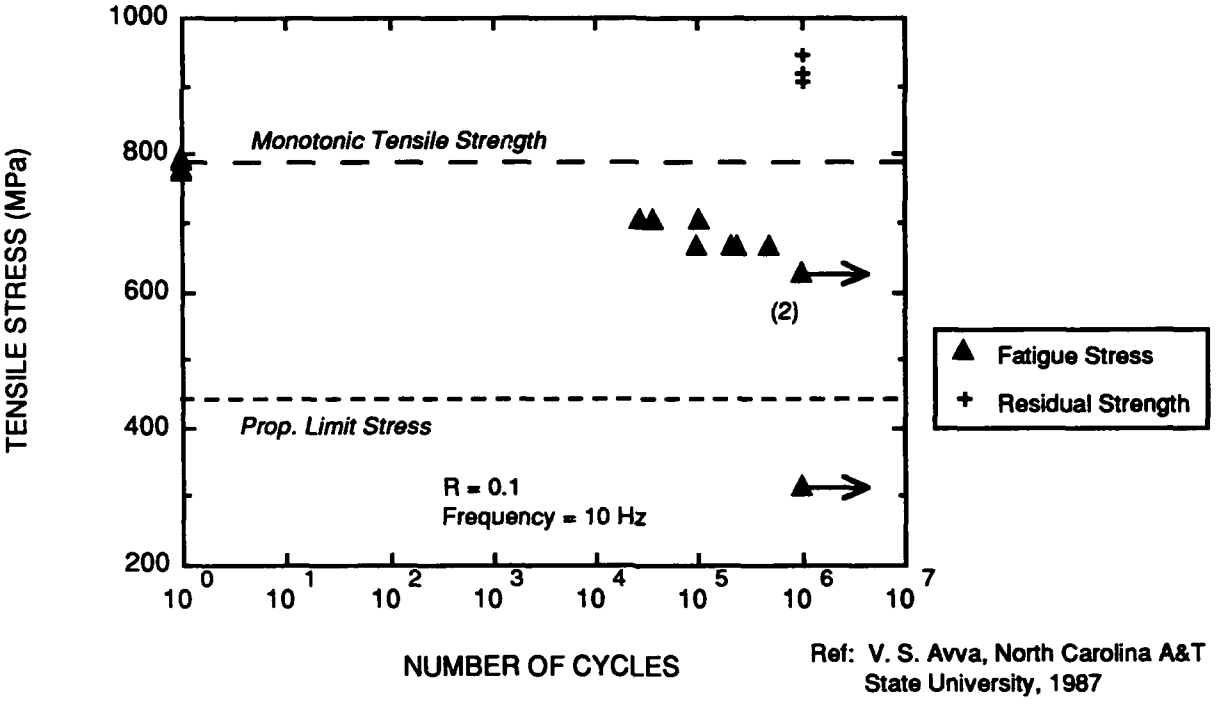

Figure II-9. Tensile Fatigue Behavior of Unidirectional HMU/BSG Composites

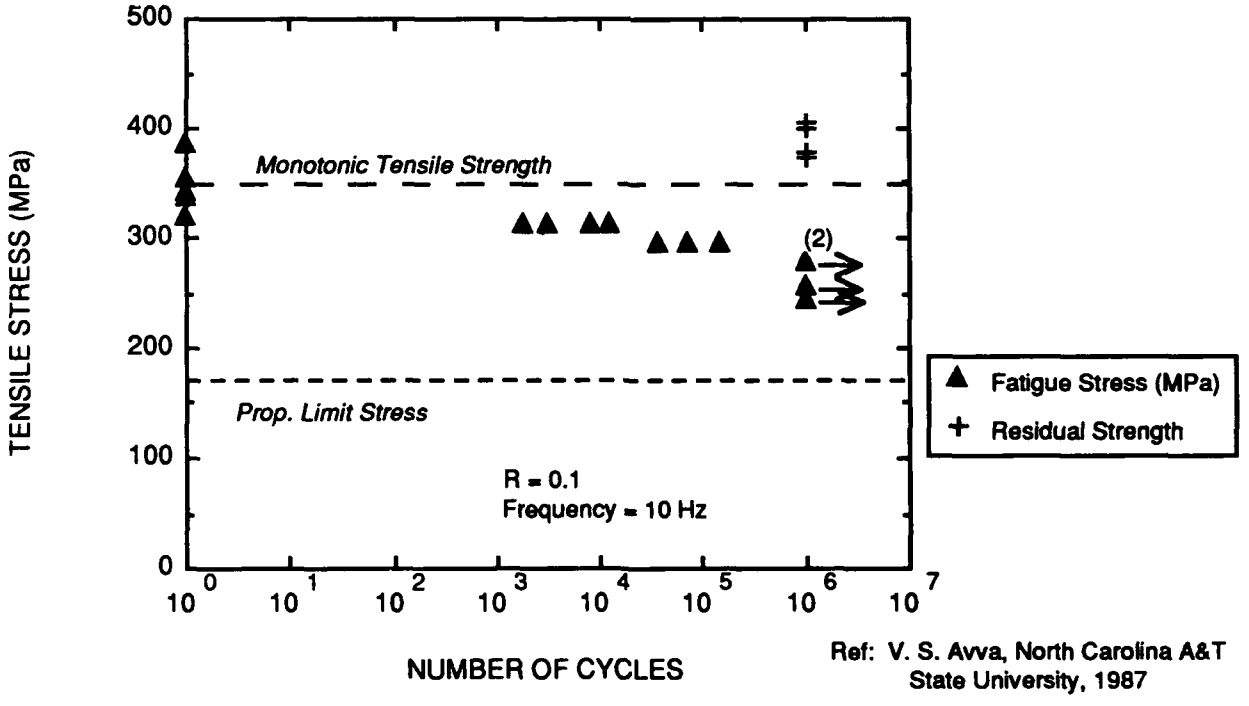

Figure II-10. Tensile Fatigue Behavior of [0/90] HMU/BSG Composites

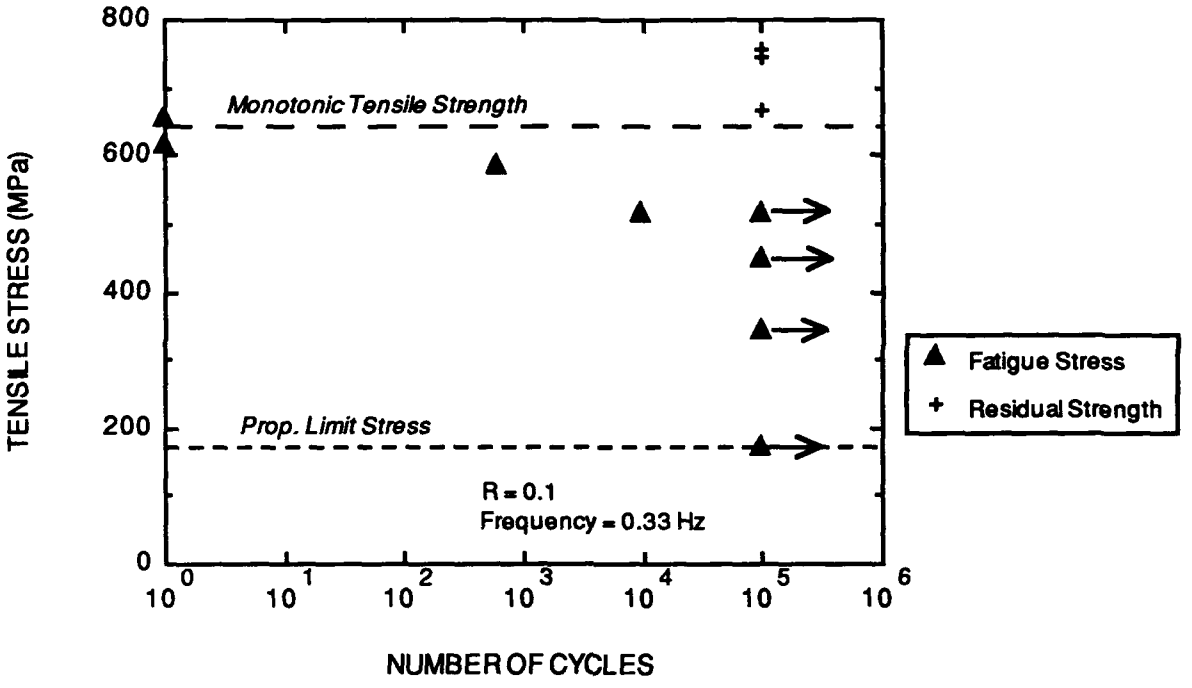

Figure II-11. Tensile Fatigue Behavior of Unidirectional FT700/BSG Composites

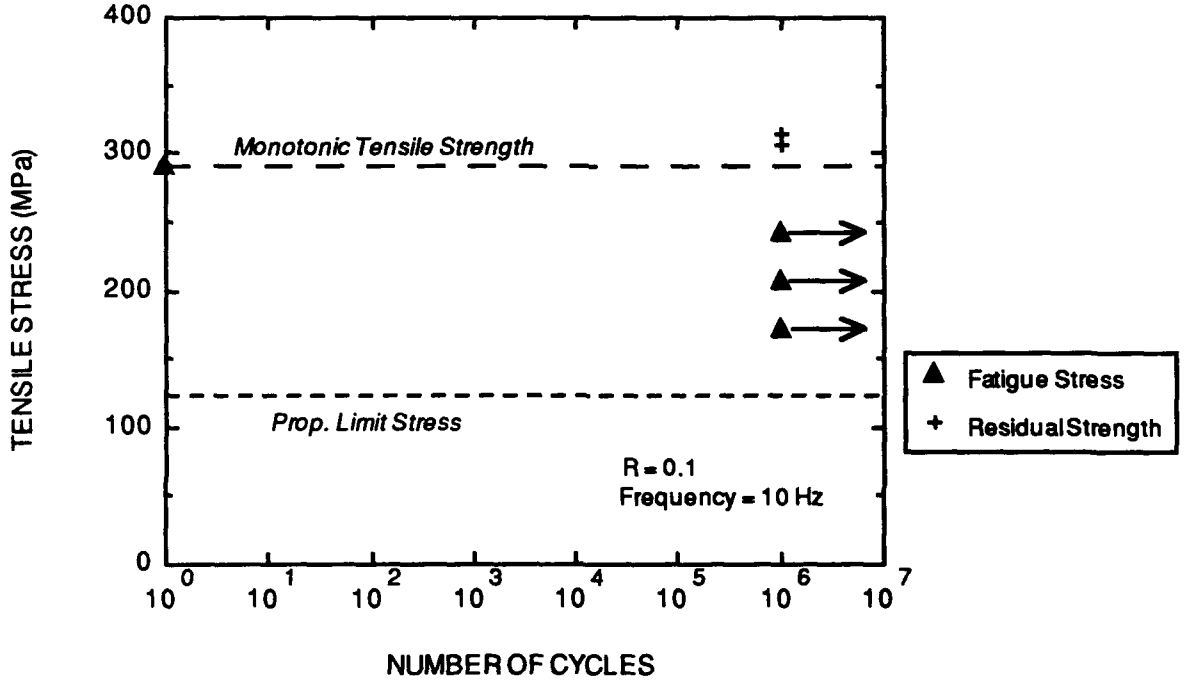

Figure II-12. Tensile Fatigue Behavior of [0/90] P-100/BSG Composites

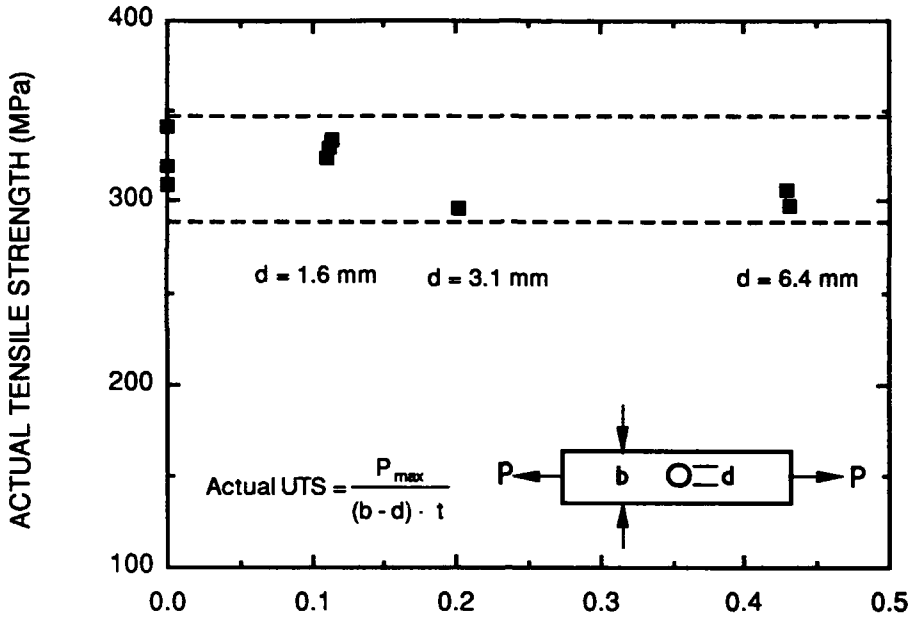

(a)

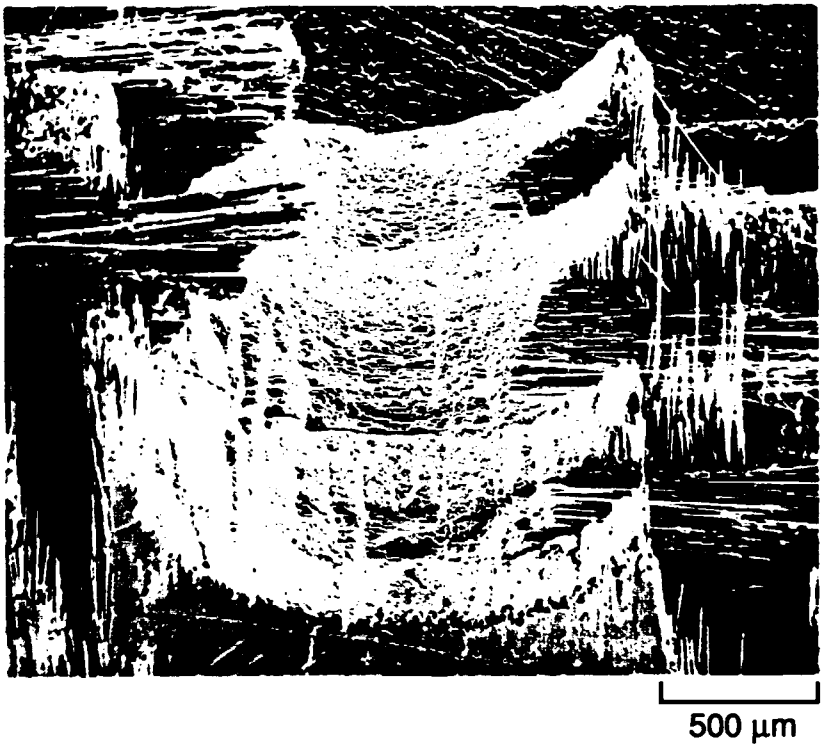

(b)

Figure II-13. (a) Tensile Strength of [0/90] HMU/BSG Composites Containing Circular Holes of Various Diameters. (b) Fracture Surface in the Vicinity of the Notch for a [0/90] HMU/BSG Composite.

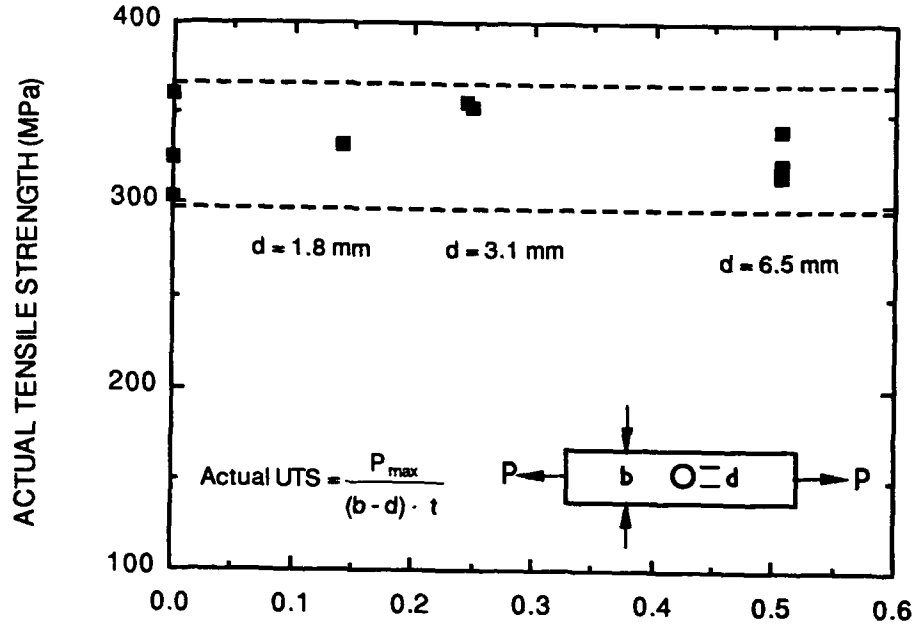

(a)

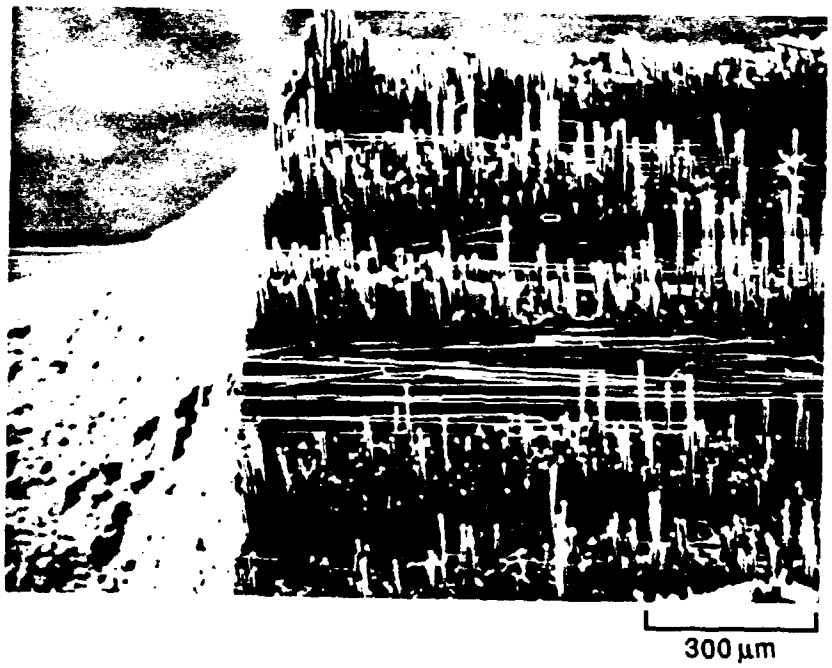

(b)

Figure II-14. (a) Tensile Strength of [0/90] FT700/BSG Composites Containing Circular Holes of Various Diameters. (b) Fracture Surface in the Vicinity of the Notch for a [0/90] FT700/BSG Composite.

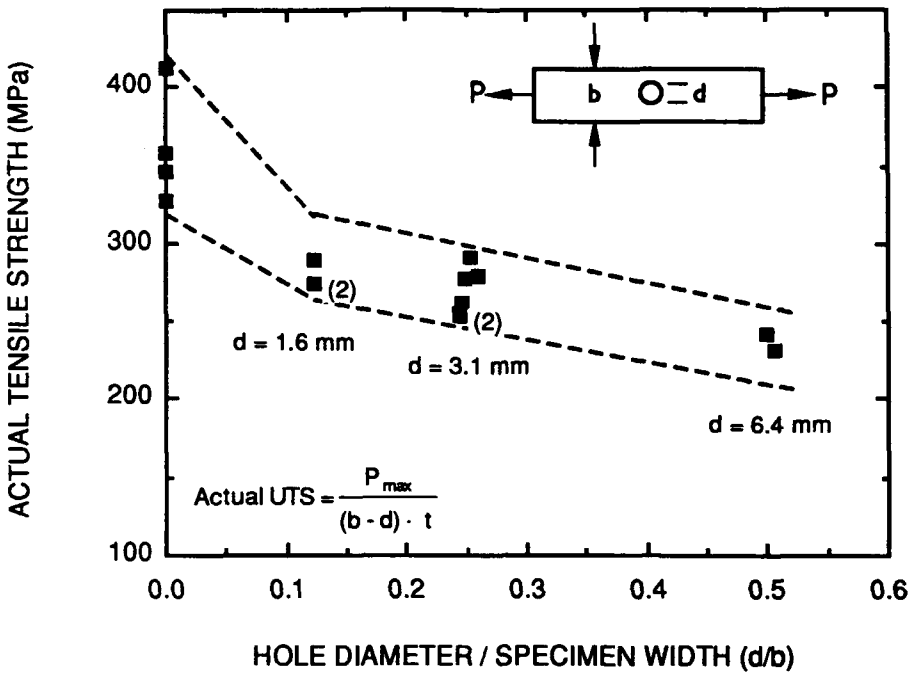

(a)

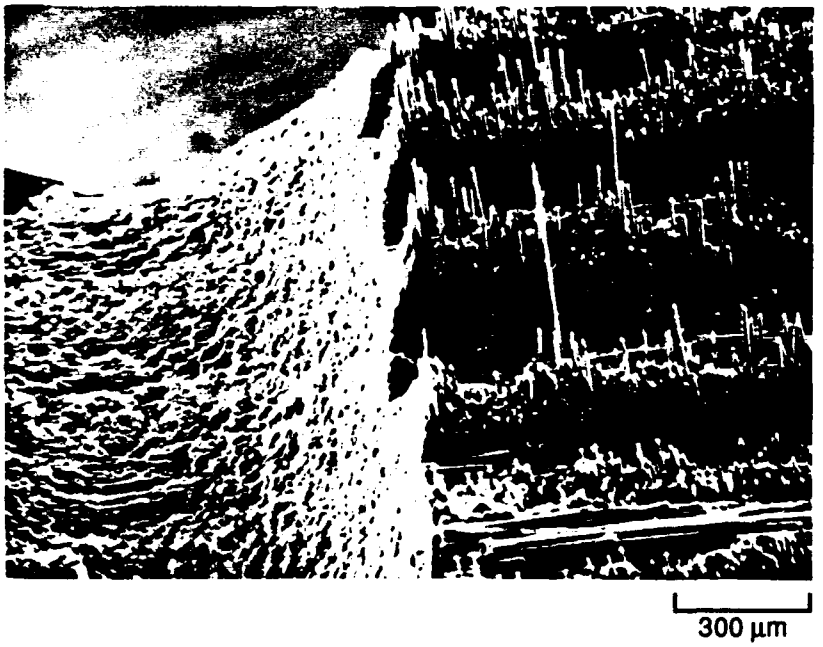

(b)

Figure II-15. (a) Tensile Strength of [0/90] P-100/BSG Composites Containing Circular Holes of Various Diameters. (b) Fracture Surface in the Vicinity of the Notch for a [0/90] P-100/BSG Composite.

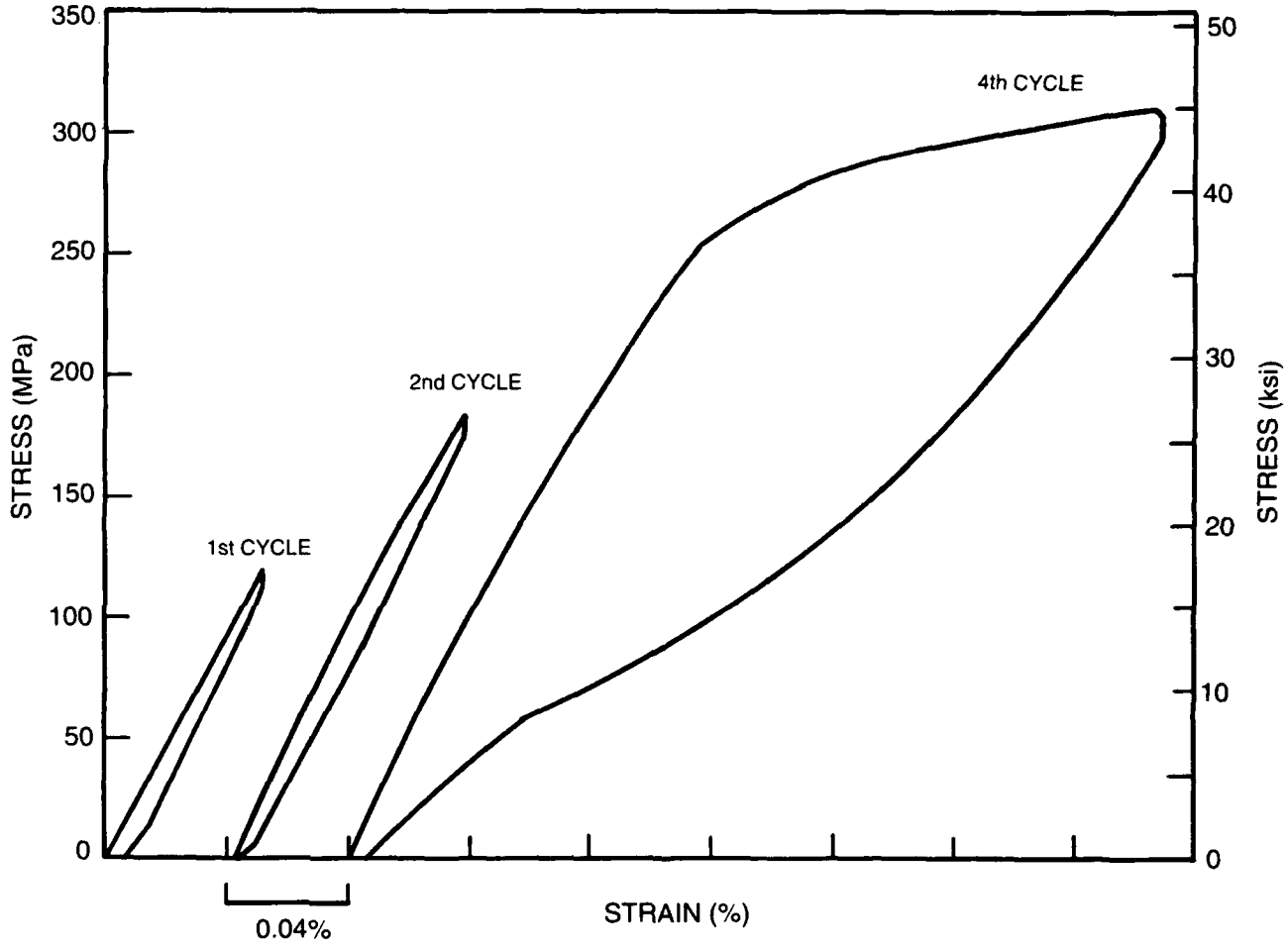

Figure II-16. Cyclic Compressive Stress-Strain Behavior for 0° P-100/BSG-2 Composites

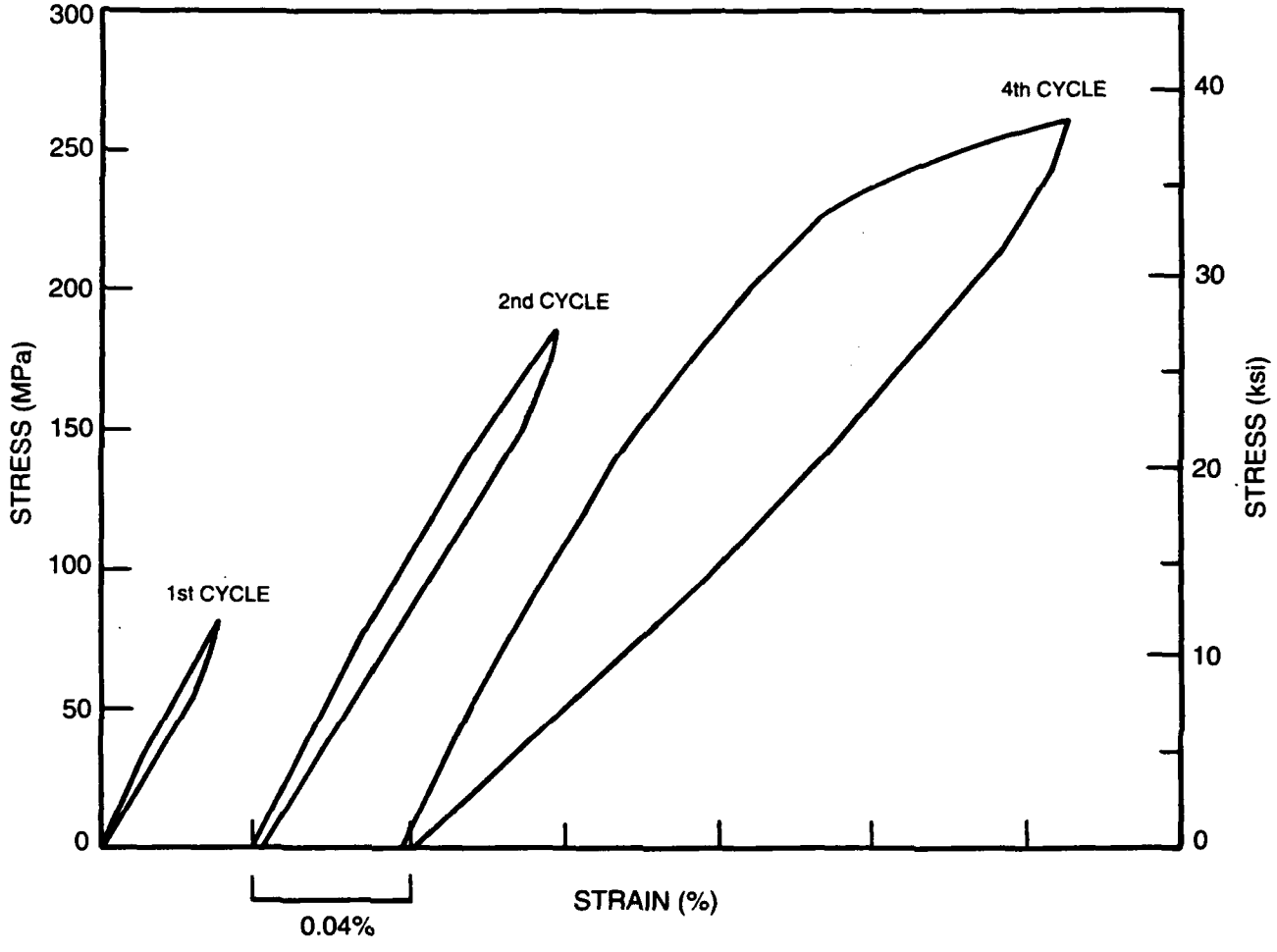

Figure II-17. Cyclic Compressive Stress-Strain Behavior for $(0/20/0)_s$ P-100/BSG-2 Composites

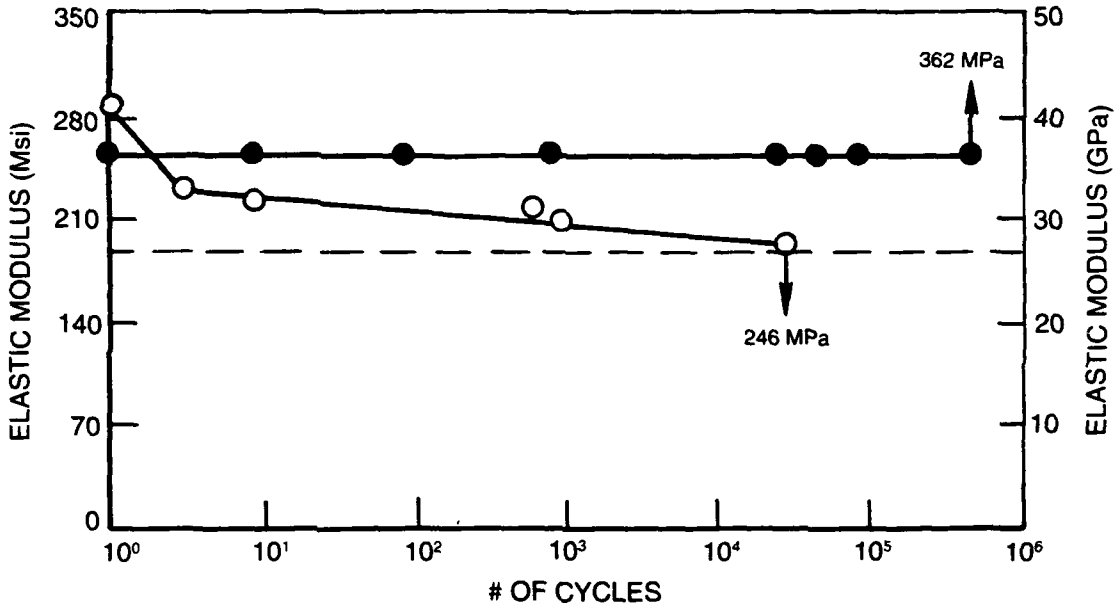

Figure II-18. Elastic Modulus Changes Measured During Compressive Fatigue Testing of Unidirectional (●) and $(0/20/0)_s$ (○) Composites. The Dashed Line Represents 191 GPa.

(A) UNIDIRECTIONAL (208.000 CYCLES, UPLOADED)

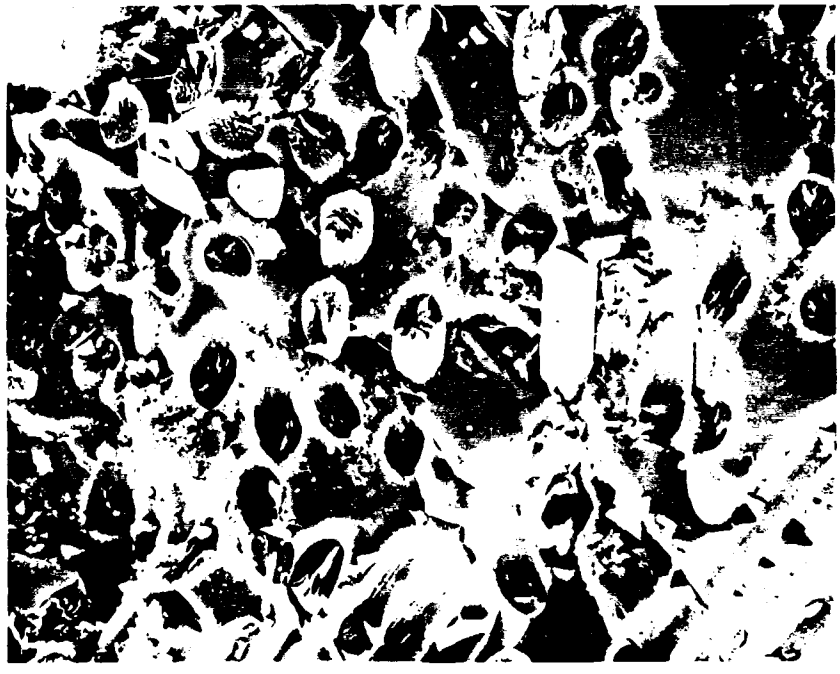

(B) $(0/20/0)_s$ (FAILED AFTER 26.000 CYCLES)

Figure II-19. Fracture Surfaces of P-100/BSG-2 Composites after Compressive Fatigue Testing

92-5-7-16

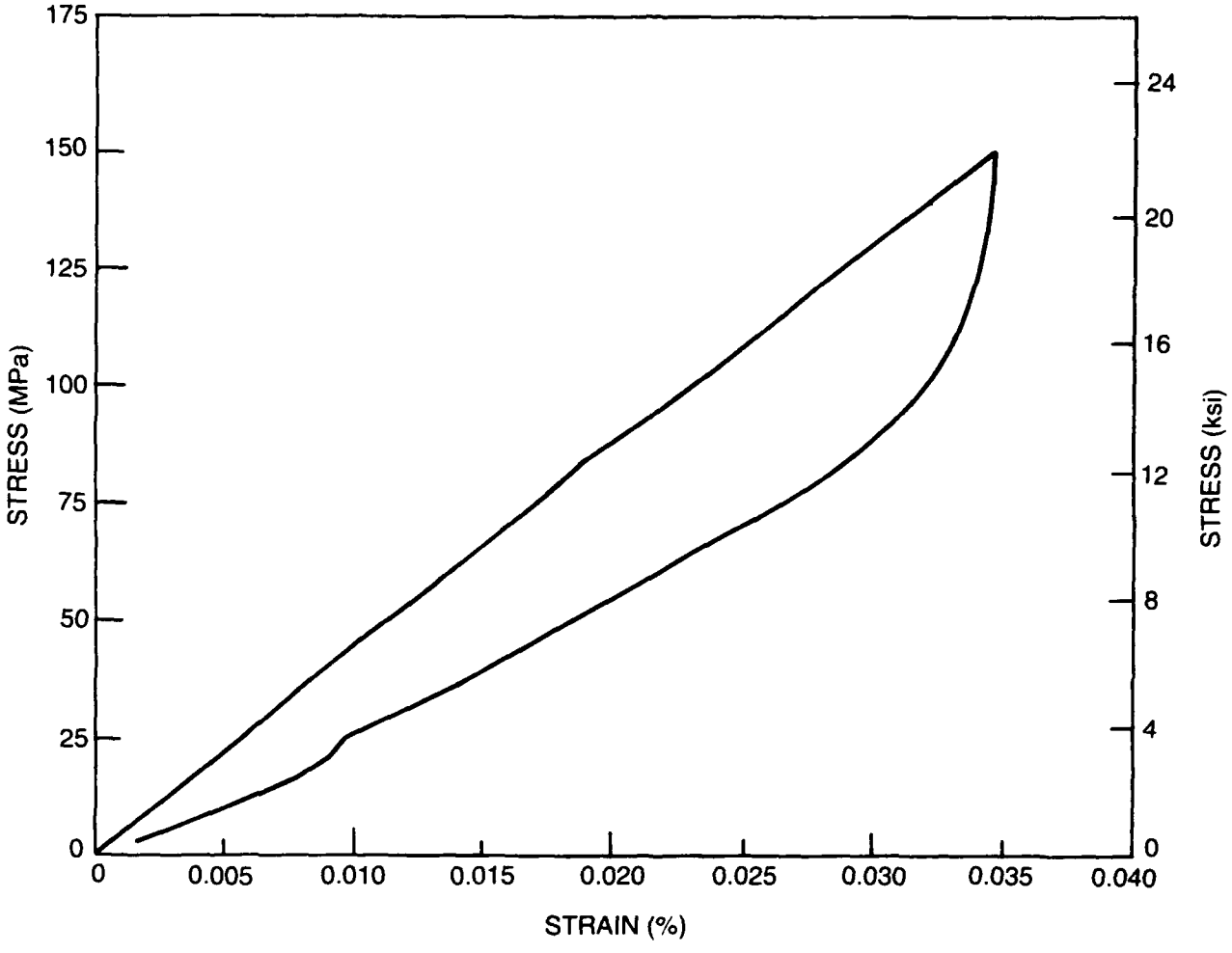

Figure II-20. Representative Hysteresis Behavior Observed for Both 0° HMU/BSG-2 and P-100/BSG-2 Composites During Compressive Pre-Stressing. Samples were Subsequently Loaded to Failure in Tension.

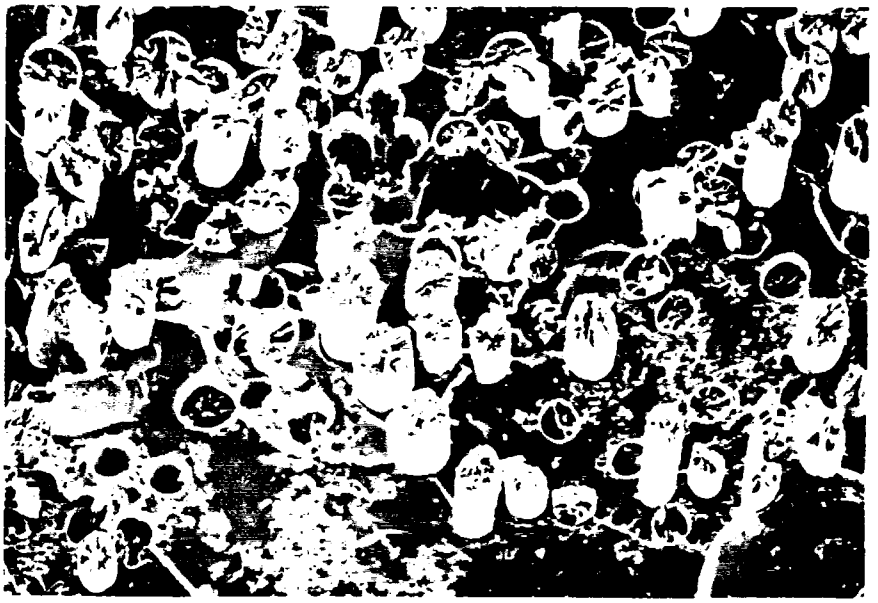

Figure II-21a. Tensile Fracture Surfaces of an as Fabricated (not Pre-Stressed) P-100/BSG-2 0° Composite

92-5-7-13

Figure II-21b. Tensile Fracture Surfaces of a Pre-Compression Stressed P-100/BSG-2 0° Composite

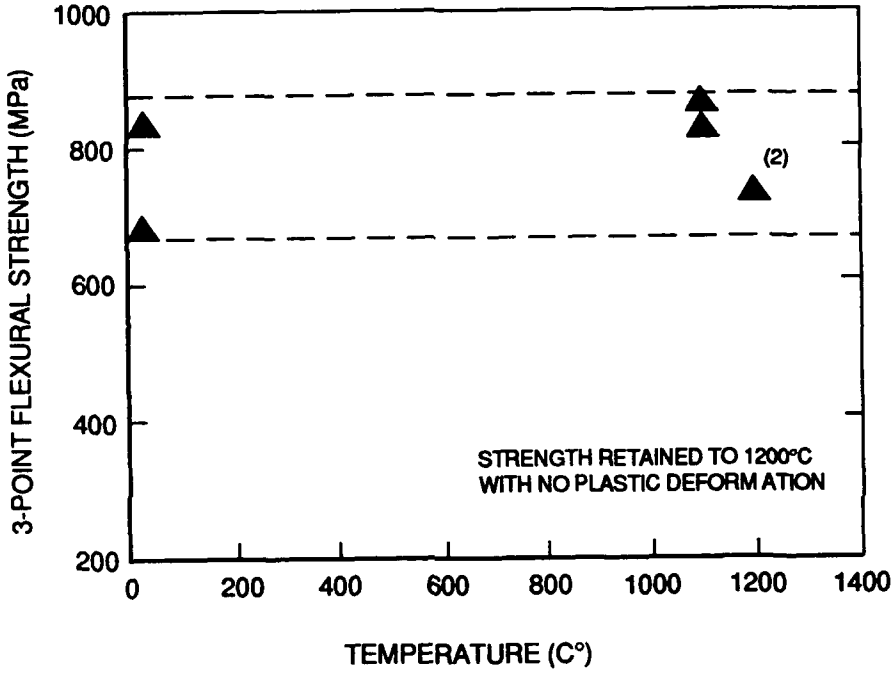

Figure II-22. 3-Point Flexural Strength as a Function of Temperature in Argon for a Unidirectional FT700/BMAS Composite

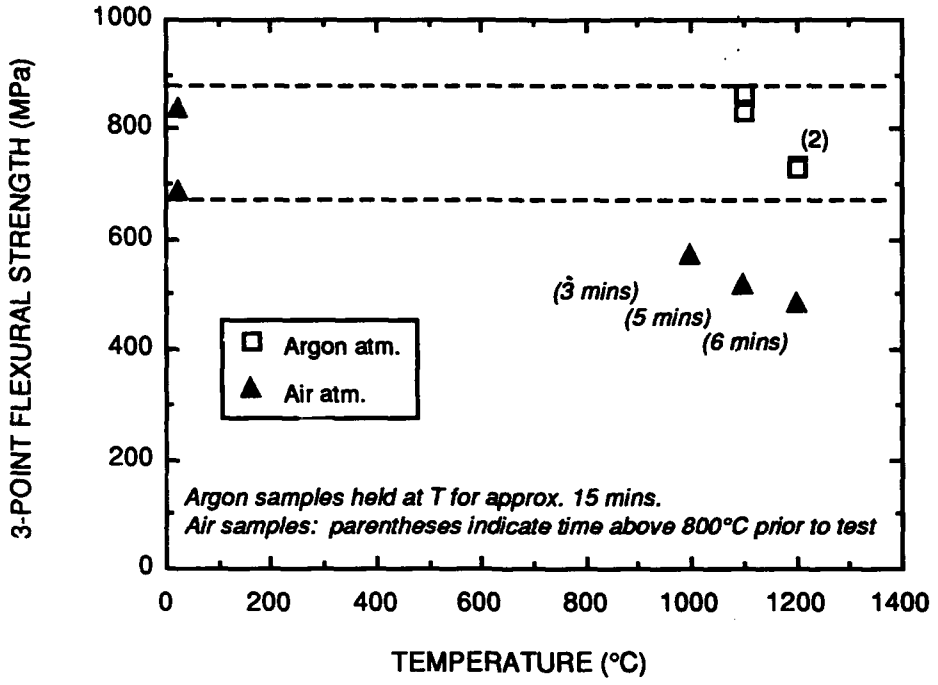

Figure II-23. 3-Point Flexural Strength vs. Temperature in Argon and in Air for a Unidirectional FT700/BMAS Composite

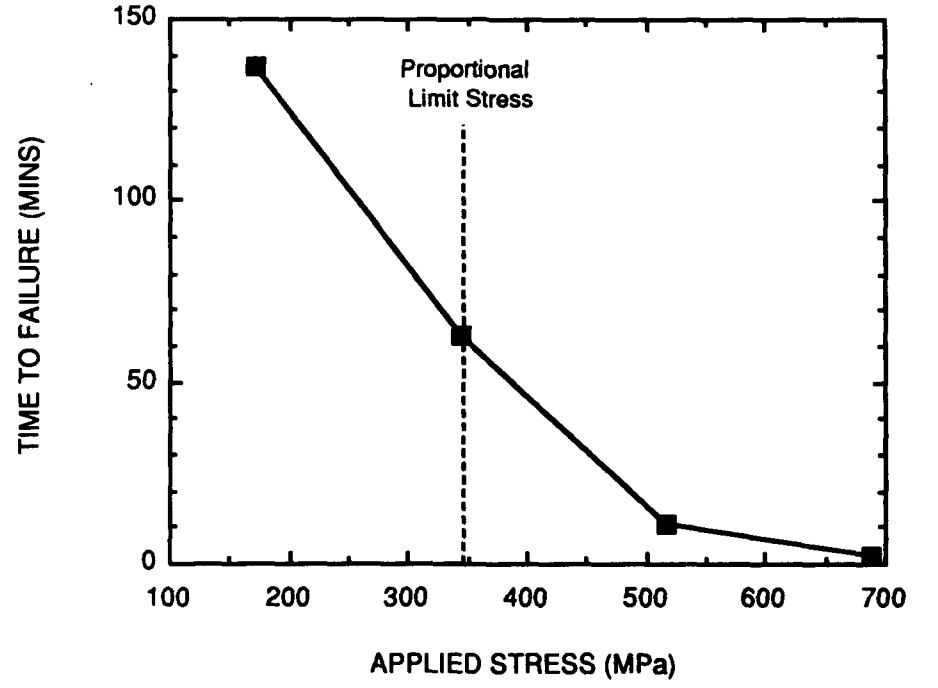

Figure II-24. Time to Failure vs. Applied Flexural Stress in Air at 800°C for a Unidirectional FT700/BMAS Composite

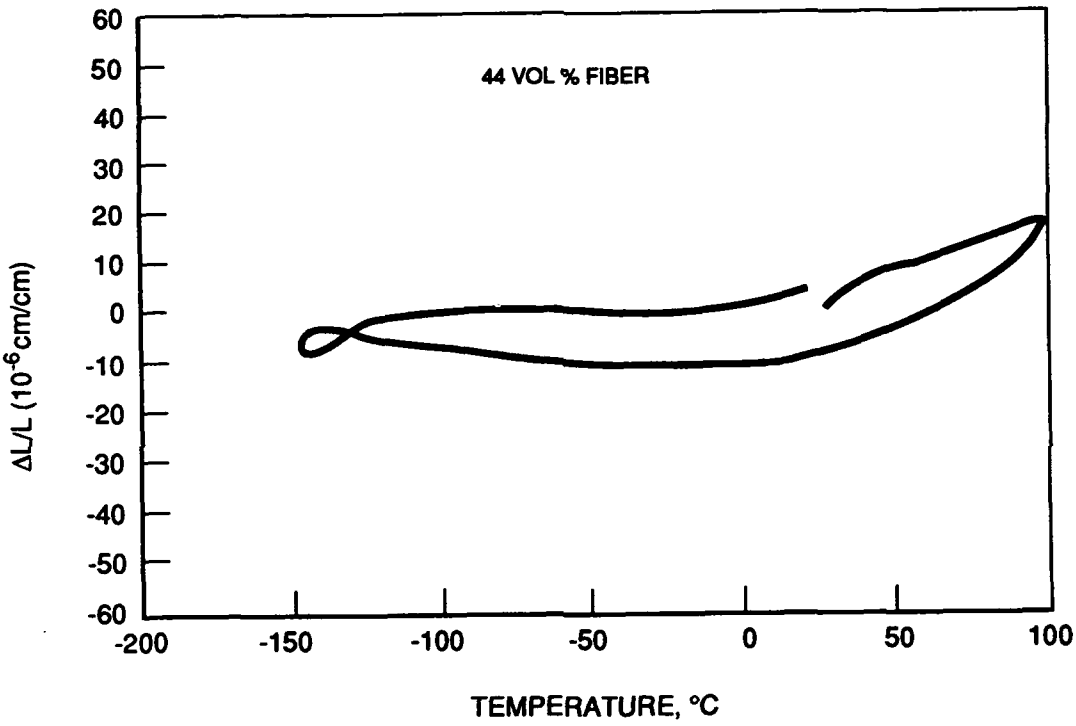

Figure II-25. Thermal Strain (ΔL/L) vs. Temperature for a Quasi-Isotropic [0/±60] Reinforced HMU/BSG Composite Exhibiting Near-zero Thermal Expansion

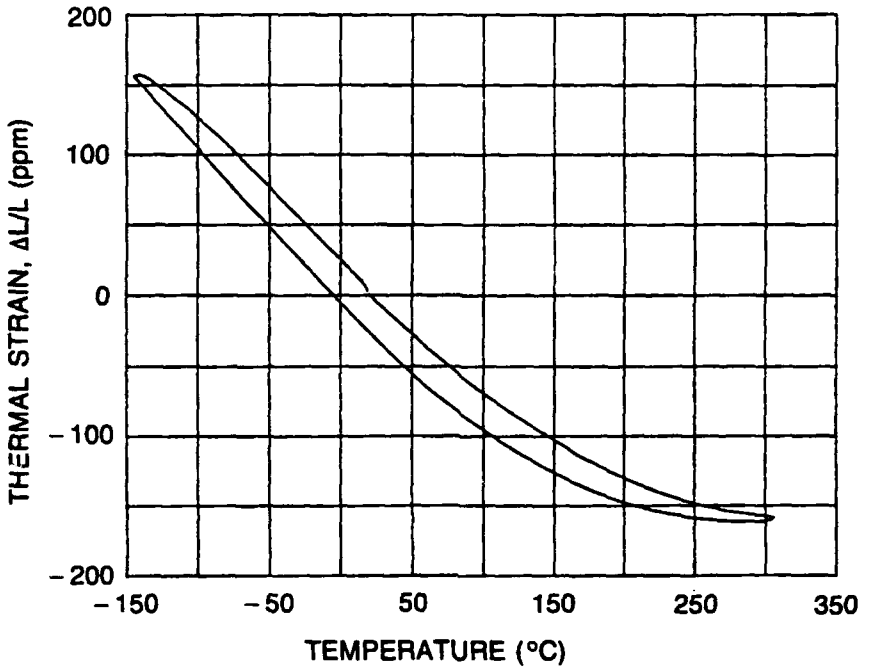

Figure II-26. Axial Thermal Strain vs. Temperature for 0°-45 v/o P-100/BSG Composite

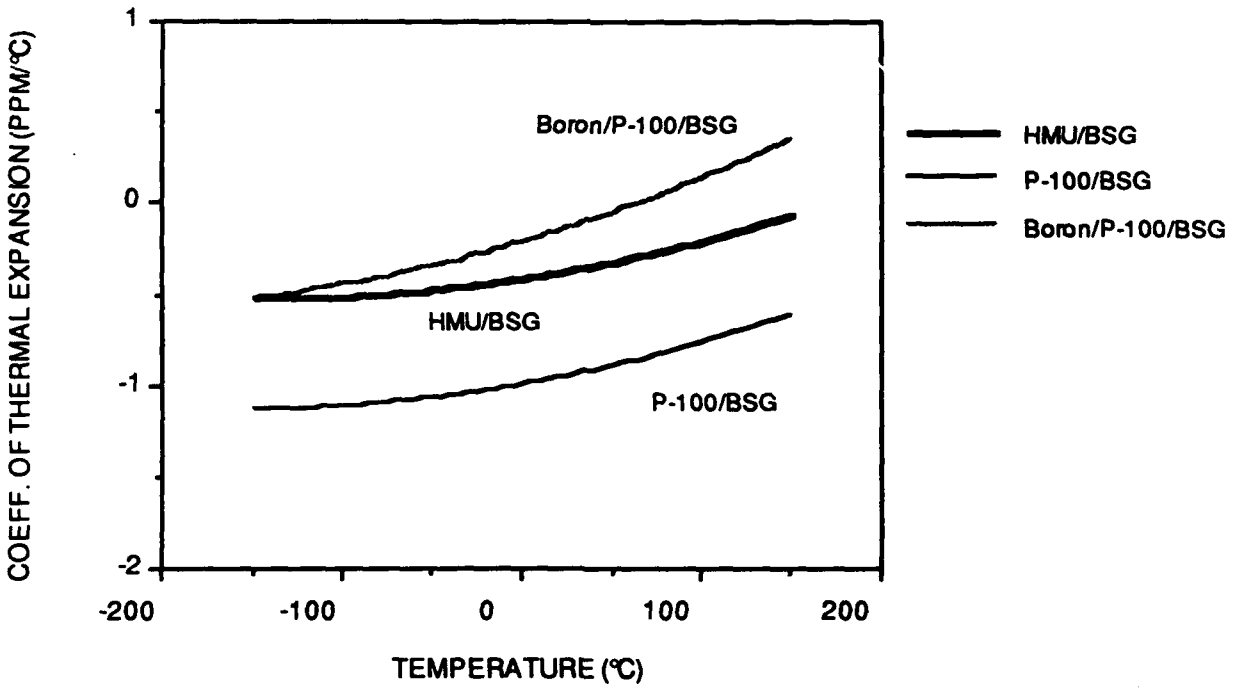

Figure II-27. Coefficient of Thermal Expansion vs. Temperature for Unidirectional HMU/BSG, P-100/BSG, and Boron/P-100/BSG Composites

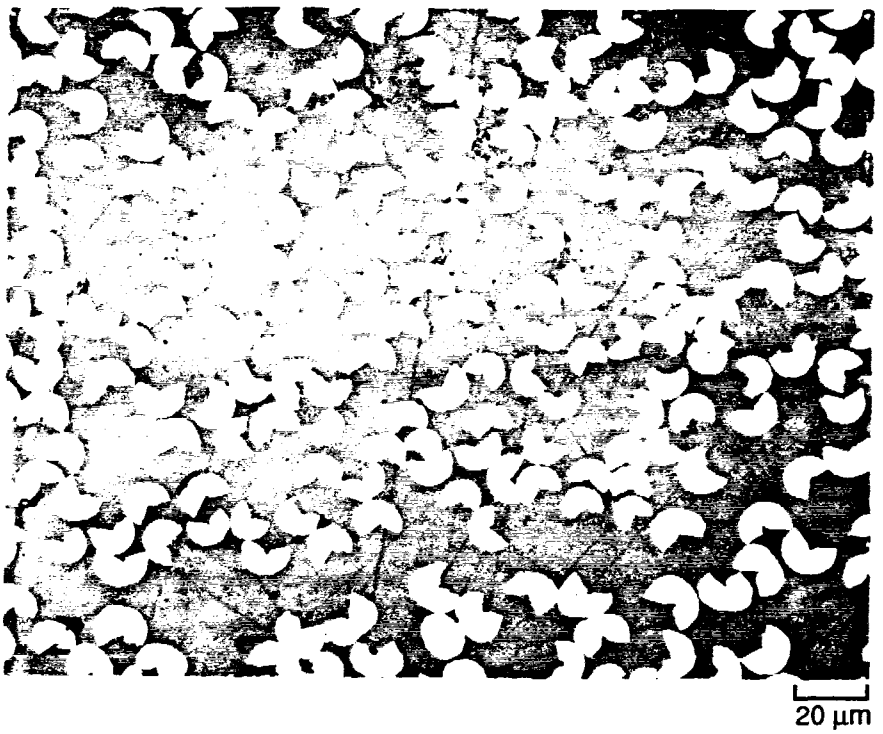

Figure II-28. Microstructure of Unidirectional K1100X/BSG Composite Showing the "Pac-Man" Fiber Structure

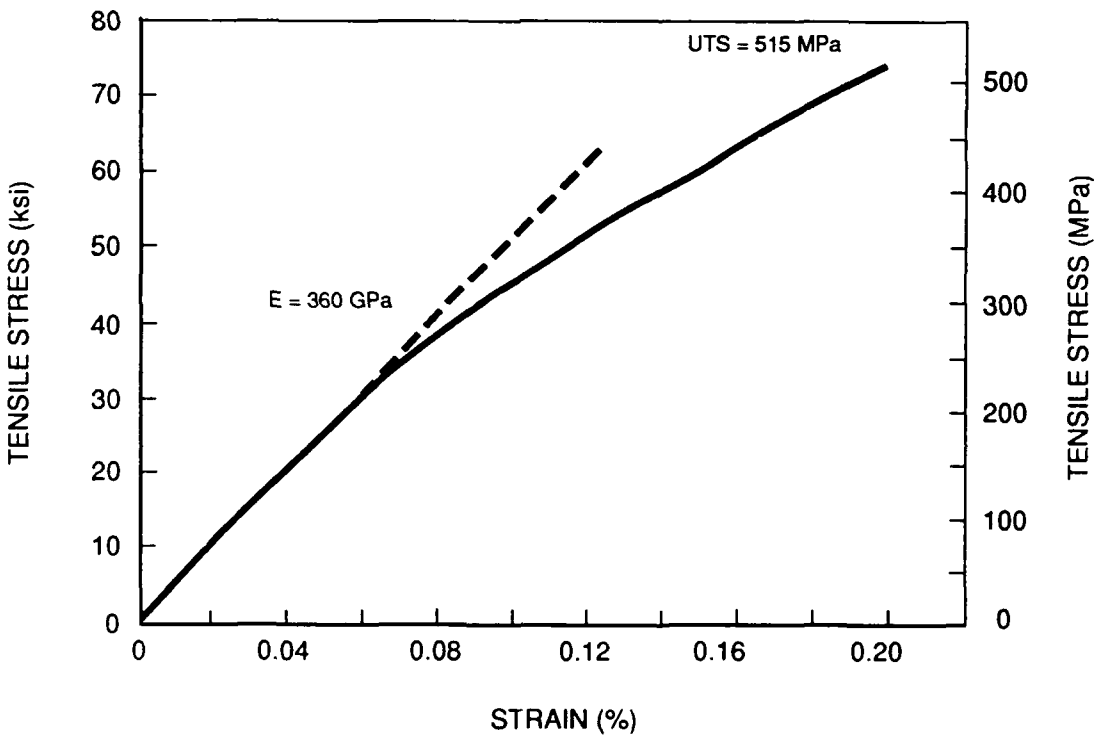

Figure II-29. Tensile Stress-Strain Behavior of a Unidirectional K1100X/BSG Composite Containing 41 v/o Fiber

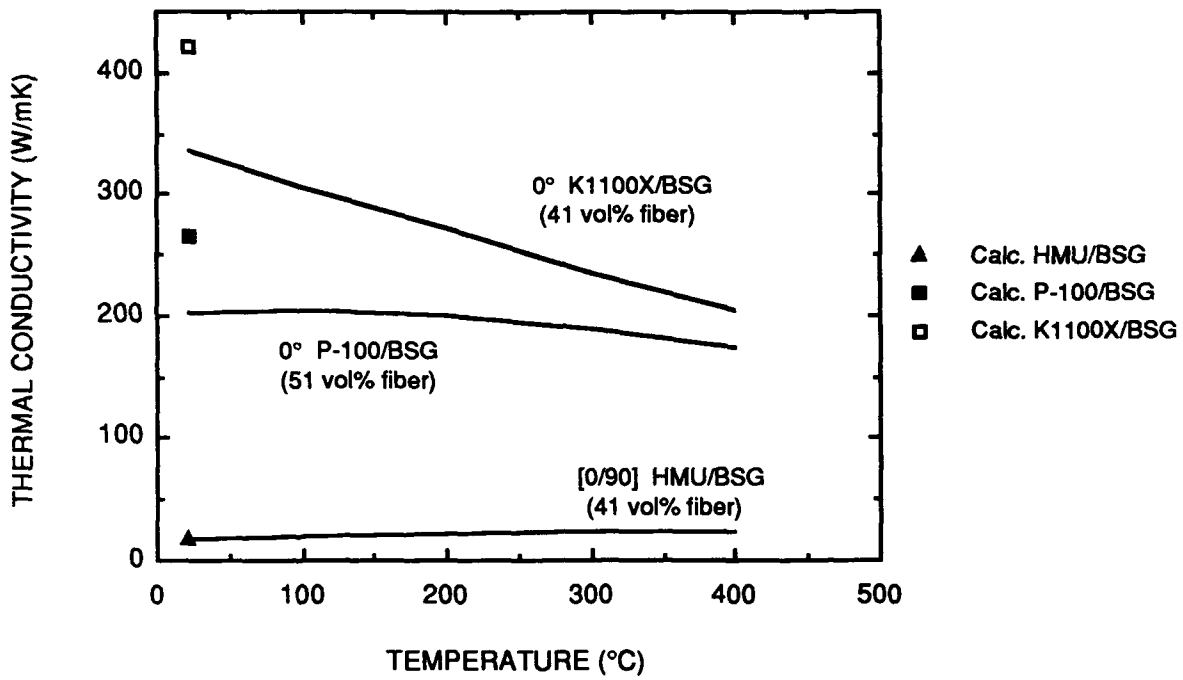

Figure II-30. In-Plane Thermal Conductivity vs. Temperature for 0° K1100X/BSG, 0° P-100/BSG, and [0/90] HMU/BSG Composites

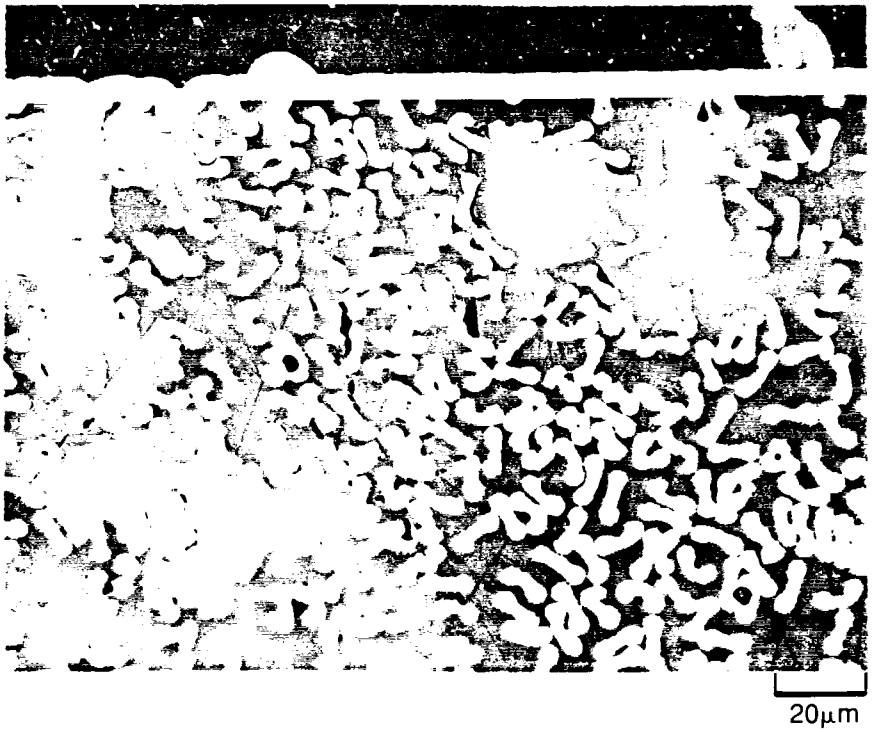

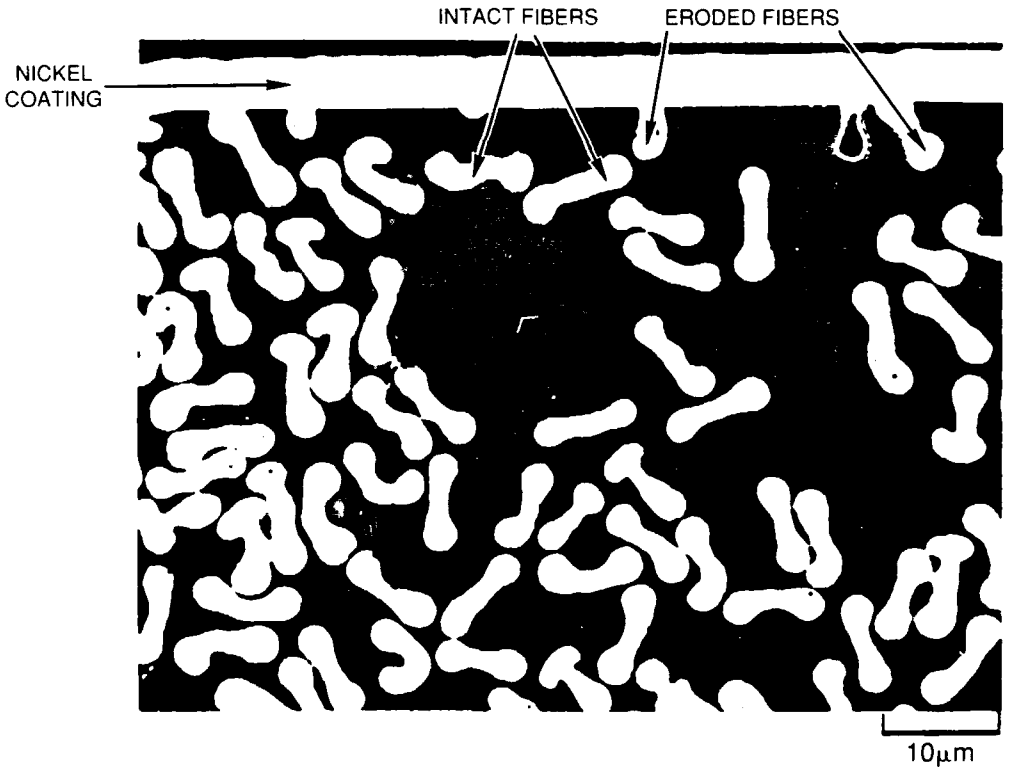

Figure II-31. Cross-Sectional View of Sample GL2-1 Showing Intact Fibers just Below the Sample Surface. Carbon Fibers that are Covered Even by Only a very Thin Layer of Glass have been Protected from AO Erosion.

91-5-46-3

III. COMPARISON OF HOT PRESSED AND HOT ISOSTATICALLY PRESSED CARBON FIBER REINFORCED GLASS COMPOSITES

III.1. INTRODUCTION

As previously described, the tow impregnation process has been used to produce a prepreg material having an intimate mixture of matrix powder and reinforcing fiber. Forming this prepreg material into a dense composite requires a consolidation step. Consolidation of C/Glass composites is typically accomplished by heating a prepreg material to a temperature sufficiently high so that the glass matrix phase has softened, then applying pressure to flow the glass matrix, consolidating the composite. It is important to heat the prepreg material above the matrix softening point, such that a completely consolidated part can be formed without damaging the reinforcing fibers via an abrasion mechanism. In order to accomplish this, independent control of pressure and temperature are required.

Typically, application of pressure is in only one direction, or unidirectional. A uniaxial hot press capable of operating in a non-oxidizing environment allows carbon fibers to be heated to temperatures sufficient to soften the glass matrix without degradation of the fiber properties. While uniaxial hot press consolidation of C/Glass has been used extensively at UTRC over the last 18 years [1], it has limitations. The two major limitations are in the size and shape of the components that can be fabricated by this method. Typical hot press units are limited to approximately 61cm x 61cm panels. These size limits arise from the inability to control ram travel such that the pressure applied is uniform across the part, and inability to maintain a uniform temperature across the entire area of the press. Although relatively small, complex shapes have been formed using hot press consolidation (truss core structures, rib stiffened panels and a variety of other shapes), hot press consolidation has never demonstrated the ability to form thin walled, hollow cross-section materials (tubular elements). It is the ability to form large, complex shaped composites, including hollow cross-section tubular elements, that makes HIPping an attractive consolidation technique.

The process for the HIP consolidation of thin-walled composite tubes was initially explored under UTRC funding and has been applied to the fabrication of C/Glass tubes on this program. Utilization of the HIP process should provide the capability to fabricate fairly large structures. Commercial HIP units exceed 3 meters in total length and 1.5 meters in diameter. As stated earlier in this report, a variety of parts having various cross sections were demonstrated during this program. Figure III-1 shows the family of shapes fabricated, which include circular tubes having diameters ranging from 2.5 - 4.5 cm and lengths up to 30 cm, a square tube, having a side length 2.5 cm, and a right angle structural beam, having a leg width of 2.5 cm. Wall thickness for all the parts ranges from 0.5 - 1.3 mm. Fiber orientation for the right angle structural beams has included unidirectional and 0/90, while for the tubular elements fiber orientation was typically $0/\pm\theta/0$, with θ ranging from 10° to 30°. As discussed previously in Section II of this report, the circular diameter tubes were fabricated and compression tested to determine the mechanical performance, and assess this performance in light of NSWC requirements for space-based structural elements.

This section of the report focuses on comparing HIP consolidation to traditional hot press consolidation for C/Glass composites. After a brief discussion regarding the mechanisms of both consolidation procedures, a comparison of composite specimens consolidated using the two processes will be presented.

III.2. COMPARISON OF HOT PRESSING AND HIPPING

While traditional uniaxial hot pressing applies pressure in only one direction, through the action of a ram, traditional HIPping applies pressure in all directions, usually through the action of a high temperature gas. These two consolidation processes are schematically depicted in Figure III-2. For monolithic materials, either process works well to produce consolidated parts; however, there are concerns that must be recognized when consolidating a continuous fiber reinforced material. Continuous fiber reinforced prepreg material has a "debulking" factor, defined as the bulk density before consolidation divided by bulk density after consolidation, of between 2 and 3. This means that during consolidation, the ply thickness of the composite decrease by a factor of 2 - 3. For 2-D laminates processed in a unidirectional hot press this is not a problem, provided the pressure is applied normal to the fiber length.

If continuous fiber reinforced prepreg material were to be processed in a traditional HIP having application of pressure from all sides, the large debulking factor would cause fiber buckling and damage in the fiber axial direction. This damage would result in a decrease in composite mechanical performance. However, UTRC has been able to modify the HIP process such that fiber buckling and damage during the HIP consolidation of continuous fiber C/Glass composites is avoided.

Both hot press and HIP consolidation allow pressure and temperature to be maintained and controlled *independently*. This is critical for the consolidation of glass matrix composites, as discussed earlier. A comparison of typical hot press and HIP profiles used for consolidation of C/Glass is shown in Figure III-3. During hot pressing, the prepreg material is heated to a temperature sufficient to soften the glass matrix prior to the application of the consolidation pressure. Neglecting any die frictional effects, all of the applied load is realized on the composite panel through a solid load train. Pressure is maintained during cooling to prevent delamination of the composite. While the HIP profile shown in Figure III-3B appears quite different than the hot press profile, the basic principals are the same. The differences seen result from a different die design, the need for a HIP can, and the application of gas pressure, not direct pressure.

Initially, UTRC's HIP chamber requires a finite pressure to protect the electronics from overheating. This pressure is not transferred to the composite prepreg because it is insufficient to overcome the strength of the canning material, and therefore distortion of the HIP can does not occur. This low pressure is maintained as the HIP chamber is heated to a temperature sufficient to soften the glass matrix. When that temperature is achieved, the pressure is slowly increased and begins to be transferred to the prepreg. The final pressure in this case, 35 MPa, is much greater than that used in the uniaxial hot press (7 MPa) due to the need for the metallic HIP can to distort and transfer the load to the prepreg. As in the hot press, pressure is maintained during cooling to prevent delamination of the composite.

To compare the two consolidation processes, flat mechanical test specimens were obtained from composites fabricated using both HIP and hot press consolidation. In the HIP consolidated composites, flat specimens were machined from the sides of right angle structural beams, while flat specimens were machined from flat panels fabricated using hot pressing. Both HMU carbon fiber reinforced borosilicate glass (HMU/BSG-2) 0/90 composites and ultra-high modulus P-100/borosilicate glass (P-100/BSG-2) unidirectional composites were investigated.

III.3. COMPOSITE PROPERTIES

III.3.1. Microstructure

As mentioned above, when HIP consolidation was used, right angle structural beams were fabricated and test specimens were machined from the flat sections of the beam, away from the right angle, as shown in Figure III-4. Care was taken to avoid cutting specimens too close to the angle in these composites, as a variation of fiber volume percent, and possibly damaged fiber could be in the test specimens. As seen in Figure III-5, the cross sectional area of the panel at the angle is greater than at the sides, causing the fiber volume in that area to be markedly less than on

the sides. Also, there is potential for fiber damage in the 0/90 ply layups, where the 90° ply has to bend around the sharp angle. Thus, to avoid breaking the very stiff P-100 fibers, only unidirectional panels were fabricated and tested.

Figure III-6 compares the polished microstructures of samples of P-100/BSG-2 composites fabricated by hot pressing and by HIPping. A difference in the porosity levels can be seen, the HIP part having greater porosity. It is believed that this porosity can be eliminated through slight alterations in process conditions, because this porosity was not seen in the HMU/BSG-2 right angle structural composites fabricated (Figure III-5), nor in thin walled tubes fabricated via HIP.

In regions of the composite away from the bend area in Figure III-5 and in Figure III-6, good fiber distribution is seen. This results from the prepreg operation, and is not believed to be dependant on the consolidation process. Aside from the porosity previously mentioned, the microstructures of hot pressed and HIPped materials are comparable.

III.3.2. Tensile Properties

Monotonic tensile properties were determined for the materials studied using straight sided specimens having a 2.54 cm gage length. Test specimen strain was measured using strain gages mounted directly on the test specimen surface. Composites investigated included 0/90 HMU/BSG-2 and 0° P-100/BSG-2 composites, fabricated by both hot pressing and HIPping.

Table III-1 lists the tensile properties measured for samples fabricated by hot pressing and HIPping. Representative stress-strain curves for the HMU fiber material are shown in Figure III-7, and in Figure III-8 for the P-100 fiber composites. Typical fracture surfaces of these materials are shown in Figures III-9 and III-10, respectively.

As the data in Table III-1 indicate, negligible difference is observed between the hot press and the HIP consolidated 0/90 HMU/BSG-2 composites. The accompanying stress-strain curves and fracture surfaces indicated comparable tensile behavior. In both cases, a great degree of fiber pull-out is seen at the fracture surfaces (Fig. III-9).

There exists a large difference in the tensile behavior of the 0° P-100 fiber reinforced material. The hot pressed composite shows almost twice the ultimate tensile strength of the HIPped material. Additionally, the tensile elastic modulus and the strain to failure are greater for the hot pressed samples (Table III-1).

The difference in strength between similar P-100/BSG-2 composites based on consolidation technique can be explained considering the microstructures of the two composites previously shown. Recall that in Figure III-6B, a high degree of fine porosity in the

unidirectional, HIPped P-100 reinforced composite was shown. Porosity such as this decreases the interfacial bond area in the composite and results in a decrease in the mechanical performance of the material. A large difference in the tensile behavior can be seen by comparing the stress-strain curves shown in Figure III-8. While the hot pressed sample (Figure III-8A) has a nearly linear curve to failure, the HIPped sample (Figure III-8B) stress-strain curve shows the onset of nonlinearity at a very low stress level. This behavior suggests microcracking of the matrix (expected to occur at a lower stress in a defect-containing matrix) and has been observed previously in C/Glass composites containing significant levels of matrix porosity [2]. Consistent with the observed interfacial porosity and decreased interfacial bond area in the HIPped sample, there is a large degree of fiber pullout for this sample compared to the hot pressed sample (Figure III-10).

Elastic modulus differences between the two P-100 composites can be explained by the difference in fiber loading of the two composites. Because of the very high modulus of the fibers (E = 758 GPa) relative to that of the matrix (E = 63 GPa) small variations in fiber volume percent of the composite result in large differences in the elastic modulus of the composite.

Table III-1 - Monotonic Tensile Properties for Hot Pressed and HIP'ed C/Glass Composites

Composite System	Consolidation Method	Fiber Vol%	UTS(MPa)	E(GPa)	Failure Strain (%)
$[(0/90)_2]_s$ HMU/BSG-2	Hot Press	40	249	78.7	0.40
	HIP	40	261	72.9	0.42
$[0°]_8$ P100/BSG-2	Hot Press	45	630	319	0.21
	HIP	38	320	285	0.16

UTS = Ultimate tensile strength
E = Elastic modulus

III.3.3. Compression Testing

Compressive properties of HMU and P-100 fiber reinforced composites were determined using straight sided samples having a 1.27 cm gage section. As in the tensile tests, sample strain was measured using strain gages mounted directly on the samples. In this instance, extensometers may have been a better choice as the strain gages seem to have buckled during loading. Because of the buckling of the strain gages during loading, strain-to-failure determination was not possible.

Table III-2 lists the compressive properties determined for the two composite systems and the two consolidation processes studied. From the tabulated data, it is apparent that the consolidation method has little effect on the compressive properties of these composites. In the HMU reinforced system, the materials have similar strengths and moduli, as was the case in the tensile tests discussed earlier. Interestingly, the P-100 fiber reinforced composites show similar ultimate strength in compression for both hot press and HIP consolidation, while a difference is shown in the compressive elastic modulus. This was of some surprise since it had been expected that matrix porosity would have affected both compressive stiffness and compressive strength.

Table III-2 - Monotonic Compression Test Results for Hot Pressed and HIP'ed C/Glass Composites

Composite System	Consolidation Method	Fiber Vol%	UCS (MPa)	E (GPa)
$[(0/90)_2]_s$ HMU/BSG-2	Hot Press	40	325	71
	HIP	40	281	80
$[0°]_8$ P-100/BSG-2	Hot Press	45	351	304
	HIP	38	366	242

UCS = Ultimate compression strength
E = Elastic modulus

Figure III-11 contains typical compressive fracture surfaces for hot press and HIP consolidated P-100/BSG-2 specimens. Both specimens show failure surfaces lacking a great deal of fiber pullout, not atypical for a compression failure surface. The structured nature of the P-100 fibers is evident, as is the primary mode of failure for the fibers, shear at a 45° angle to the fiber axis.

III.4. SUMMARY/CONCLUSIONS

Two different consolidation procedures, hot pressing and hot isostatic pressure (HIP) processing, were investigated and compared to each other to determine the ability to use either to fabricate carbon fiber reinforced glass matrix composites. Hot pressing has been used for over 18 years as the primary consolidation process for fabricating flat panels, but is limited in capability for forming hollow cross-section, thin walled composites such as tubes. HIP consolidation has been demonstrated for fabricating structural elements, such as thin walled tubes, and also has the capability to form very large composites.

It has been shown that either of these two consolidation processes provide the necessary independent control of pressure application and temperature required for forming glass matrix composites. Using HMU and P-100 carbon fiber and a borosilicate glass matrix, a variety of composite panels were fabricated and evaluated to ascertain the similarity of the two consolidation processes. Polished microstructures, monotonic tensile testing and monotonic compression testing have shown that no difference in composite properties exists based on the fabrication process used. This important conclusion allows databases generated using hot press consolidated specimens to be used in the modelling of properties expected for HIP consolidated materials.

REFERENCES

1. K. M. Prewo, J. J. Brennan and G. K. Layden, "Fiber Reinforced Glasses and Glass-Ceramics for High Performance Applications," *Am. Ceram. Soc. Bull.*, **65** (1986) 305-313.

2. W. K. Tredway and K. M. Prewo, "Carbon Fiber Reinforced Glass Matrix Composites for Space Based Applications," UTRC Contract Report R87-917470-1, Office of Naval Research Contract N00014-85-C-0332, August 30, 1987.

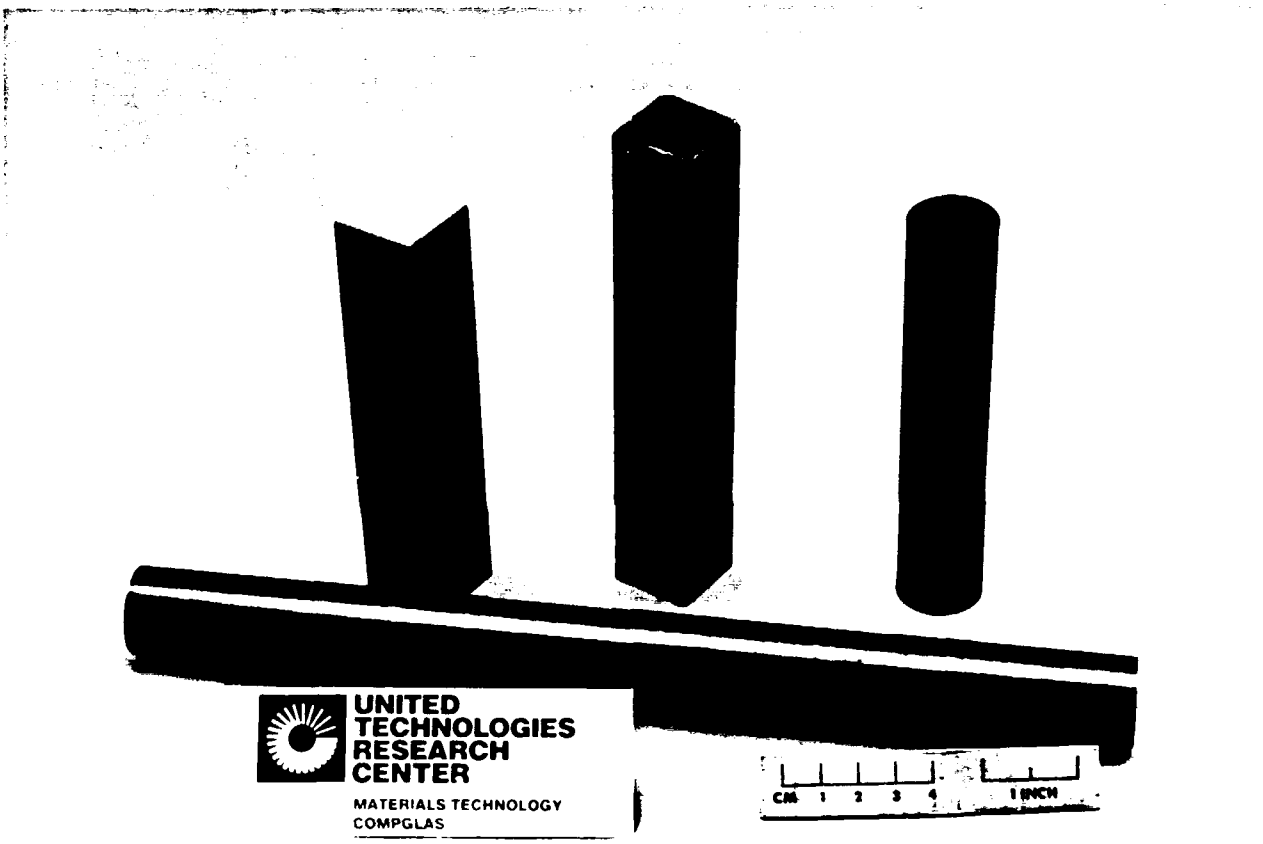

Fig. III-1 Continuous Carbon Fiber Reinforced Glass Composites Fabricated by HIP

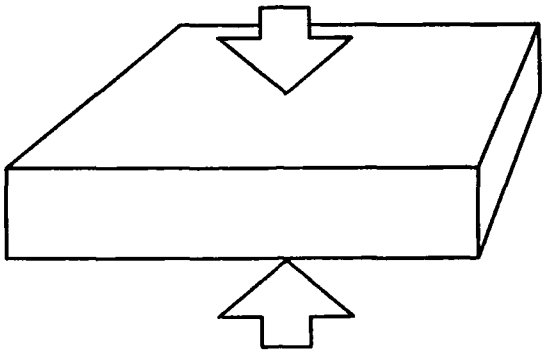

A) HOT PRESSING

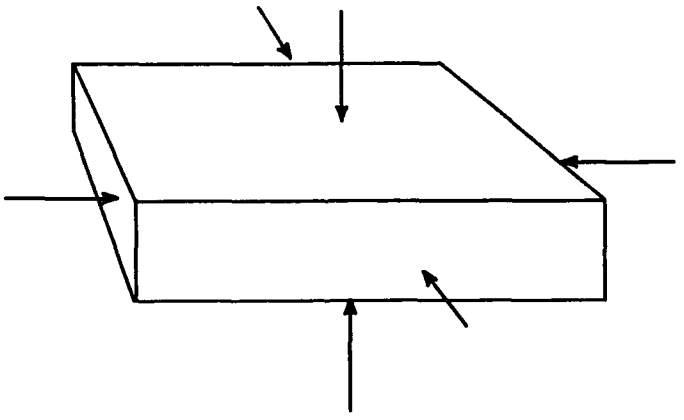

B) HOT ISOSTATIC PRESSING (HIP)

Fig. III-2 Schematic Representation of Two Consolidation Methods Used for Forming C/GI Composites

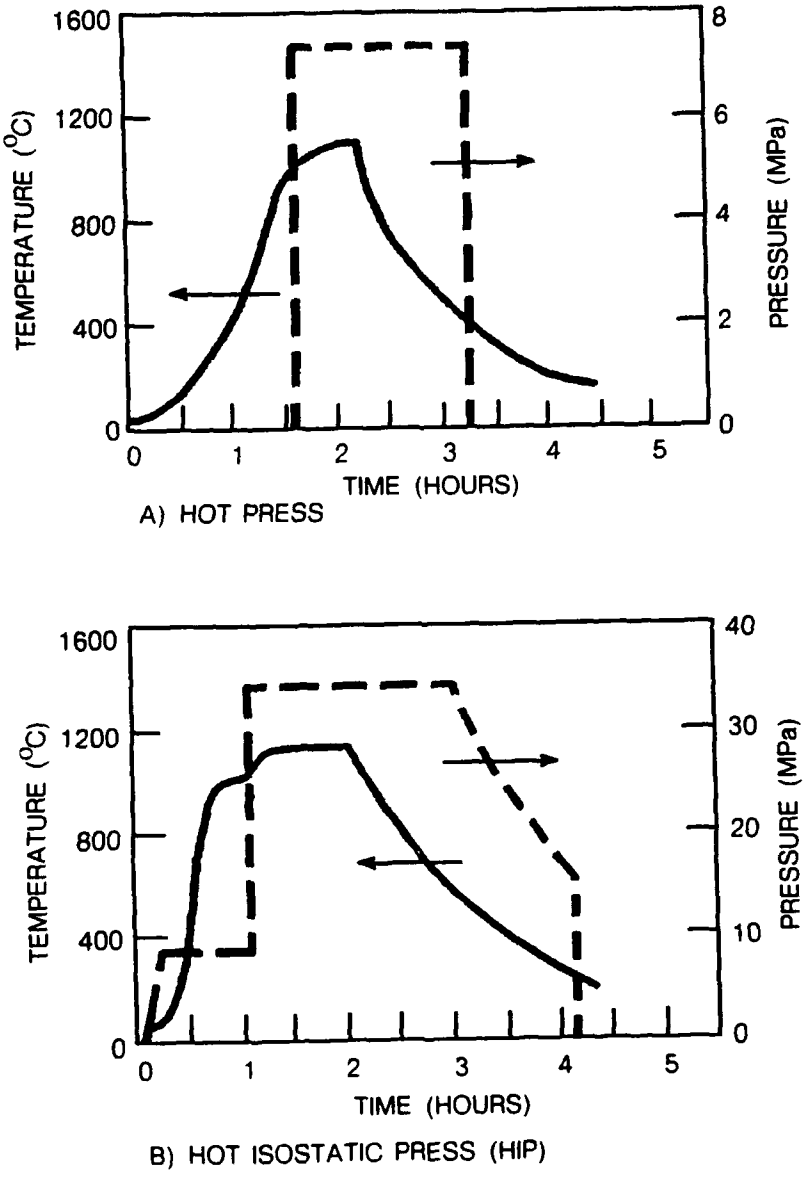

Fig. III-3 Comparison of A) Hot Press and B) HIP Consolidation Processing Conditions

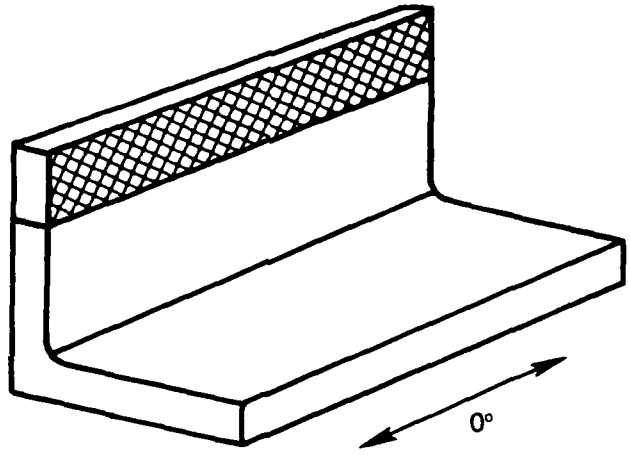

Fig. III-4 Schematic Representation of the Area that Test Specimens were Machined From

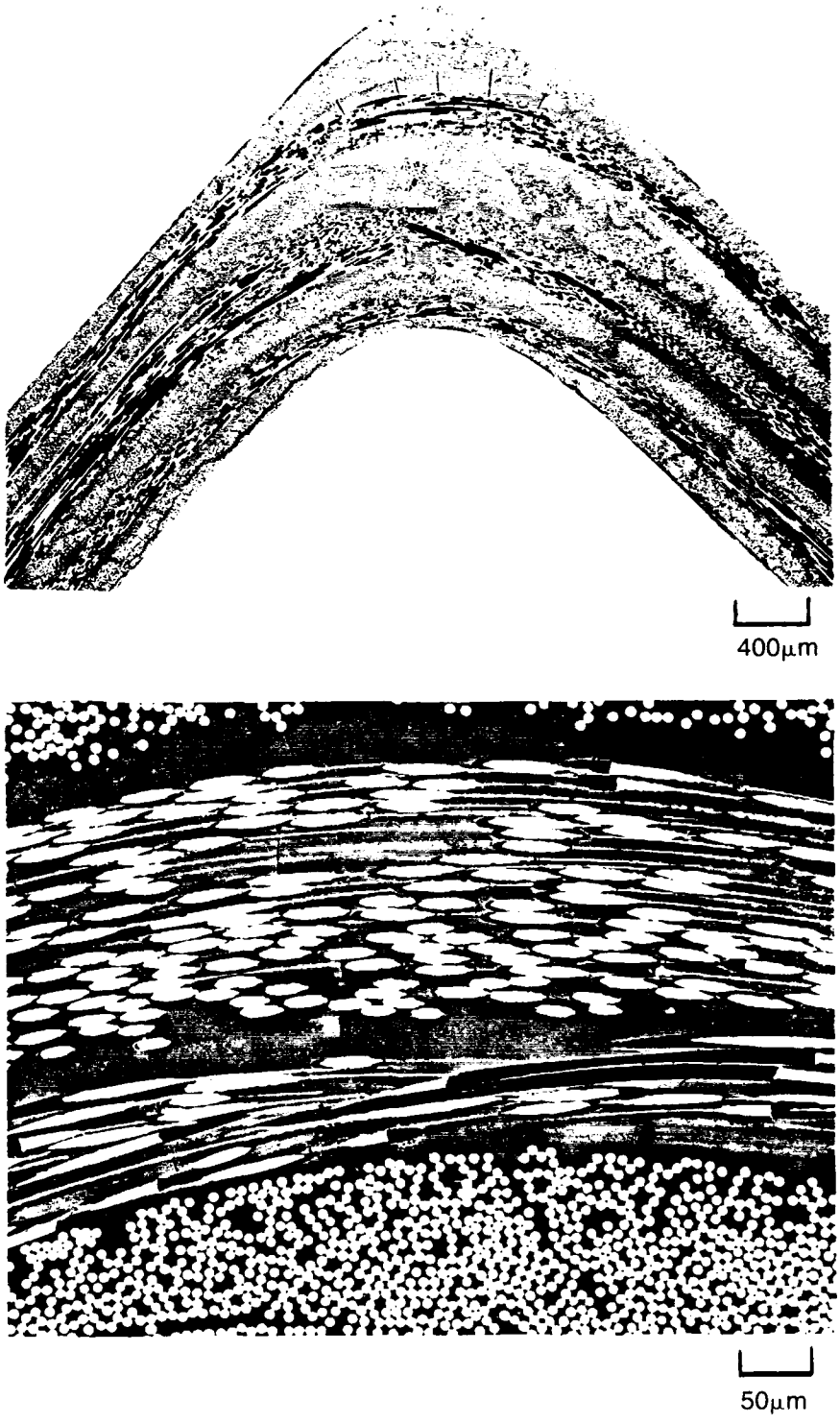

Fig. III-5 Polished Microstructures of HMU/BSG-2 HIP Consolidated 'L' Beam. Notice the Width at the Angle is Greater than at the Sides.

92-5-7-5

R92-917981-2

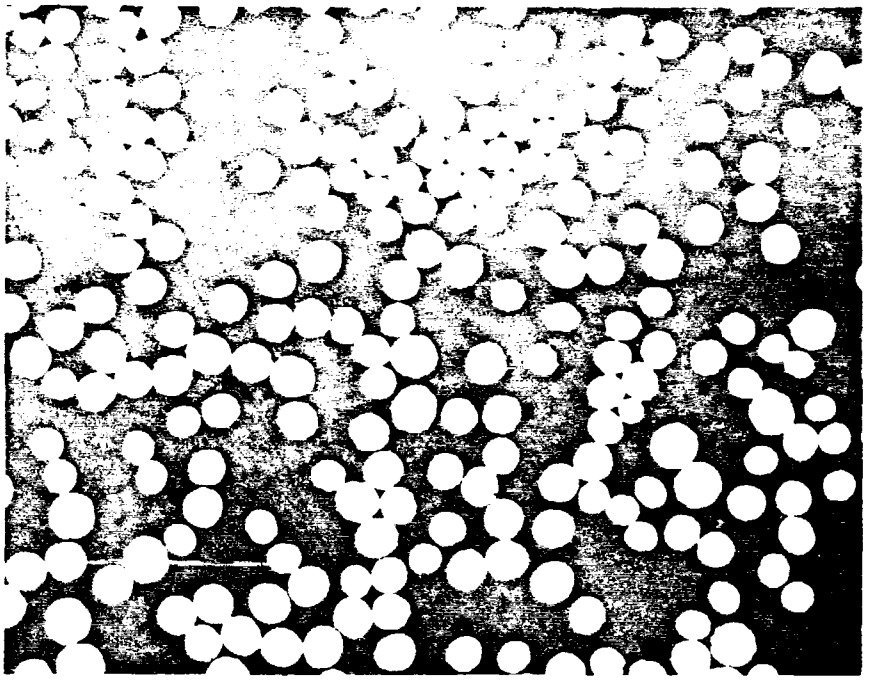

(A) HOT PRESS CONSOLIDATED

20μm

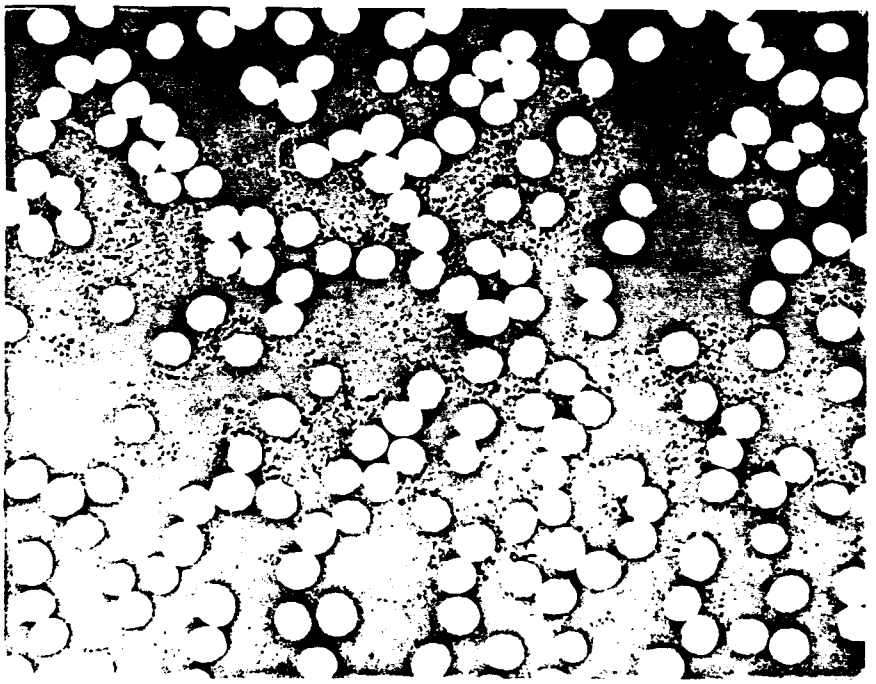

(B) HIP CONSOLIDATED

20μm

Fig. III-6 Polished Photomicrographs of P-100/BSG Composites Fabricated Using A) Hot Press and B) HIP Consolidation

92-5-7-4

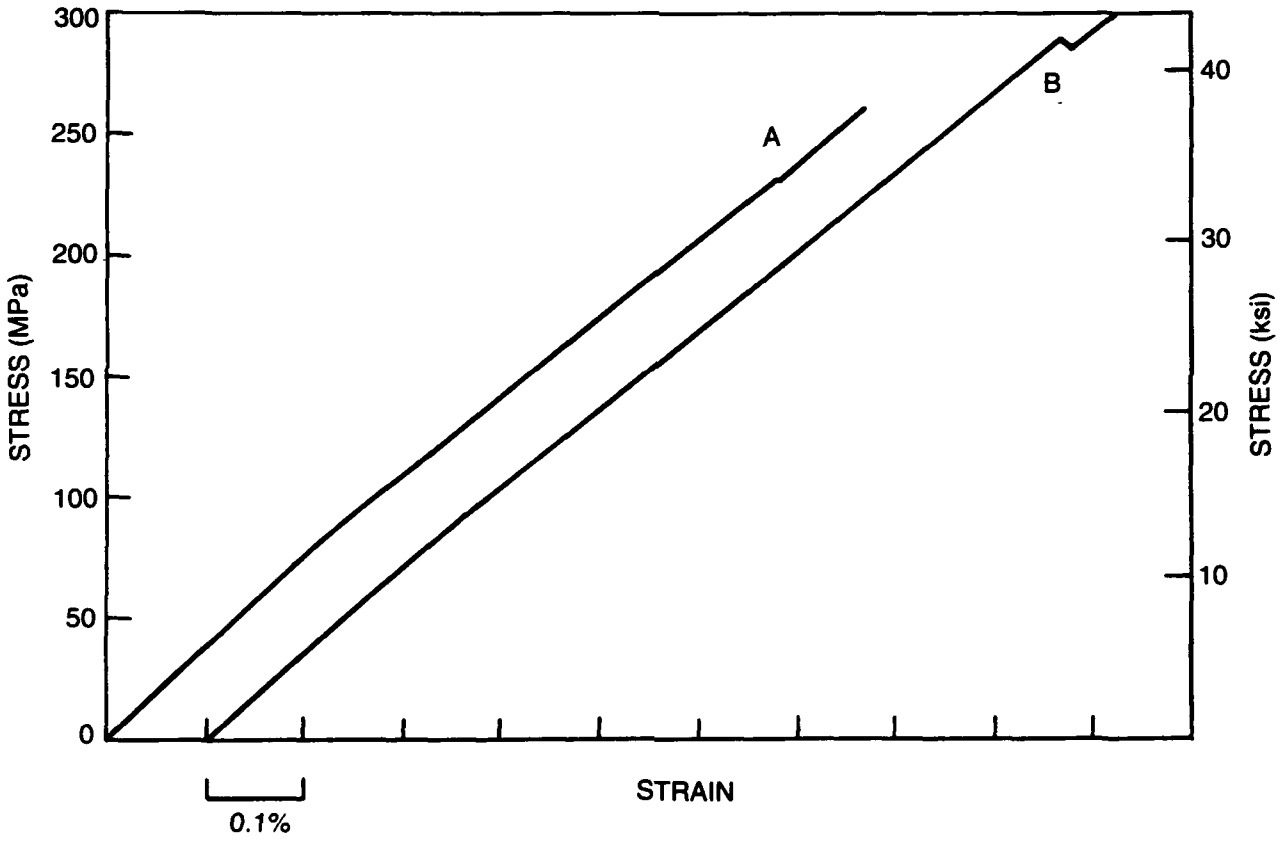

Fig. III-7 Typical Stress-Strain Response for 0/90 HMU/BSG-2 Composite Specimens Consolidated by (A) Hot Pressing and (B) HIPping

92-5-7-11

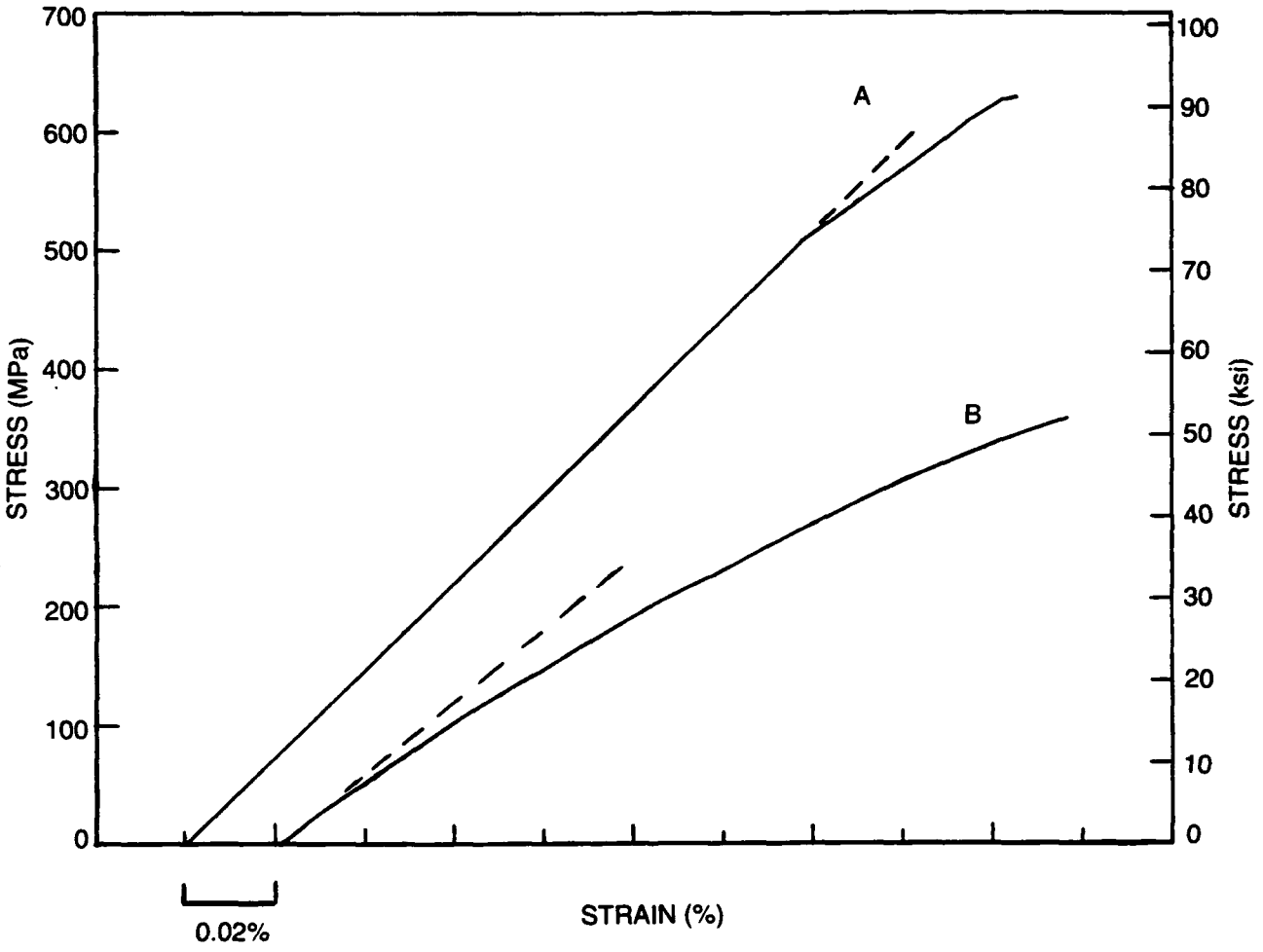

Fig. III-8 Longitudinal Tensile Stress-Strain Behavior for 0° P-100/BSG-2 Composites Consolidated by A) Hot Pressing and B) HIPping

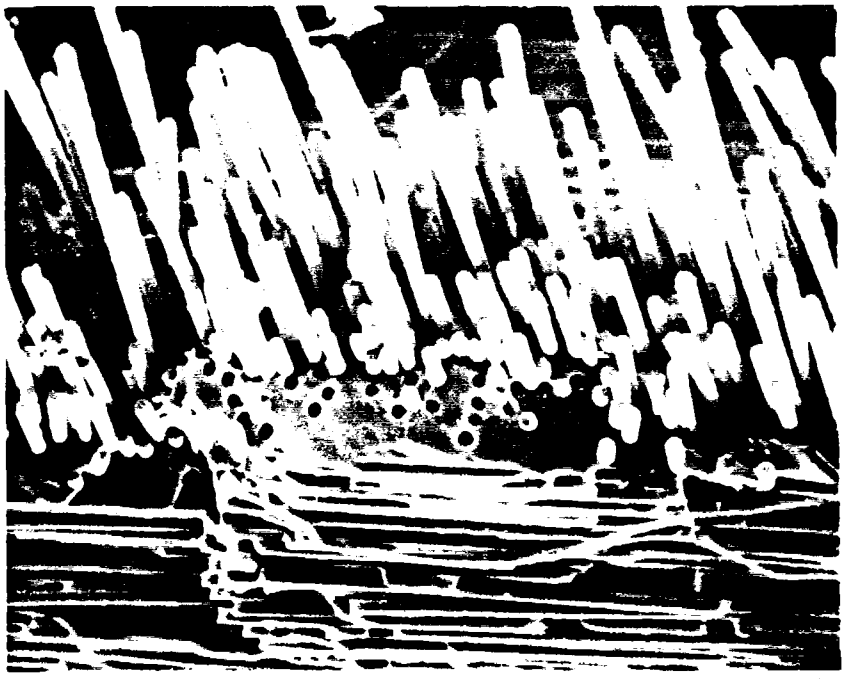

(A) HOT PRESS

20μm

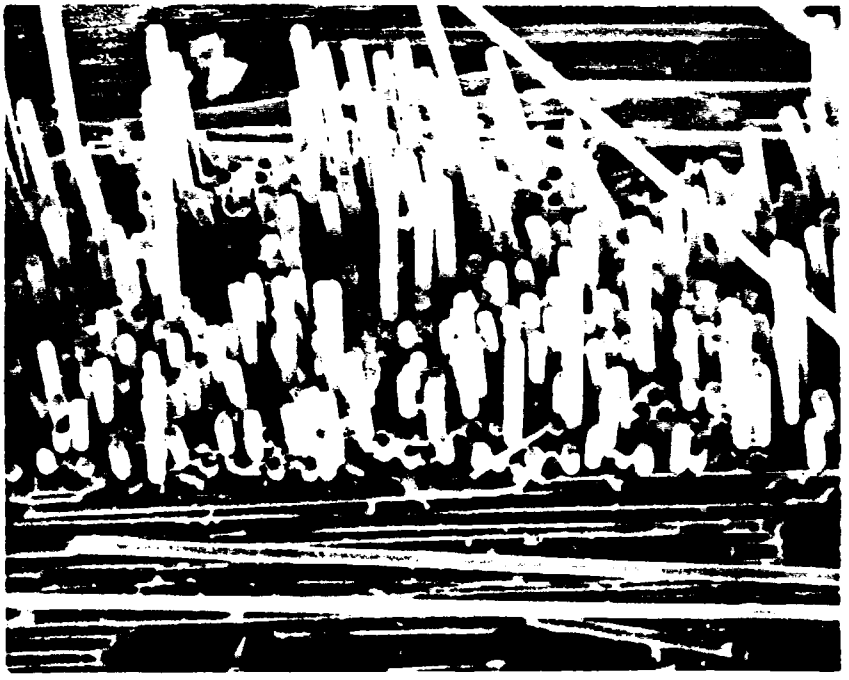

(B) HIP

10μm

Fig. III-9 Tensile Fracture Surfaces of HMU/BSG-2 0/90 Composite Specimens

92-5-7-3

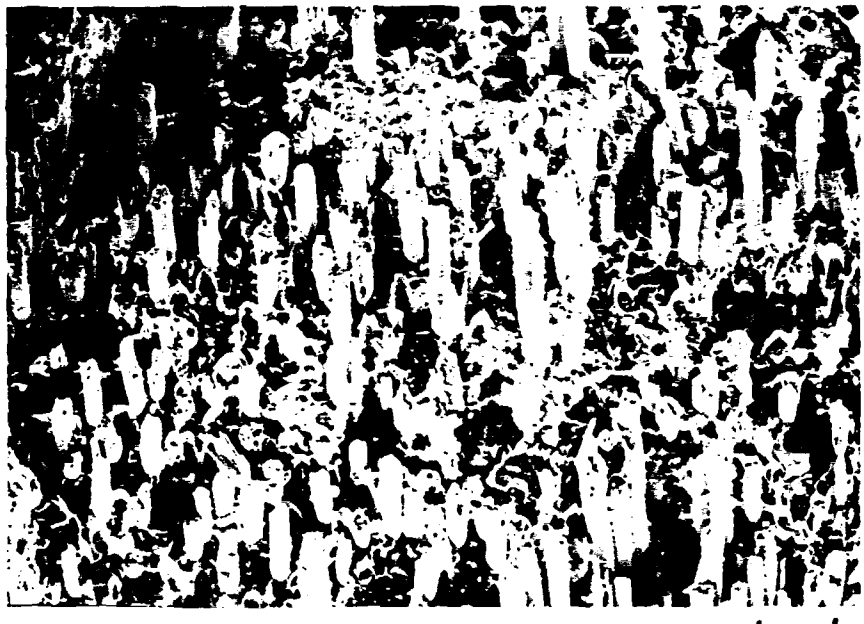

(A) HOT PRESS

40μm

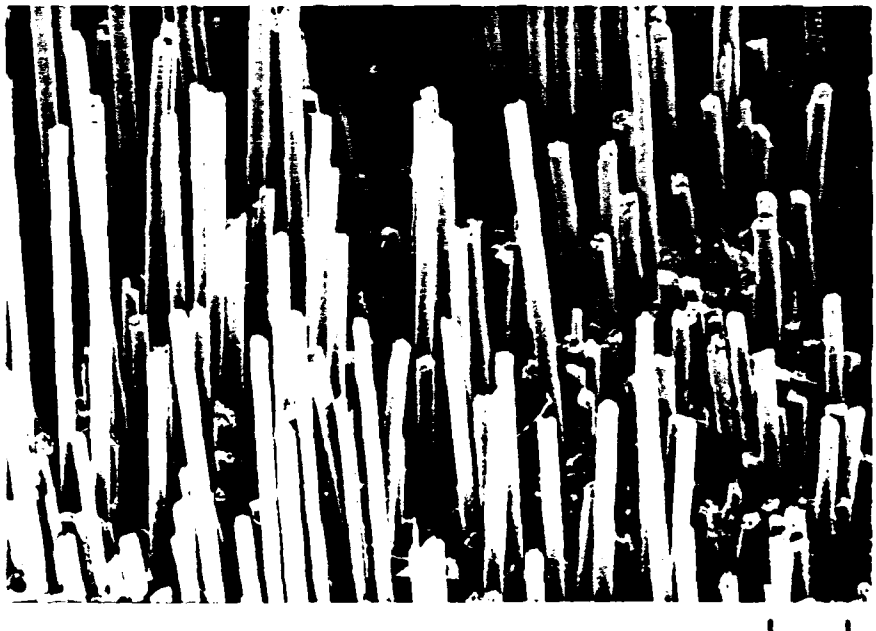

(B) HIP

40μm

Fig. III-10 Tensile Fracture Surfaces of P-100/BSG-2 0° Composite Specimens

Fig. III-11 Compression Fracture Surfaces of P-100/BSG-2 0° Composite Specimens

IV. METHODS OF IMPROVING THE PROPORTIONAL LIMIT STRESS IN C/GLASS COMPOSITES

The proportional limit (PL) stress of a composite material is often regarded as a type of "design allowable" stress, *viz.* a practical upper limit of useful strength for structural applications. This thinking stems from the common association of the PL with matrix microcracking, fiber debonding, and the onset of damage within the composite that could lead to accelerated degradation through oxidation or other environmental factors. Naturally, the implication of this is that PL stress needs to be maximized for any type of fiber reinforced ceramic composite. However, as was described in a previous section, the PL does not always coincide with matrix microcracking, and, in the case of the P-100/BSG and FT700/BSG systems, cyclic tensile behavior indicates that loading well beyond the PL does not lead to permanent damage of the composite. Nevertheless, increasing the PL in C/Glass composites is probably desirable purely from the standpoint of having linear elastic behavior over a larger range. For this reason, several approaches for increasing the PL in C/Glass composites have been demonstrated at UTRC over the past few years. These techniques will be described below.

As was described in a previous section, thermal expansion differences between the fiber and matrix in C/Glass composites lead to residual tensile stress in the matrix in a direction parallel to the fiber during cooling from the fabrication temperature. Reducing the magnitude of the residual matrix stress should lead to a greater degree of external mechanical load that can be applied before the matrix stress reaches its ultimate strength and begins to crack, which should translate to an increase in PL stress. One method of reducing the residual matrix stress is to vary the composition of the BSG matrix in such a way as to lower either the matrix coefficient of thermal expansion (CTE), matrix elastic modulus (E_m), and/or the glass strain point temperature (T_{strain}). These factors are all related to the degree of residual tensile stress in the matrix through the expression

$$\sigma_m = \frac{(CTE_f - CTE_m)\,\Delta T\, E_f V_f}{1 + V_f\left(\frac{E_f}{E_m} - 1\right)} \quad , \qquad \text{(IV-1)}$$

where σ_m is the residual matrix stress, CTE_f and CTE_m are the fiber and matrix thermal expansion coefficients, respectively, ΔT is the temperature difference below T_{strain}, V_f is the fiber volume fraction, and E_f and E_m are the fiber and matrix moduli, respectively. This

expression assumes that the stress is one-dimensional (i.e., neglecting transverse CTE mismatch) as well as that the CTE's and moduli of the fiber and matrix are independent of temperature over the ΔT range. Table IV-1 shows the effect of changing to a matrix composition with both a lower elastic modulus and a lower T_{strain} on the PL stress of several different C/Glass composites. It is clear that reducing the residual matrix tensile stress produced a profound effect on increasing the PL stress in all of the systems shown. Figure IV-1, which shows a plot of the dependence of the measured composite PL stress on the calculated matrix stress, further illustrates the strong relationship between these parameters. The trend of data shown in the figure suggests that this relationship is fairly linear.

Table IV-1 - Effect of Residual Matrix Stress on Composite PL Stress for Unidirectionally Reinforced C/Glass Composites

Fiber/Matrix	Fiber Vol %	Calculated Residual Matrix Stress (MPa)*	Prop. Limit Stress (MPa)	Ultimate Tensile Strength (MPa)
HMU/BSG	45	107	400	944
HMU/BSG-2	45	87	604	944
P-100/BSG	40	138	134	650
P-100/BSG-2	33	106	412	661
FT700/BSG	45	135	96	792
FT700/BSG-2	43	106	441	523

* Calculated using equation IV-1

Another approach that has been shown to lead to higher PL stresses in C/Glass composites is to add boron nitride (BN) platelets to the composite as a secondary reinforcing phase. Table IV-2 shows the effect of adding approximately 25 vol% BN to the BSG matrix for several different C/Glass systems. It is clear that the addition of the BN platelets leads to a considerable increase in composite PL stress. In these C/Glass composites, the "matrix" can be considered to be the combination of the BSG glass and the BN platelets, a kind of "micro composite" within the coarser scale fiber reinforced composite. The enhancement in PL stress is believed to stem from a combination of a lower effective "matrix" CTE as well as improved toughness of the "matrix" resulting from uniform dispersion of the BN platelets within the BSG glass.

Measurements of the thermal expansion behavior of BSG glass containing 25 vol% BN (without fiber reinforcement) have shown that the CTE is about 1.6×10^{-6}/°C, compared to 3.2×10^{-6}/°C for pure BSG glass. As discussed earlier, a lower matrix CTE leads to less thermal residual tensile stress in the matrix. The relationship between matrix toughness, or fracture energy (γ_m), and matrix cracking strain (ε_{mc}) has been expressed through the well-known ACK equation [1], given as

$$\varepsilon_{mc} = \left[\frac{12\,\tau\,\gamma_m\,E_f\,V_f^2}{E_c\,E_m^2\,r\,V_m} \right]^{1/3} . \qquad \text{(IV-2)}$$

Equation IV-2 indicates that an increase in matrix fracture energy should lead to an improvement in matrix cracking strain (and stress) if all of the other factors in the equation remain unchanged. Measurements of the fracture energy of pure BSG and pure BSG with 25 vol% BN platelets using the single-edge notched beam technique in a 3-point flexure configuration have shown that γ_m for the glass with the BN platelets (91 J/m^2) is about 50% higher than that of the pure glass (61 J/m^2). The combination of the increase in matrix toughness provided by the BN platelets together with the lower effective CTE of the "BSG+BN" matrix is believed to be responsible for the increase in PL stress in the composite systems shown in Table IV-2.

Table IV-2 - Effect of BN Additions on Composite PL Stress and Strain for Unidirectionally Reinforced C/Glass Composites

Fiber/Matrix	Fiber Vol %	BN Type	BN Vol %	Prop. Limit Stress (MPa)	Prop. Limit Strain (%)
P-100/BSG	39	---	0	103	0.03
	30	Cerac*	17	345	0.12
FT700/BSG	45	---	0	96	0.04
	43	Cerac*	13	413	0.12
	40	MW-5**	14	345	0.11
	40	ESK†	14	324	0.10
	45	HCP**	13	393	0.12

* Cerac, Inc., Milwaukee, WI

** UCAR Advanced Ceramics, Cleveland, OH

† Type S, ESK Engineered Ceramics, New Canaan, CT

Still another approach that has been investigated as a means of improving composite PL stress is annealing of composite samples following fabrication. This approach again is based on the idea of reducing the degree of residual tensile stress in the matrix. Annealing has long been recognized as a means of reducing stresses in monolithic glass that are built up during cooling due to thermal gradients within the glass [2]. Typically, pieces of monolithic glass are heated to a temperature where internal stresses can be relieved through viscoelastic relaxation of the glass structure, but below a temperature where softening or deformation of the glass would occur. The annealing range is typically near the glass transition temperature (T_g). After being held in the annealing range for a suitable period of time, the glass is cooled very slowly to minimize the generation of thermal gradients that lead to the build-up of more internal stress. In the case of C/Glass composites, matrix stress is built up continuously during cooling once the temperature drops below a temperature in the range of T_g. This makes it seem that while annealing of composite samples may relieve matrix stresses at the annealing temperature, these stresses will simply reappear on cooling regardless of the cooling rate. However, the dependence of the magnitude of the matrix stress on cooling rate is unknown, suggesting that a slower cooling rate may result in less matrix stress. For this reason, it seemed reasonable to explore annealing as a potential means of reducing residual matrix stress and in the process improve composite PL stress.

Samples of unidirectionally reinforced P-100/BSG and FT700/BSG composites were annealed in a gettered argon atmosphere using several different time-temperature schedules. The samples were then cooled to 400°C (well below the annealing temperature) at a rate of 1°C/min, followed by rapid cooling to room temperature. Table IV-3 shows the results of annealing on the ultimate tensile strength (UTS) and PL stress and strain for the two composite systems. Each value reported in the table is an average of either two or three samples. The data in the table show that annealing produced interesting but very different effects in the two composite systems. In the P-100/BSG system, the changes in PL stress were minor, with the biggest improvement resulting from the 522°C anneal (50%). Changes in UTS were unexpected; however, the 540°C anneal resulted in a considerable increase in strength, from 541 MPa to 626 MPa. In the FT700/BSG system, the shape of the stress-strain curve changed significantly with annealing, becoming noticeably less non-linear after annealing. The UTS decreased about 25% after annealing, and the PL stress increased to nearly the value of the UTS after the 560°C anneal due to the near-linear shape of the stress-strain curve. These results observed in these two systems cannot be readily explained. However, it is clear that annealing definitely had an affect on the tensile stress-strain behavior in these materials, presumably by changing the nature of the residual matrix stress and also possibly the nature of the fiber-matrix interface. Additional experiments will be necessary to gain further insight into the effects of annealing on the performance of C/Glass composites.

Table IV-3 - Effect of Annealing on the Mechanical Performance of Unidirectionally Reinforced C/Glass Composites

Fiber/Matrix	Annealing Schedule	Ultimate Tensile Strength (MPa)	Prop. Limit Stress (MPa)	Prop. Limit Strain (%)
P-100/BSG	None	541	101	0.03
	522°C, 138 mins	517	152	0.05
	540°C, 60 mins	626	125	0.04
	560°C, 30 mins	563	84	0.02
FT700/BSG	None	863	279	0.09
	540°C, 60 mins	704	190	0.06
	560°C, 30 mins	657	648	0.22

Increases in PL stress and strain have also been realized in C/Glass composites through methods designed to improve microstructural homogeneity. In the HMU/BSG composite system, it has been previously demonstrated that using fiber with a tow size of 1000 filaments leads to considerable increases in PL stress and strain compared to fiber with 3000 filaments per tow [3]. This improvement was attributed to a more uniform fiber distribution resulting from the smaller 1000 filament tows. More recently on the current program, it has been demonstrated that the PL stress and strain of pitch fiber reinforced glasses can be improved significantly by reducing the thickness of the individual laminae within the composite. This is accomplished during the fiber prepregging operation by increasing the fiber spacing on the take-up mandrel followed by manual spreading of the fiber tows. Figure IV-2 shows the effect of reducing the ply thickness from 246 μm to 67 μm on PL stress and strain in a BSG matrix composite reinforced with either P-100 or FT700 fiber. The improvement in performance with decreasing ply thickness is obvious. As with the HMU/BSG system described above, the improvement is thought to result mainly from more uniform distribution of fiber within the composite. Spreading the fiber out to a greater degree within the ply reduces the amount of fiber tow "bunching" as well as reducing the thickness of any glass-rich regions that may exist between

plys. Micromechanics theory also predicts that reduced ply thickness leads to increased matrix cracking stress and strain in the transverse plys of [0/90] reinforced composites. Although it is not clear how this would translate to unidirectionally reinforced composites, there may be some small effect resulting from this as well.

REFERENCES

1. J. Aveston, G. A. Cooper and A. Kelly, "Single and Multiple Fracture," *The Properties of Fibre Composites*, Conference Proceedings, National Physical Laboratory, 1971, pp. 15-26.

2. S. R. Scholes, *Modern Glass Practice*, CBI Publishing Company, Inc., Boston, MA, 1975.

3. K. M. Prewo, "Carbon Fibre Reinforced Glass Matrix Composite Tension and Flexure Properties," *J. Mater. Sci.*, **23** (1988) 2745-2752.

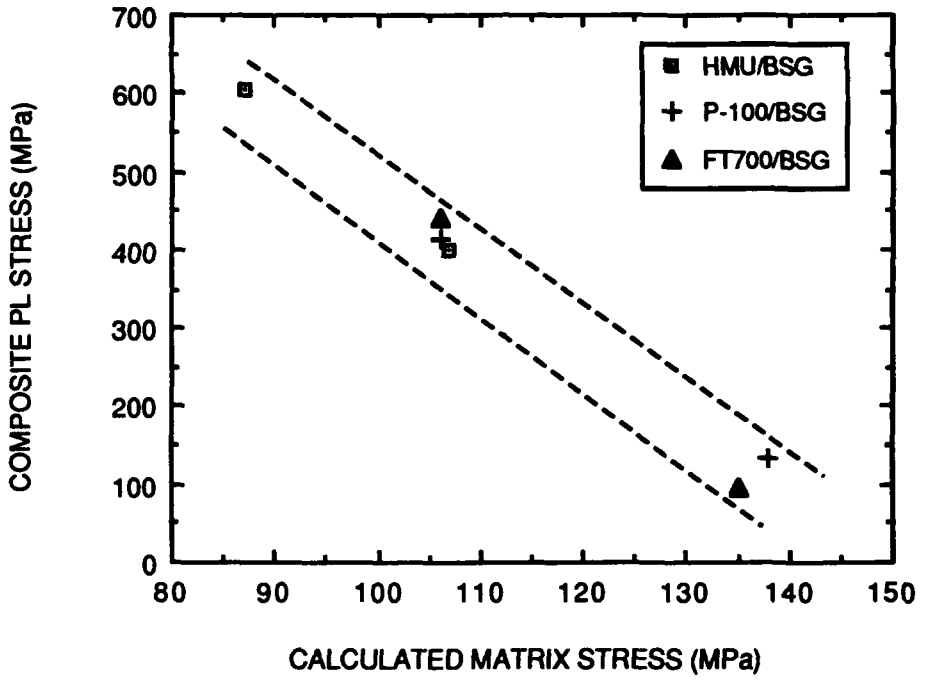

Figure IV-1. Dependence of composite proportional limit (PL) stress on calculated residual matrix stress for C/Glass composites.

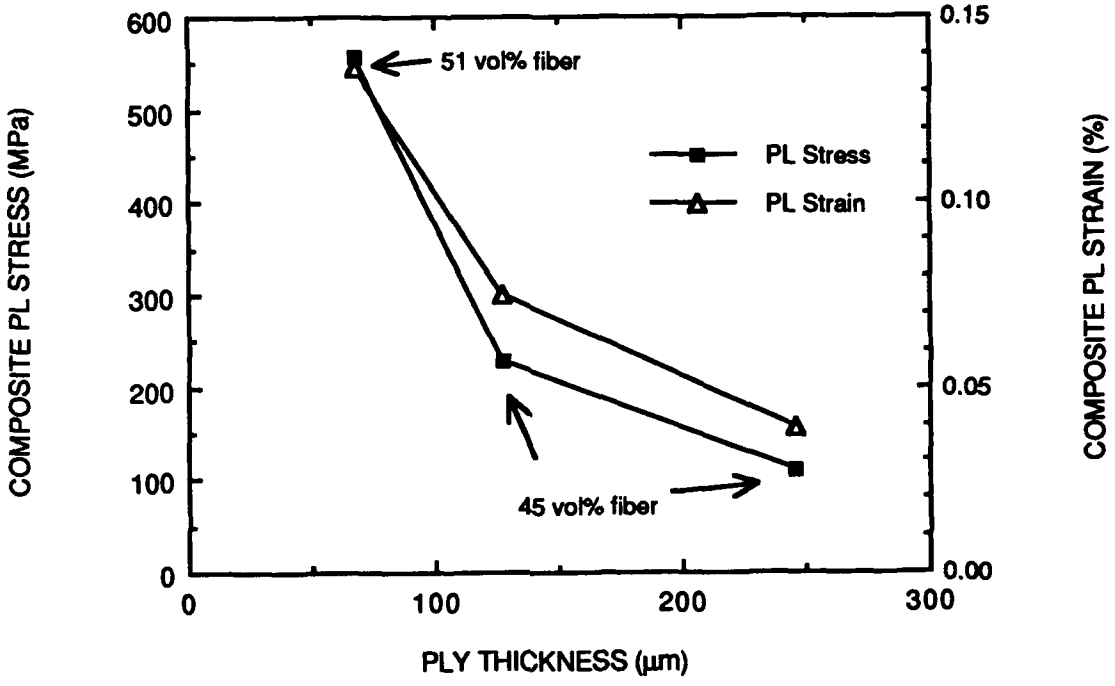

Figure IV-2. Effect of ply thickness on average proportional limit (PL) stress and strain of pitch fiber reinforced glass matrix composites.

V. APPLICATIONS FOR CARBON FIBER REINFORCED GLASS IN SPACE STRUCTURES

As described previously, the C/Glass composite system can provide an attractive alternative to polymer matrix, metal matrix and carbon/carbon composites. The glass matrix provides increased dimensional and environmental resistance while it also permits ease of composite fabrication. The following analyses are referenced here to illustrate these points. Materials Sciences Corporation (MSC), located in Blue Bell, PA, recently performed a study of C/Glass composites in which they modeled the mechanical behavior of these materials and then used the results of that model to identify potential space-based structural applications [1]. Two applications that were identified as being ideal for the implementation of C/Glass composites were satellite truss structures and radiator fins for space power applications. The results of these studies are described here in brief.

VII.1 SATELLITE TRUSS STRUCTURE

Critical requirements for satellite truss tubes were identified as being high modulus (170-340 GPa), near-zero CTE ($\pm 1.4 \times 10^{-6}$ cm/cm K), low density (< 2.5 g/cm^3), and the ability to withstand liftoff and maneuvering stresses of approximately 200 MPa. Other issues considered were AO resistance and the capability to withstand brief excursions into an elevated temperature regime (> 1000°C). Unidirectionally reinforced P-100/BSG and P-100/BMAS composites containing 12 volume % SiC monofilament were evaluated against unidirectionally reinforced P-100/Epoxy composites containing 17 volume % SiC monofilament and against ±17° reinforced P-100/Al composites in terms of meeting the key requirements described above. The results of this evaluation showed that all the materials fulfilled the modulus, CTE, and density requirements. However, the P-100/BSG and P-100/BMAS composites exhibited significantly higher maximum use temperatures than either of the other two composites and were far superior to the epoxy matrix composite in terms of AO resistance. The two C/Glass composites were therefore recommended for satellite truss applications where thermal stability and long-term durability are essential requirements.

Based in part on the results of this trade study, UTRC and MSC collaborated to design and fabricate thin-walled P-100/BSG tubes that would meet the requirements of an existing NSWC program known as Satellite Applications for Carbon-Carbon II (SACC II). These tubes were then supplied to NSWC for compression testing at Southern Research Corporation as part of the SACC II program. A detailed description of the design, fabrication, and testing of these tubes can be found in a previous report [2]. As summarized in this report, the P-100/BSG tubes were found to meet all the design requirements of the SACC II program with respect to tube geometry and mechanical properties and were comparable in performance to C-C tubes that were tested on the SACC II program.

VII.2 RADIATOR FIN

Radiator fins for the dissipation of waste heat in space power systems require lightweight materials that have high thermal conductivity in a direction normal to the heat pipe. Other critical requirements can be elevated temperature capability if the working fluid temperature is high and AO resistance if the space vehicle will be in low earth orbit for an extended period of time. For the trade study, radiator fin length was determined for each individual material by optimizing the power capability, or heat dissipation rate per unit weight. A multitude of different materials were then compared based on this optimized power capability parameter. Unidirectionally reinforced P-100/BSG and P-100/BMAS composites were evaluated against several metal fins (Cu, Al, Mg, Ti) as well as a number of other composite materials reinforced with P-100 fiber, such as P-100/Epoxy, P-100/Al, P-100/Cu, and P-100 C-C. The results of this evaluation were that all of the materials containing P-100 fiber exhibited the highest values of power capability for their respective optimized fin lengths (even greater than monolithic Cu), with all of them being essentially equivalent at approximately 100 W/kg. This indicates that the high thermal conductivity P-100 fiber dominates the response of the material regardless of the thermal conductivity of the matrix.

Another result of the study was that for fin thicknesses of 0.25-0.50 mm, which are typical for satellite radiator fins, matrix thermal conductivity was found to have a minimal effect on overall radiator performance, suggesting that low through-thickness conductivity is not a critical factor for thin-gauge structures such as fins. The overall recommendation of the study was that P-100 fiber should be used as the reinforcement and that matrix selection should be based on concerns other than heat transfer, such as AO resistance and temperature capability. For radiators requiring AO resistance and either survivability or operating temperatures in excess of 300°C, P-100 reinforced glass matrix composites were recommended as the best material.

A key aspect of radiator fin technology is the capability of producing a thin-gage material with a thickness in the range of 0.25-0.37 mm that exhibits enough transverse strength to enable it to be handled without damage to the fin. UTRC has recently demonstrated the ability to fabricate 0° reinforced P-100/BSG and K1100X/BSG composites in this thickness range. Extra transverse strength is built into the composites by adding thin layers of discontinuous carbon fiber paper, known as "scrim cloth". Addition of the scrim in between unidirectionally aligned plies gives the thin-gage composites superior handleability and a transverse tensile strength in the range of 25-30 MPa, compared to transverse tensile strengths on the order of 5-10 MPa in composites without scrim. The strain to failure in the transverse direction is approximately 0.4% in the composites containing scrim. This accomplishment is believed to be significant in light of the fact that C-C and metal matrix composites have yet to demonstrate that they can be fabricated in such thin-gage form.

REFERENCES

1. D. Volk, C. F. Yen and K. Buesking, "Structural Development of Fiber Reinforced Glass Matrix Composites," Materials Sciences Corporation Contract Report MSC TFR 2112/8601, Office of Naval Research Contract N00014-89-C-0211, June, 1990.

2. W. K. Tredway and P. H. McCluskey, "Compression Testing of Continuous P-100 Fiber Reinforced Glass Matrix Composite Tubes," UTRC Contract Report R91-917981-1, Office of Naval Research Contract N00014-89-C-0046, October 1, 1991.